



FRIEDRICH-SCHILLER-
UNIVERSITÄT
JENA

DIRECTED MOTILITY OF BENTHIC DIATOMS

DISSERTATION

(KUMULATIV)

zur Erlangung des akademischen Grades
doctor rerum naturalium (Dr. rer. nat.)

vorgelegt dem Rat der Chemisch-Geowissenschaftlichen Fakultät
der Friedrich-Schiller-Universität Jena von Diplom-Chemikerin

von

M.Sc. (Marine Science) Karen Grace V. Bondoc

geboren am 03.06.1988 in Amulung, Cagayan, Philippinen

Dissertation, Friedrich-Schiller-Universität Jena [2017]

Gutachter:

1. Prof. Dr. Georg Pohnert, Friedrich-Schiller-Universität Jena
2. Prof. Dr. Wilhelm Boland, Friedrich-Schiller-Universität Jena
3. Prof. Dr. Knut Drescher, Philipps-Universität Marburg

Tag der Verteidigung: 14 Dec 2017

For the One who created the oceans.

"But I don't want to go among mad people," Alice remarked.
"Oh, you can't help that," said the Cat: "we're all mad here. I'm mad. You're mad."

"How do you know I'm mad?" said Alice.
"You must be," said the Cat, "or you wouldn't have come here."

— Lewis Carroll, *Alice in Wonderland*

TABLE OF CONTENTS

TABLE OF CONTENTS.....	V
SUMMARY.....	VII
ZUSAMMENFASSUNG.....	XI
ABBREVIATIONS	XV
LIST OF FIGURES.....	XVI
1 INTRODUCTION.....	1
1.1 Characteristics and ecology of diatoms	1
1.1.1 Motility	2
1.1.2 Reproduction	4
1.2 Diatom biofilms: success in patchiness	6
1.3 From small-scale to large-scale processes: Bigger impacts of behaviour	11
1.3.1 Behaviour	11
1.3.2 Investigations in motility.....	12
2 SCOPE OF THE STUDY	17
3 PUBLICATIONS	19
3.1 Publication A.....	19
3.2 Publication B.....	37
3.3 Publication C	51
4 DISCUSSION AND FUTURE PERSPECTIVES	99
4.1 Nutrient attraction across the life cycle	99
4.1.1 Nutrient starvation and recovery.....	100
4.1.2 Behavioural response to nutrient starvation	102
4.1.3 Nutrient uptake enhanced by motility	104
4.2 Pheromone-mediated chemoattraction of sexual cells.....	105
4.3 Sensing mechanisms: How do diatoms find chemical signals?.....	108
4.4 Prioritization mechanisms: Food vs. sex on sexually-available diatoms.....	108
4.5 Implications of directed motility – evolutionary aspects and ecological cascades	110
4.6 Future perspectives	112
5 REFERENCES.....	115
6 DECLARATIONS.....	125

Selbstständigkeitserklärung.....	125
Weitere Erklärungen	125
Einverständniserklärung des Betreuers.....	126
AFTERWORD.....	127

SUMMARY

Diatoms are a group of highly diverse microalgae dominating aquatic systems and contributing to a quarter of the global primary production. They have a unique morphology including a biomineralized silicate-based cell wall. This rigid cell wall leads to cell size reduction during mitosis followed by size restoration through sexual reproduction. In intertidal sediments, they significantly contribute to microphytobenthic biofilm communities, thereby playing an important role in ecosystem functioning. A biofilm is a complex and dynamic environment where growth and reproduction are under the control of signal molecules and nutrient resources. As diatoms are key players for biogeochemical cycling, collective behaviour and interactions can create a cascade of events with global-scale consequences.

I used the model pennate diatom *Seminavis robusta* to determine how benthic diatoms forage for nutrients and locate their mating partners. Like most pennate diatoms, *S. robusta* moves by gliding back-and-forth across surfaces through excretion of extrapolymeric substances (EPS) from the raphe, a slit on its cell wall. The sexual phase of this microalga is pheromone-mediated, with both mating types (MT^+ and MT^-) secreting sex-inducing pheromones (SIP^+ and SIP^- , respectively) as priming signals for each other once they reach sexual size threshold (SST). MT^- cells then produce the attraction pheromone diproline for chemoattraction of MT^+ . Hotspot sources of stimuli were mimicked using specific beads that adsorb dissolved nutrients or the pheromone diproline. Upon medium contact, beads release the stimuli, forming a diffusion gradient. A combination of video monitoring, trajectory analysis, and statistical modelling was utilized to determine how nutrient-starved or sexually-induced cells responded to the signal gradients formed. As cells in both vegetative and sexual phases of *S. robusta* were used for the attraction assays, this study is the first to provide comprehensive knowledge on a microorganism's behavioural motility across its life cycle.

I tested the responses of diatoms to the macronutrients dissolved silicate (dSi), phosphate (dP), and nitrate and ammonium (dN). Foraging cells were attracted to dSi and dP, but not to any form of dN. Cells accumulated around the nutrient-loaded bead within ~5 min for dSi and ~20 min for dP, respectively, while control beads did not elicit attraction. The observed dSi response was universal, as no inter- and the intra-specific difference in reaction of different strains of *S. robusta*, as well as of another pennate diatom, *Navicula sp.* was found. Additionally, the dSi response was substrate-specific, as gradients of germanium dioxide (dGe), which have comparable chemical characteristics as dSi, elicited a negative response. Since dSi elicited the fastest response among the tested nutrients, I verified the differential behaviour of large-sized vegetative cells (>50 μm) and cells of two sexual sizes

below the sexual size threshold (SST): medium- ($\sim 40 \mu\text{m}$) and critically small-sized (24-27 μm) cells. No variability in the response towards dSi was observed, albeit, large-sized cells required a longer starvation time. Foraging cells utilized a simultaneous tactic and kinetic approach in locating nutrient resources. Changes in the gliding behaviour enable the cells to locate the stimulus and maximize their encounter rate with it. Overall, the fine tuning of motility parameters while foraging increased nutrient uptake up to 170-fold, which may circumvent severe limitation scenarios in the benthic environment.

Sexual MT⁺ cells additionally exhibited an attraction to diproline once they crossed SST. However, the factors affecting their response varied. Cells accumulated around diproline-loaded beads rapidly ($\sim 5 \text{ min}$) and exhibited the same tactic and kinetic finding mechanism similar to those of foraging cells. However, with critically small-sized cells, an unprecedented attraction to diproline even in the absence of priming (SIP⁻) was also observed. Sexual cells on the verge of extinction can exhibit an emergency mechanism by bypassing the pheromone priming for sexualization and move toward diproline when it is encountered, thereby prioritizing mating to escape cell death. Diproline-sensing is sensitive, with cells recognizing the stimuli even in a picomolar range. Both bypassing priming and sensitivity to diproline are mechanistic ways that could ensure survival in a complex landscape where signals from different microorganisms can co-occur.

In silico comparisons of motility parameters of cells encountering dSi and diproline showed that the latter affected the search patterns of cells drastically. There was increased directionality and diffusivity of cells during pheromone location. Since benthic diatoms face co-occurring signals in their natural environment, I designed an experiment to determine their decision-making mechanism under different physiological constraints. Medium and small-sized cells were exposed to various combinations of dSi-starvation and sex-priming, and individual beads (dSi or diproline) were applied. Medium-sized cells have clear had physiological control over their attraction. They only exhibited diproline attraction when sexually-induced, and dSi attraction when starved. However, sexual pressure on small-sized cells influenced them to be more sensitive to diproline. Even if only trace amounts of dSi were present, cells were attracted to the pheromone. Nonetheless, if both stimuli were missing, self-priming was not observed. Since dSi is essentially required for cell wall formation after pairing, cells require this resource before locating a mating partner. When cells simultaneously faced both dSi and diproline-loaded beads, the response was consistent with the one-bead experiment, highlighting the role of trace dSi before mating can progress. It is highly possible that there is a cross-talk between motility, dSi-sensing, and mating, that increase fitness under nutrient-limitation or sexual pressure in a complex landscape depending on the physiological condition of the cells.

The interplay between nutrient acquisition and mating in *S. robusta* is a complicated mechanism involving signalling events and regulation of behaviour. The performance of diatoms on a complex microhabitat is dependent on the adaptive motility behaviour that can be triggered by nutrient limitation and sexual pressure. Moreover, the capacity to prioritize between co-occurring stimuli

highlights the fine control mechanism of cells to their behaviour depending on their physiological constraint. The results suggest that diatom motility not only allows cells to respond and position themselves along nutrient and pheromone gradients to exploit them, but it also plays a major role in exploiting fine-scale spatial heterogeneity in available resources. The active searching behaviour can potentially contribute in shaping the aquatic environment on a microscale by influencing patchiness of biofilm communities, and on a global scale by affecting sediment-water nutrient fluxes and biogeochemical cycles.

ZUSAMMENFASSUNG

Diatomeen (Kieselalgen) bilden eine sehr diverse Gruppe von Mikroalgen, die in aquatischen Systemen oft zu den dominanten Primärproduzenten zählen. Durch ihre große photosynthetische Aktivität tragen sie zu ca. einem Viertel der globalen Primärproduktion bei. Die einzigartige Morphologie der Diatomeen ist durch ihre charakteristischen biomineralisierten, silikatbasierten Zellwände geprägt. Aufgrund der starren Zellwand führt die mitotische Zellteilung bei vielen Diatomeen zur Abnahme der Zellgröße. Diese kann nur durch sexuelle Reproduktion wiederhergestellt werden. In den Gezeitenzonen tragen Diatomeen signifikant zu den mikrophytobenthischen Biofilmen bei und spielen damit eine wichtige Rolle im Ökosystem. Ein Biofilm ist eine komplexe und dynamische Umwelt, in der Wachstum und Reproduktion durch Signalmoleküle und Nährstoffverfügbarkeit beeinflusst werden. Da Kieselalgen eine Schlüsselfunktion in biogeochemischen Kreisläufen übernehmen, kann ihr kollektives Verhalten und ihre biotischen Interaktionen Auswirkungen auf globaler Ebene haben.

Um zu ermitteln, wie motile pennate Diatomeen Nährstoffe und Paarungspartner finden, untersuchte ich die Modellkieselalge *Seminavis robusta*. Wie die meisten pennaten Diatomeen bewegt sich *S. robusta* durch Ausscheidung von extrapolymeren Substanzen (EPS) die zu einer gleitenden vor- und rückwärts-Bewegung führt. Die sexuelle Reproduktion dieser Mikroalge ist oft durch Pheromone mediert. Bei *S. robusta* sekretieren beide Paarungspartner (MT^+ und MT^-) Sex-induzierende Pheromone (SIP^+ und SIP^-) als initierendes Signal sobald eine kritische Zellgröße unterschritten wird. MT^- Zellen produzieren anschließend das Attraktionspheromon Diprolin zur Chemoattraktion von MT^+ . Punktquellen des Pheromons und anorganischer Stimuli wurden durch die Nutzung spezieller Partikel, die gelöste Nährstoffe oder Diprolin adsorbieren, erzeugt. Durch Kontakt mit Medium geben die Partikel die Stimuli frei und es bildet sich ein Diffusionsgradient. Mittels einer Kombination aus Videobeobachtung, Zellbewegungsanalysen und statistischer Modellierung wurde untersucht, wie nährstofflimitierte oder sexuell-induzierte Zellen auf Gradienten der Signalstoffe reagierten. Da sowohl vegetative als auch sexuelle Zellen in Attraktionsassays untersucht wurden, ist diese Studie die erste, die umfangreiches Wissen über das Bewegungsverhalten eines Mikroorganismus in seinem Lebenszyklus aufzeigt.

In der Arbeit wird die Reaktionen der Diatomeen auf das Attraktionspheromon und auf die gelösten Makronährstoffe Silikat (dSi), Phosphat (dP) und Nitrat und Ammonium (dN) untersucht. Nährstoff-suchende Zellen wurden durch dSi und dP, aber nicht durch dN, angezogen. Sie

akkumulierten in Partikelnähe in ~5 min für dSi und ~20 min für dP, während Kontrollpartikel keine Attraktion zeigten. Die gefundene dSi-Antwort ist universell, da keine inter- oder intraspezifische Differenz in der Reaktion verschiedener *S. robusta* Stämme oder einer anderen pennaten Diatomee *Navicula sp.* gefunden wurde. Ferner ist die dSi-Antwort substratspezifisch, weil Germaniumdioxid (dGe), welches vergleichbare chemische Eigenschaften wie dSi aufweist, negative Antwort auslöste. Da dSi die schnellste Reaktion im Vergleich zu den anderen Nährstoffen zeigte, untersuchten wir das differentielle Verhalten von großen, vegetativen Zellen (<50 µm), von Zellen die die Grenzgröße zur sexuellen Vermehrung gerade unterschritten haben (mittelgroß, ~40 µm) und von Zellen mit kritisch-kleiner Größe (24-27 µm). Es wurde keine Variabilität in der Reaktion zu dSi festgestellt, außer dass große Zellen eine längere Limitierungsdauer benötigten, um dSi Affinität zu zeigen. Nährstoffsuchende Zellen benutzen gleichzeitig Taxis und Kinesis, um Nährstoffquellen zu finden. Ich habe die Veränderungen im Bewegungsverhalten charakterisiert durch die Zellen die Stimuli lokalisieren und ihre Auffindungsrate erhöhen können. Insgesamt erhöhte das genaue Abstimmen der Motilitätsparameter während der Nahrungssuche die Nahrungsaufnahme um bis zu einem Faktor von 170, was der Zelle helfen könnte drastisch limitierende Szenarien im Benthos zu vermeiden.

Sexuelle MT⁺ Zellen zeigten eine Attraktion zu Diprolin, sobald sie die SST unterschreiten, wobei die beeinflussenden Faktoren variierten. Induzierte Zellen akkumulierten schnell um Diprolinpartikel (~5 min) und zeigten einen taktisch-kinetischen Mechanismus vergleichbar zur Nahrungssuche. Mit kritisch-kleinen Zellen wurde eine bisher unbekannte Attraktion zu Diprolin selbst ohne Sex-Induzierendes Pheromon (SIP-) beobachtet. Sexuelle Zellen können anscheinend kurz vor dem Zelltod einen Notfallmechanismus nutzen, indem sie die Pheromoninduktion zur Sexualisierung umgehen. Sie orientieren sich nach der Wahrnehmung des Attraktionspheromones auf dieses zu und priorisieren dadurch die Paarung, um einem Zelltod zu entgehen. Die Diprolinwahrnehmung ist dabei so empfindlich, dass die Zellen die Stimuli selbst im picomolaren Bereich wahrnehmen können. Sowohl das Umgehen der Induktion als auch die Sensitivität der Diprolinwahrnehmung sind mechanistische Wege, die das Überleben in einer komplexen Umgebung, in der sich Signale verschiedener Mikroorganismen überlagern können, sicherstellen.

In silico Vergleiche der Motilitätsparameter von Zellen während der dSi- und Diprolinaufnahme zeigen, dass letzteres die Suchmuster der Zellen drastisch verändert. Während der Partnersuche sind Direktionalität und Diffusionsvermögen der Zellen erhöht. Da benthische Diatomeen in ihrer natürlichen Umwelt überlappenden Signalen begegnen, entwickelte ich ein Experiment, um deren Entscheidungsfindung unter verschiedenen physiologischen Restriktionen zu bestimmen. Mittelgroße und kleine Zellen wurden unter unterschiedlichen Kombinationen von dSi-Limitierung und Sex-Induktion kultiviert und verschiedene Partikel (dSi oder Diprolin) wurden zugegeben. Für mittelgroße Zellen ergab sich dabei eine klare physiologische Kontrolle über die Attraktion. Sie zeigten nur unter sexueller Induktion eine Diprolinattraktion und nur, wenn sie hungrten, eine dSi-Attraktion. Dagegen

führte die Dringlichkeit zur Reproduktion bei kleinen Zellen zu einer erhöhten Empfindlichkeit für Diprolin. Selbst bei geringen Mengen dSi wurden die Zellen vom Pheromon angezogen. Dennoch wurde, wenn beide Stimuli fehlten, keine Selbstinduktion beobachtet. Da dSi essentiell für die Zellwandbildung nach der Paarung ist, benötigen die Zellen diese Ressource vor der Partnerfindung. Bei gleichzeitiger Verwendung von dSi- und Diprolinpartikeln zeigten die Zellen die gleichen Reaktionen wie in den Experimenten mit einzelnen Partikeln, was die Rolle von geringen Mengen an dSi vor der Paarung hervorhebt. Es ist sehr wahrscheinlich, dass es eine Verknüpfung von Motilität, dSi-Wahrnehmung und Paarung gibt, welche die Fitness unter Nährstofflimitierung und sexueller Dringlichkeit in einer komplexen Umgebung in Abhängigkeit der physiologischen Kondition der Zellen erhöht.

Das Zusammenspiel zwischen Nährstoffaufnahme und Paarung ist ein komplizierter Mechanismus, der Zellsignale und Verhaltensregulation beinhaltet. Der Erfolg in einem komplexen Mikrohabitat ist abhängig von dem adaptiven Bewegungsverhalten der Zellen, das durch Nährstofflimitierung und Paarungsbereitschaft ausgelöst werden kann. Die Fähigkeit zwischen überlagernden Signalen zu entscheiden, unterstreicht die Feinabstimmung des Verhaltens der Zellen in Abhängigkeit der physiologischen Einschränkungen. Diese Ergebnisse implizieren, dass das Bewegungsverhalten der Diatomeen, auf Nährstoff- und Pheromongradienten zu reagieren und sich zu positionieren. Durch ihr Bewegungsverhalten sind Diatomeen in der Lage, selbst auf verdünnte Nährstoff- und Pheromongradienten zu reagieren und sich gerichtet fortzubewegen. Dieses aktive Suchverhalten hat Auswirkungen auf das aquatische System, sowohl im Mikromaßstab durch einen Einfluss auf die (Un)Gleichmäßigkeit des Biofilms, als auch im globalen Maßstab über eine Beeinflussung biogeochemischer Nährstoffzyklen und -flüsse in der Sediment-Wasser-Grenzschicht.

ABBREVIATIONS

BrCN	Cyanogen bromide
cAMP	Cyclic adenosine monophosphate
cGMP	Cyclic guanosine monophosphate
D	Diffusivity
DFAA	Dissolved free amino acid
dGe	Dissolved germanium dioxide
DMS	Dimethyl-sulfoxide
DMSP	Dimethyl-sulfoniopropionate
dN	Dissolved inorganic nitrogen
DOP	Dissolved organic phosphorus
dP	Dissolved inorganic phosphate
dSi	Dissolved inorganic silicate
EPS	Extracellular polymeric substances
GC/PDE	Guanylyl cyclase/phosphodiesterase
L	Trail length
Micro-PIV	Micro-particle image velocimetry
MPB	Microphytobenthos
MT ⁺	Migrating mating type
MT ⁻	Attracting mating type
NO	Nitric oxide
PCD	Programmed cell death
Pe	Peclet number
Sh	Sherwood number
SIP	Sex-inducing pheromone
SST	Sexual size threshold

LIST OF FIGURES

Figure 1. Examples of the diversity of diatoms and the unique structure of their siliceous cell wall.....	1
Figure 2. Diagram of the frustule in centric (A) and pennate (B) diatoms.....	2
Figure 3. A simplified model of locomotion model for <i>Navicula sp.</i> , a raphid benthic diatom.....	3
Figure 4. The life cycles of a centric (A) and pennate (B) diatom.....	5
Figure 5. Schematic diagram of a benthic biofilm (A) and niche partitioning in a biofilm (B).	6
Figure 6. The activity of epipelagic diatoms and the vertical distribution of environmental factors within the biofilm.....	9
Figure 7. Schematic diagram of fundamental processes affecting behaviour.....	11
Figure 8. Methods in analysing motility in microbial systems.....	14
Figure 9. The adaptive motility of <i>Seminavis robusta</i> towards nutrient and pheromone sources across its life cycle.....	96
Figure 10. Suggested experimental set-up to determine nutrient foraging and mate-locating in a patchy environment.....	110

1 INTRODUCTION

1.1 Characteristics and ecology of diatoms

The diatoms (Bacillariophyta) are a highly productive algal group, representing a mere 0.2% of global biomass, and are responsible for nearly half of the global net primary production¹. They also have the highest diversity in all algae, with more than 200,000 extant species inhabiting a broad range of aquatic environments (Fig. 1), serving as the basis of most aquatic food webs and are significant players to global nutrient cycling¹⁻⁴. Diatoms are broadly classified under stramenopiles or heterokonts together with brown algae, oomycetes, and opalinids. They are part of the Chromalveolata supergroup together with haptophytes, cryptophytes, and alveolates⁵.

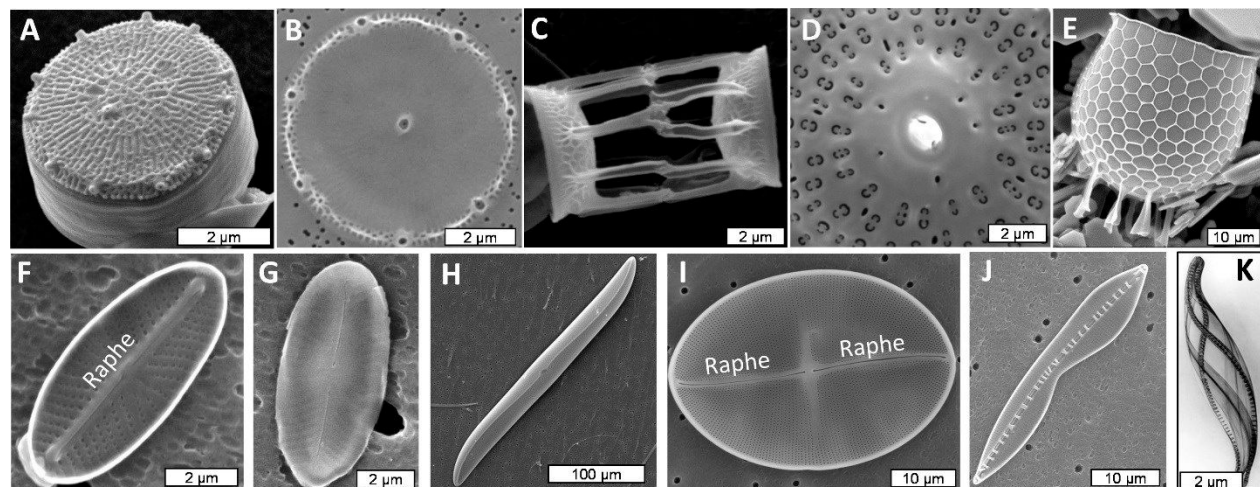


Figure 1. Examples of the diversity of diatoms and the unique structure of their siliceous cell wall. (A) *Thalassiosira pseudonana*, (B) *Thalassiosira oceanica*, (C) *Skeletonema costatum*, (D) *Ditylum brightwellii*, (E) *Stephanopyxis turris*, (F) *Navicula pelliculosa* proximal surface, (G) *N. pelliculosa* distal surface, (H) *Gyrosigma balticum*, (I) *Cocconeis* sp., (J) *Bacilaria paxillifer*, (K) *Cylindrotheca fusiformis*. (A)–(E) are centrics, (F)–(K) are pennates. The location of the raphe is noted in (F) and (I). Figure from Hildebrand and Lerch 2015⁶, Copyright License No. 4153661016377.

One of the defining traits of diatoms is the diversity of their intricately-shaped cell walls—called frustules—composed of hydrated silica (SiO_2) (Fig. 1). The frustule can be described as a ‘glass box’ with overlapping top and bottom valves that resemble a pill box or petri dish (Fig. 2). The larger and older valve (epitheca) overlaps with the smaller and younger valve (hypotheca) through several girdle bands that bind them together⁶. The top of the frustule also contains micro- and nanometer-sized perforations, allowing diffusion of molecules in and out of the cell and permitting the contact to

substrates in the environment⁷. Additionally, the surface structure of the frustule acts as a sieve against harmful particles, bacteria, or viruses and increase diffusion efficiency by inhibiting fouling of the diatom surface⁸. This biomineralized cell wall also functions as a very effective armour against predators by providing mechanical protection⁹.

Diatoms are traditionally divided into two morphological groups: the centrics and pennates. Centric diatoms (Mediophyceae) are characterized by having valves with radial symmetry and are often components of the pelagic phytoplankton. Whereas, pennate diatoms (Bacillariophyceae) possess valves with bilateral symmetry and often inhabit the benthos, dominating biofilm communities¹⁰ (Fig. 2). Pennate diatoms were estimated to diverge from centrics only from 90 Mya but had diversified immensely⁴. Pennates can be further subdivided into two groups depending on the presence of a raphe, a slit on the valve of their cell wall involved in surface adhesion and movement. Raphids can possess a raphe on one side of their frustule (monoraphid) or both (biraphid). Most of them move by gliding, although several that have adnate or stalked growth forms are sessile. Whereas, araphids lack a raphe, and are thus immotile, except for a few species that can glide slowly^{11,12}. The raphe has a ‘tongue-in-groove’ curvature that protects the valve from stress and runs along the long central axis of the valve either continuously or interrupted by a silicified central nodule^{6,10}.

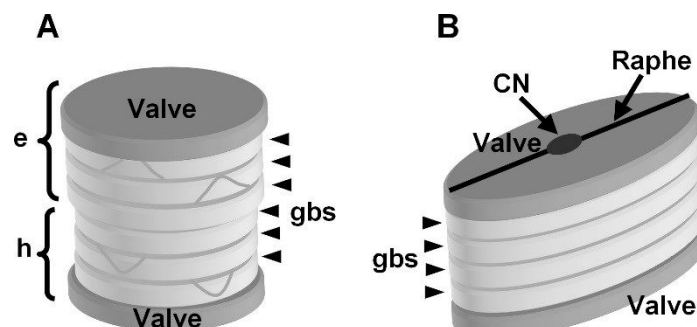


Figure 2. Diagram of the frustule in centric (A) and pennate (B) diatoms.

The epitheca (e) and hypotheca (h) are connected through overlapping girdle bands (gbs). In pennate diatoms, the raphe can be absent (araphid), or present in one (monoraphid) or both (biraphid) valves. The structure runs the whole length of the valve either continuously or interrupted by the central nodule (CN) and runs along the entire length of the valve. Figure from Hildebrand and Lerch 2015⁶, Copyright License No. 4153661016377.

1.1.1 Motility

Some centric diatoms move along the water column even in the absence of a raphe by altering their buoyancy through their vacuoles, resulting in a sink-and-stop movement. Ion regulation of the cell sap controls the density of a cell¹³. However, only large-sized cells were reported to finely control their sink-and-stop behaviour in response to nutrient stress in the water column. Briefly, cells exhibit a buoyant state when nutrients are sufficient; once resources become scarce, they sink fast with a similar rate as that of senescent and dead cells to increase nutrient uptake¹⁴.

Motility of raphid pennate diatoms is through gliding, which is characterized by shunting back and forth with jerky and irregular patterns¹⁵. Locomotion is achieved through the excretion of adhesive mucilaginous compounds, called extracellular polymeric substances (EPS), which aid in adhering to and moving on surfaces¹⁵⁻¹⁷. Adhesion to surfaces is a prerequisite for subsequent movement as raphe contact to the substratum is needed to initiate gliding¹⁸. This process is highly dependent on both Ca²⁺ for both marine and freshwater diatoms, with the former requiring millimolar amounts^{19,20}. Intracellular nitric oxide (NO) levels can regulate adhesion by blocking secretion of EPS and enabling the cells to detach from the surface and glide²¹.

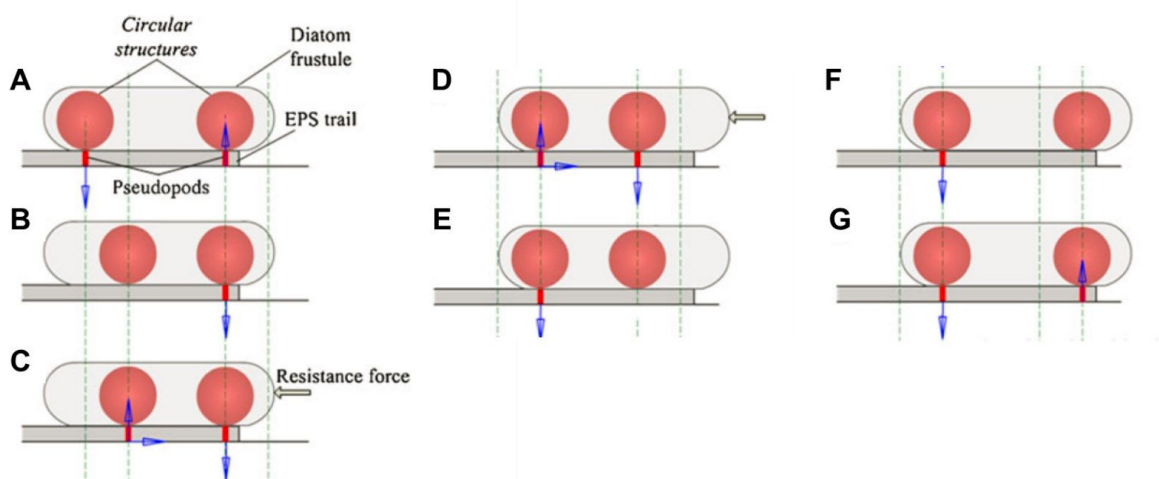


Figure 3. A simplified model of locomotion model for *Navicula sp.*, a raphid benthic diatom.

Two circular structures made from actin (**A**) protrude as pseudopods. One pseudopod (right circular structure) adheres and press on the substrate (**B**). The exerted downward force enables the other pseudopod (left circular structure) to roll towards the right (**C-D**). Afterwards, the right pseudopod is retrieved, and the left pseudopod presses the substrate that allows the former to roll as well towards the right (**E-G**). The alternating push-pull off movement from the two pseudopods create a force for the back-and-forth movement. Figure from Wang *et al.* 2013²², Copyright License No. 4153670917250.

According to a gliding model, an actin-myosin complex was hypothesized to control/regulate diatom movement. Actin filaments act as “intracellular railways” while myosin provides the tractional force for movement^{15,17}. However, an updated model from Wang *et al.*²² showed a more mechanistic and realistic model where movement is made possible by two or more pseudopods or stalks made from actins protruding from the raphe (Fig. 3). The pseudopod form two actin-circular structures inside the frustule located on both ends of the cell. To initiate movement, one of the pseudopods presses on the substrate, initiating the other pseudopod to pull off and the circular structure to roll in the direction of movement. The stalks alternately adhere and put pressure on the substrate which produces the friction for movement. The high-speed motility of the stalks enables the cells to move fast. Additionally, cell rotation is achieved through a torque produced from strong adhesion to the substrate²². The speed of raphid diatoms can range from ~1–29 µm s⁻¹¹⁵, and their horizontal speed is 10-fold higher than their vertical speed²³. Speed does not correlate with diatom length, and the cells

can perform motility in a wide range of pH and osmolarity²⁰. However, cells have the capacity to utilize directed movement towards signals such as species-specific light wavelength requirement^{24,25} and monosaccharide resources²⁶.

1.1.2 Reproduction

Another unique characteristic of most diatoms is their diplontic life cycle (Fig. 4), characterized by a relatively long vegetative phase (months to years) and short sexual reproduction (hours to weeks). In the vegetative division, one daughter cell will inherit one theca, and within this constraint, the other half of the frustule will be formed through the incorporation of silicate. The daughter cell inheriting the larger epitheca will have an identical cell size to the parental cell, while the other one possessing the smaller hypotheca will have a gradual decrease in cell size for each mitotic division^{27,28}. After successive vegetative division and reaching a species-specific sexual size threshold (SST), typically 30–40% of their original size, cells switch to sexual reproduction²⁹ to reconstitute their cell size and escape programmed cell death (PCD)²⁷. For both diatom types, only cells that reach SST can be sexualized²⁷.

Centrics and pennates have different modes of sexual reproduction and factors that can affect reproduction success. Centric diatoms exhibit oogamy, wherein flagellated motile sperms fuse to a large immotile egg. Gametogenesis can occur from one clonal population, hence the system is homothallic and cells can essentially self-fertilize^{27,28}. Additionally, the process is governed by species-specific environmental cues such as light, temperature, ammonium concentration, or salinity^{27,28,30}. While primary copulation in centrics is exclusively via gametes (gametogamy), the gametangia of pennates can also pair, subsequently producing gametes either through anisogamy (gametes are different morphologically and/or behaviorally) or isogamy (gametes are similar morphologically and/or behaviorally). Additionally, two separate but sexually-compatible mating types from different clonal populations can mate, making the system heterothallic. Besides cell-cell interaction, environmental factors such as light can also affect reproduction success²⁷. After successful pairing of gametes, a zygote is formed and develops into an auxospore, which is subsequently enveloped by new thecae, completing the constitution of a new initial large cell^{27,28}.

In recent years, experimental research has been done regarding the factors affecting reproduction success. An exemplary model for centric sexual reproduction is *Thalassiosira pseudonana* (Fig. 4A), which was previously assumed to be asexual as it does not exhibit cell-size reduction³¹. Dose-dependent concentrations of ammonium—not nitrate—triggered the production of oogonia, spermatogonia, and subsequently auxospores and initial cells. This observation also extends to the other centric diatoms *Thalassiosira weissflogii* and *Cyclotella cryptica*³⁰. In pennate diatoms, both araphids and raphids are sexualized by the presence of the opposite mating types, and the mating

process can either be mediated by the presence or absence of pheromones³²⁻³⁵. A model system for the pheromone-mediated mating is the sexual reproduction of raphid pennate, *Seminavis robusta* (Fig. 4B). In a first step, both the migrating (MT⁺) and the attracting (MT⁻) mating types produce sex-inducing pheromones, SIP⁺ and SIP⁻, respectively, which serve as signals of their sexualized state and presence within the vicinity. Subsequently, the production of the attracting pheromone, the L-proline-derived diketopiperazine, octahydro-5H,10H-dipyrrrolo[1,2-a:1,2-d]pyrazine-5,10-dione (in the following abbreviated as diproline) in MT⁻ is triggered, and the diproline receptor in MT⁺ is potentially produced or upregulated. Diproline production enhances reproduction success by improving mate finding probability and subsequent pairing. Indeed, previous attraction assays showed that MT⁺ cells could migrate towards polymer beads that gradually release diproline signals^{33,36}.

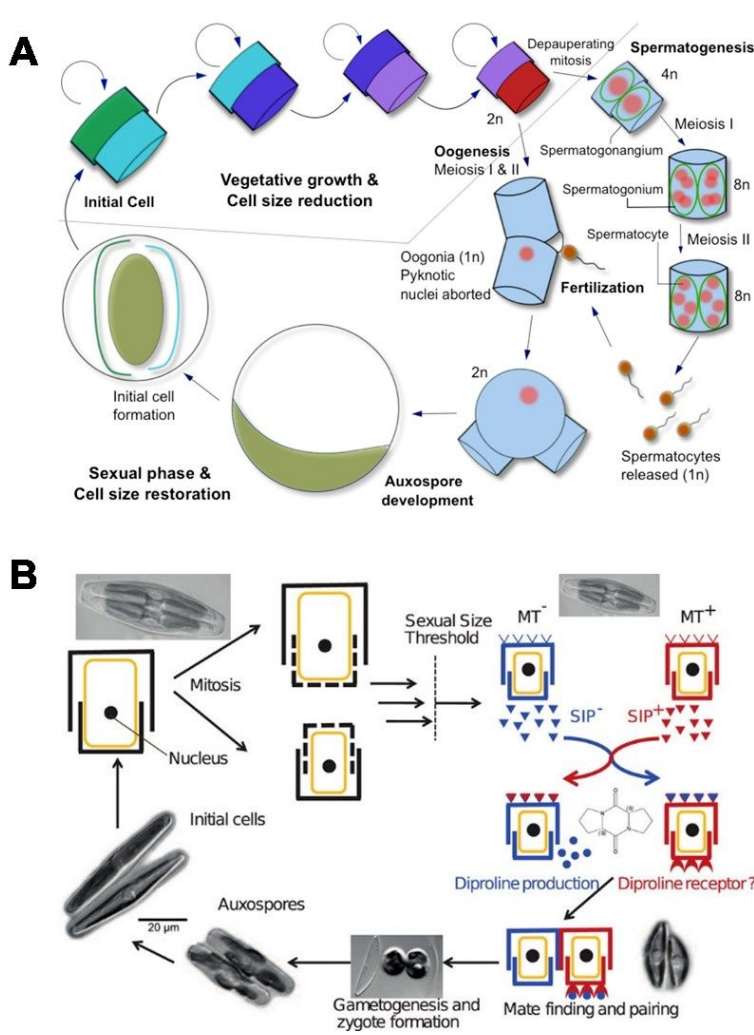


Figure 4. The life cycles of a centric (A) and pennate (B) diatom.

Vegetative mitotic division in diatoms leads to decreased cell size as a result of inheritance of differing sizes of the theca. At a certain point, cells cross a species-specific sexual size threshold (SST) and switch to sexual reproduction. Sexual cells can continue to mitotically-divide, but only mating can reinstate the original cell size, thereby escaping a programmed cell death. **(A)** For centric diatoms, like *Thalassiosira pseudonana*, spermatogenesis and oogenesis produce haploid motile spermatoocytes and a non-motile egg, respectively that can undergo fertilization, and subsequently, auxospore development, and a production of initial cells. Figure from Moore et al. 2017³⁰, Copyright under the Creative Commons Attribution License.

(B) For the pennate model diatom *Seminavis robusta*, the life cycle is pheromone-mediated. Upon crossing SST, MT⁻ and MT⁺ cells produce sex-inducing pheromones (SIP). This triggers the production and release of the attracting pheromone, diproline from MT⁻ and the possible upregulation of diproline receptor in MT⁺. MT⁺ uses diproline to track the location of MT⁻ to mate. After successful pairing, gametogenesis can occur releasing gametes that fused into a zygote, and subsequently, develop into an auxospore, and finally to an initial cell. Figure from Moeyns et al. 2016³⁶, Copyright under the Creative Commons Attribution License.

1.2 Diatom biofilms: success in patchiness

Motility of pennates enabled them to dominate ecosystems within deposited sediments³⁷, mainly forming microphytobenthos (MPB) and colonizing intertidal and tidal areas globally^{37,38}. The biofilm community is also composed of aggregated prokaryotes and photosynthetic microeukaryotes embedded within a matrix of EPS³⁷⁻³⁹ (Fig. 5A). Within the MPB, diatoms are the crucial component, specifically motile types^{11,38} dominating 40% of the topmost 2 mm layer of biofilms⁴⁰. The high level of activity of benthic diatoms in a few cm thick environment can surpass the primary production activity of phytoplankton in the overlying water column. They can contribute 29–314 g C m⁻² a⁻¹, which is approximately 50% of the primary production in estuarine systems. Thus, the communities they inhabit are ranked as one of the most productive ecosystems in the world³⁸ and are considered critical links between terrestrial and aquatic systems⁴¹. As autotrophic organisms, benthic diatoms also act as the base of estuarine food webs, serving as a food source for different macro- and meiofauna, and providing dissolved organic matter (DOM) to heterotrophic bacteria^{42,43}. They can also emit chemical signals that act as settlement and habitat cues for marine invertebrate larvae that live on the benthos⁴⁴. Biogeochemical cycling rates are also high in this microenvironment and can lead to regulation of nutrient fluxes in the sediment-water interface^{38,45-47}. Additionally, they can influence sediment properties and stabilization^{11,48}.

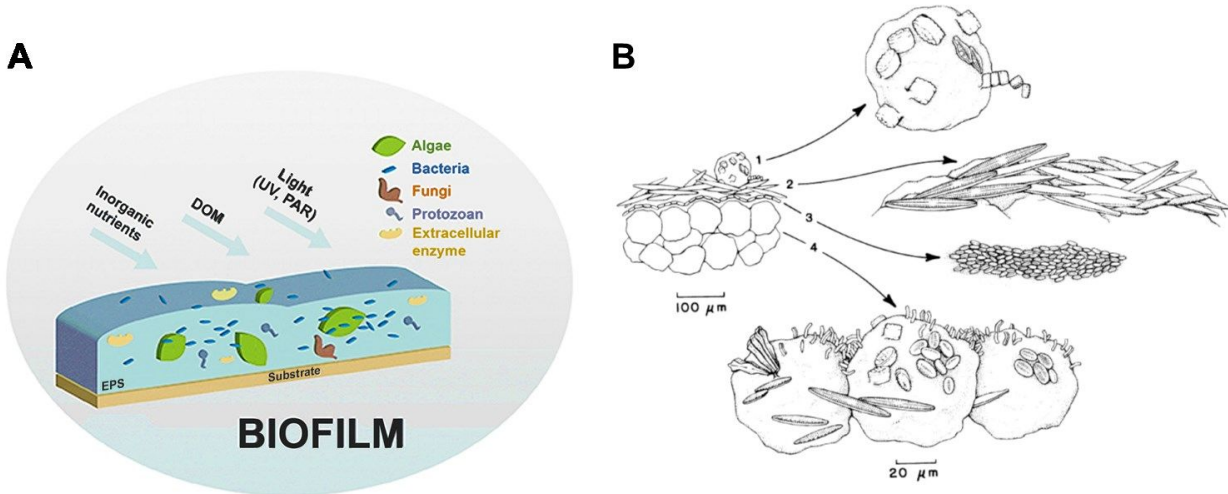


Figure 5. Schematic diagram of a benthic biofilm (A) and niche partitioning in a biofilm (B).

(A) A benthic biofilm is composed of microalgae, predominantly of diatoms, and together with bacteria are enclosed in extrapolymeric substances (EPS). The microhabitat can experience an array of fluctuating conditions. Figure from Battin *et al.* 2016⁴⁹, Copyright under the Creative Commons Attribution License. (B) A cross section of a benthic biofilm with cells distributed according to their niche. (1) Some sediment particles on the upperstory can be inhabited by stalked and adnate-forms of raphid diatoms that are both sessile. (2) The rest of the upperstory is composed of epipellic and episammic motile biraphids primarily *Navicula sp.* and *Nitzschia sp.* The species-specific timing of vertical migration recycles the composition of cells in the upperstory. (3) In the underlying understory, smaller cells, primarily episammic pennates form a mat. (4) A close-up of the sediment grain shows that both motile, sessile, and relatively sessile taxa co-exist. Figure from Pringle 1990⁵⁰, Copyright License No. 4153680429032.

A requirement for biofilm development is the formation of a ‘conditioning film’ on a submerged substrate through adsorption of organic molecules from the overlying water. The ‘conditioning film’ alters the surface properties and attracts bacteria as initial colonizers. Bacteria can actively select suitable surfaces and can employ a variety of adhesion mechanism, depending on the surface energy and chemistry, through reversible attachment¹⁸. Once the bacteria fully shift to surface-associated growth, the physicochemical properties of the substrate are altered. It is hypothesized that settled bacteria produce sugars and sugar-like monomers which attract migration of diatoms and presumably other microalgae^{18,26}.

Benthic diatoms on biofilms can have densities of 10^5 – 10^7 cells cm⁻³ depending on sediment properties, location, and season³⁷. They also exhibit different spatial distribution depending on the observation scale involved. On a microscale, the mean patch size for a microalgal community in a biofilm is 4–100 cm². On this scale, organism aggregations are homogeneous, showing self-similarity spatially, thus implying that there is also the homogeneous distribution of physical and chemical factors^{51,52}. Collectively, the cm-scale patches form random-mosaic patterns, which, when viewed on a larger scale, shows that diatom distribution is heterogenous. There is a fractal spatial distribution of diatoms in a biofilm; the smaller patches have a high degree of self-similarity, but larger scale observations are highly variable⁵². On a microscale, interspecific interactions are responsible for patch formation; whereas, abiotic conditions like tidal currents, wave action, or resources are prevailing factors for large-scale distribution^{51,52}. However, these observations are made through integrating vertical core measurements, making the assumptions applicable only for the horizontal aspect of biofilms. Vertical variability is high in this habitat, with the top layers of the sediments experiencing a region of strong and steep gradients of irradiance, water velocity, pH, oxygen (O₂), sulphide (H₂S), and nutrients that are also temporally and spatially dependent^{37,40,53–55 56} (Fig. 6).

The observed self-similarity in between the microscale patches can arise from niche partitioning of different diatom growth types (Fig. 5B). Biofilm community studies that focus on species succession and response to nutrient addition confirm the grouping of diatoms based on their adaptive physiological and behavioural traits^{50,57}. Those that typically inhabit biofilms are either epipelic or epipsammic pennates. Epipelic diatoms are large raphid pennates (>10 µm) that are highly motile and can move freely between sediment particles of mudflats. Whereas, epipsammic diatoms (<10 µm) are either attached to sediment particles or can freely move in between the particles of sand flats, and can be comprised of both araphid and raphid pennates, and centric diatoms^{37,58}. Non-motile epipsammic pennates are considered part of the low profile guild diatoms that can withstand low nutrient and light levels. They are positioned in the low disturbance part of the biofilm, which is the understory. Their growth can be stimulated by nutrient addition, but this could also attract motile epipsammic and epipelic diatoms to form thick mats and dominate the upperstory of a forming biofilm. Thus, the motile guild of pennates is considered free of resource and disturbance stress as they have

the capability to position themselves to better environments^{50,57} (Fig. 5B). There are also some epipsammic pennates that can inhabit the upperstory of a biofilm by having physiological photoprotective mechanisms rather than behavioural motility^{58,59}.

Organisms within the biofilms experience an array of complex and fluctuating conditions on both micro- and/or mesoscale. They are constantly exposed to fluctuating conditions such as wave and tide action, UV radiation, temperature and salinity variations, desiccation, and nutrient availability^{38,60}. The EPS produced by diatoms act as a matrix to neutralize the effects of daily fluctuating conditions, making the biofilm a relatively protective microhabitat³⁹. However, resource variability and microbe-microbe interactions within the biofilm are still a complicated landscape that diatoms have to interact with. Bacteria are essential components and partners of diatoms in a biofilm, and their relationship can range from synergistic, competitive, or parasitic⁶¹. Diatom-diatom interaction can also lead to one species dominating a biofilm⁵¹. For example, allelopathic interactions in diatoms have been reported through the use of light-activated production of cyanogen bromide (BrCN). Briefly, the benthic diatom *Nitzschia cf. pellucida* can release BrCN that can cause chloroplast bleaching of other diatoms shortly after sunrise, which highlights the coupled mechanism of BrCN production to vertical migration⁶².

The ability to migrate is often perceived as an adaptive behaviour towards fluctuating conditions in the biofilm, nutrient foraging, and stress avoidance^{38,50,63-66}. One remarkable example of the motile behaviour of diatoms is their vertical migration which increases survival of cells against burial and erosion^{64,67}. The photic depth in the substrata is shallow as light is easily dissipated within this material. Specifically, only 1% of light attenuation can pass through 0.1–13 mm, depending on the sediment's properties³⁷. Raphids need to migrate to the surface to gain energy through photosynthesis coinciding with a diurnal cycle. Cells reach the surface of the sediment a few hours before sunrise and form an intense peak a few hours after sunrise^{40,64,67,68}. Both phototaxis and gravitaxis play a role in vertical migration. The upward migration during the daytime, where cells are attracted to specific irradiance intensities throughout the day, is a positive phototactic behaviour. For example, during the early morning, small naviculoids and nitzschiods are in the upperstory. Some large cells (*i.e.* *Pleurosigma* sp.) migrate up when the ambient light levels increase while the smaller cells migrate down⁶⁹. However, this phototactic response can be combined with a negative photokinetic mechanism characterized by cells speeding up as fluence rate decreases, helping cells to disperse^{70,71}. However, when cells are in prolonged darkness, gravitaxis prevails wherein the upward migration is a negative gravitactic behaviour synchronized with diurnal or semi-diurnal tidal cycle. Gravitaxis occurs before phototaxis as cells can be observed moving up in the photic zone before sunrise^{72,73}. After accumulating carbon reserves and before tidal submersion, cells migrate downward. On the deep layers of the sediment, both nutrient uptake and cell cycle dynamics occur⁴⁰.

Vertical migration is a circadian response since cells exposed in continuous darkness still exhibit migratory behaviour^{64,67}. Additionally, in some communities, exogenous factors such as tidal

cycles and the length of day:night can control light attenuation and temperature, hence, affect the innate behaviour^{68,74}. For example, migrating down before tidal immersion can be a survival mechanism against physical disturbance which can wash away cells⁶⁴. Interestingly, raphids have taxon-specific rhythms and can micro-migrate leading to niche segregation^{66,69} and daily cycling of cells in the upperstory of a benthic mat⁶⁹. On a community level, this behaviour may result in a constant productivity of a biofilm since there is always a diatom taxon migrating towards the surface to photosynthesize^{66,69}.

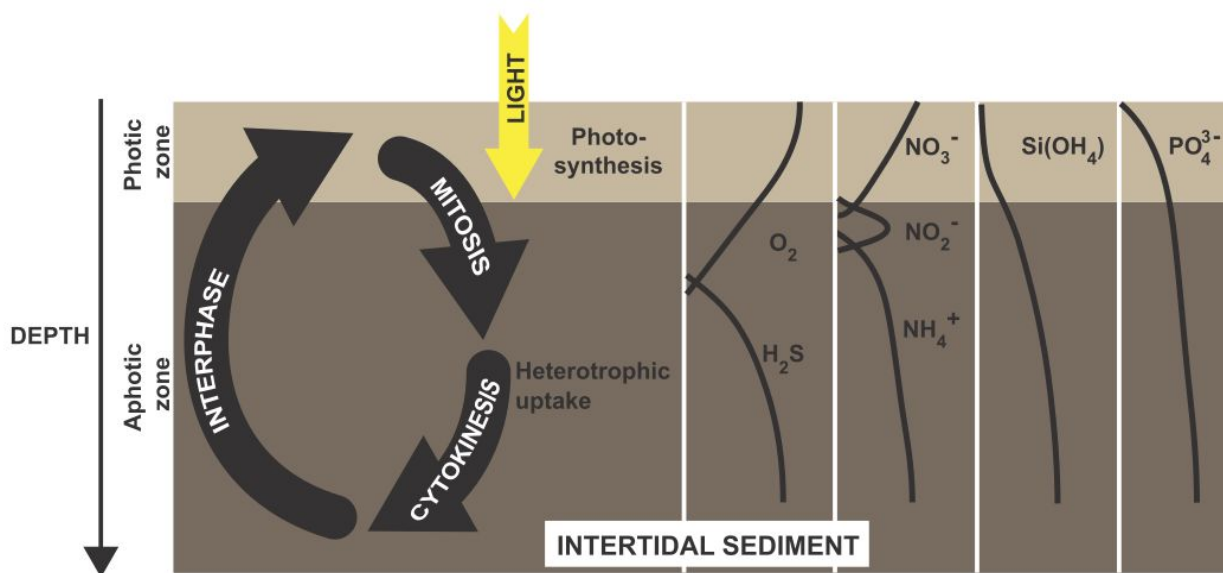


Figure 6. The activity of epipelagic diatoms and the vertical distribution of environmental factors within the biofilm.

The intertidal sediment that biofilms inhabit is divided into two zones: the photic and aphotic zones. Vertical migration aids diatoms to shuffle between these two zones and undergo growth and division. Nutrient concentrations can vary with depth. Adapted and redrawn from Saburova and Polikaprov⁴⁰.

The aphotic regions of the sediment are also anoxic zones containing rich sinks of inorganic nutrient on their reduced form. Benthic diatoms are known to uptake these nutrients supported by vertical migration^{55,56,75}. Nitrogen in the form of nitrate (NO_3^-) and ammonium (NH_4^+) are both taken up by biraphids, and can result in increased density for individual cell experiments, as well as community studies^{50,76-81}. However, NH_4^+ is preferred even if NO_3^- (both forms termed as dN unless specified) is present⁸². NH_4^+ can be directly used for amino acid biosynthesis⁷⁶. However, high NH_4^+ concentrations (~0.5 mM) can be harmful to benthic algae, especially when combined with high pH and irradiance⁸³. Phosphorus is also a crucial nutrient for diatom growth. It exists only in one inorganic form, orthophosphate (PO_4^{3-} , in the following termed as dP). Studies on planktonic algae showed that each P atom could be cycled only twice before it is deposited on the sea bed⁵⁵. Unique to other algae, diatoms also require silicon. Soluble inorganic silicate exists as the monomers $Si(OH)_4$ (in the following

termed as dSi) and SiO_4H_3^- , with the former being the most common form (~95%) and the preferred monomer for uptake, although polymerized versions could also exist^{84,85}. For planktonic diatoms, a Si atom can be incorporated into the frustule and recycled back to the marine system 40 times before being buried in the deep sea and sediment⁸⁵. All of these inorganic nutrients exists in gradients in the benthic environment, with NH_4^+ , dP, and dSi being highly correlated to each other because all of them exhibit an increase of concentration with sediment depth. On the other hand, NO_3^- and NO_2^- have decreased concentration with depth because of denitrification processes^{53,54,56} (Fig. 6). Overall, the concentration in the porewater and sediment of all the inorganic nutrients is always higher than what is found in the overlying water⁵³⁻⁵⁶. Sediment porewater concentrations of dP, dSi, NO_3^- and NO_2^- were one order of magnitude greater than in the overlying water while NH_4^+ concentration was two orders of magnitude higher^{53,54}. The concentration range for nutrients in the benthos depending on season are 70–900 μM NH_4^+ , 0–200 μM dP, 20–380 μM dSi, and 0.20–20 μM NO_3^- and NO_2^- ⁵³.

Photosynthetic and respiratory processes can change pH and oxygen distribution in a depth-dependent manner (Fig. 6). The shift of oxic and anoxic conditions relative to day:night and tidal cycles can affect the distribution of nutrients, pointing to a combined temporal and spatial variation. Anoxic conditions due to increased respiratory processes during emersion periods and night/darkness can trigger remineralization of nutrients from the sediment layers, particularly silicate and phosphate^{45,86-89}. On the other hand, inorganic nitrogen concentrations in the sediment are controlled by nitrification and denitrification processes, and concentration of nitrogen in the water column^{88,89}.

Because of exclusive access to rich sources, benthic diatoms can control nutrient fluxes across the sediment-water interface and hence can indirectly affect the productivity of planktonic diatoms^{45,46,50,86,90}. Of all the three nutrients, dSi is strongly influenced by benthic diatoms, as they consume it rapidly, thus lowering outflux from the sediment. This can shift species composition by inducing the growth of non-siliceous organisms, thereby increasing chances of harmful algal blooms^{45,90,91}. The outflux of silicate is temperature-dependent. At higher temperatures, there is a greater dissolution of silicate from particulate mineral sources, and the uptake of benthic diatoms is negligible since there is enough dSi outflux to the water column. However, at a lower temperature (<20°C) there is lower dissolution and diffusion rates, thereby uptake controls the outflux⁴⁵.

Downward vertical migration towards a more stable and nutrient-rich environment can also provide a better condition for growth and cell division since the surface layer would be exposed to more fluctuating conditions that can be stressful for the cell⁴⁰ (Fig. 6). Before cells commit to cell division, enough nutrients for cell growth should be already accumulated within the cell. Since pennates undergo girdle-to-valve relocation of chloroplasts before the G1-phase (i.e., silica biomineralization phase), the raphe is blocked and movement is inhibited⁹². In biofilms, mitotically-dividing cells can be exclusively found in the aphotic anoxic zone of the sediment, and their density correlates with increasing depth⁴⁰. Sexual reproduction in the sediments can be more complicated

than vegetative growth since mating types should be able to find each other in a diverse microenvironment filled with co-occurring signals. Additionally, migration should also be suspended once cells start sexual reproduction⁹³. Pheromone-mediated sexual reproduction might aid in increasing search efficiency and pairing³³ before cells commit to meiosis.

1.3 From small-scale to large-scale processes: Bigger impacts of behaviour

1.3.1 Behaviour

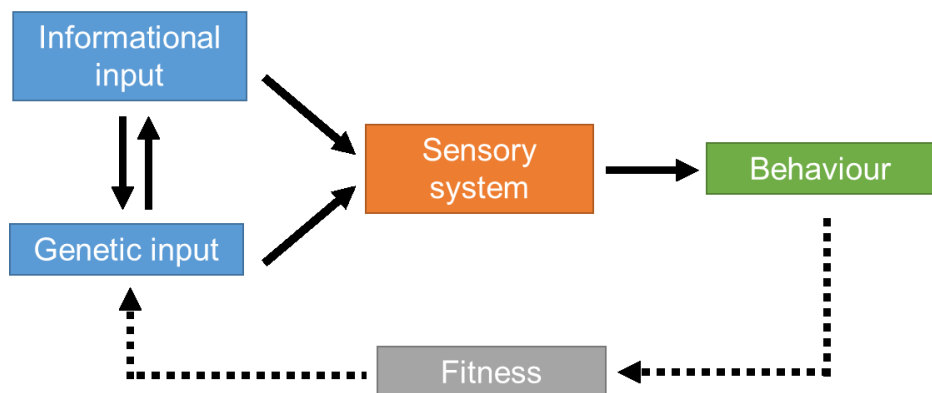


Figure 7. Schematic diagram of fundamental processes affecting behaviour.

Behaviour is influenced by both genetic and informational inputs that constantly interact with each other. While the genetic factor defines the sensory system of an organism, the informational input provides data on the abiotic and biotic environmental setting. After the sensory system processing, the output is a behaviour which could potentially increase the fitness of the organism. Behavioural adaptations in response to specific stimuli can be retained through evolution. Solid lines indicate direct relationship while dashed lines indicate a probable effect.

The behaviour of an organism can be defined as ‘internally coordinated responses (actions or inactions) of whole living organisms (individuals or groups) to internal and/or external stimuli, excluding responses more easily understood as developmental changes’⁹⁴. The behavioural capacity of an organism is imprinted on its genome. The genetic input provides the organism a sensory system consisted by defined sensing mechanism, processing abilities, and motor skills. However, an organism can only respond depending on the degree of environmental input received and its interaction to the physiology of the organism, which is in turn defined by the genome. Informational input provides data about the environmental setting, in the form of abiotic and biotic factors ranging from environmental (*e.g.* temperature, light, turbulence) to cell–cell interactions and chemical signals released by conspecifics or heterospecifics, respectively. The received information act as stimuli which can trigger the sensory system of an organism. When the produced behaviour increases the fitness of the population, it could be retained as an adaptive trait throughout evolution and can be used to predict the behaviour of the organism (Fig. 7)^{95,96}. As an example, the previously described vertical migration of benthic diatoms is an endogenous trait inscribed in the genome^{64,67,68,74}. However, a constant

informational input of light fluence is needed by a diatom to locate parts of the sediment precisely⁶⁹. Migration then is both a product of genetic and environmental that controls the sensory systems of the diatom and ultimately the behaviour.

1.3.2 Investigations in motility

The searching behaviour of motile organisms is among the well-studied and common types of behaviour, particularly in animal ecology^{95,96}. Searching behaviour is defined as active motility of an individual or group towards resources, whether foraging for food, finding a mate, avoiding stress or predators, or settling in a new habitat⁹⁵. In the last decade, studies on motility shifted to focus on microbial systems, as microbial motility not only affect the organism's interaction with diverse environmental or chemical stimuli or cell-cell interactions. It can also affect large-scale processes such as biogeochemical cycling and primary productivity⁹⁷⁻¹⁰⁰. However, defining a useful scale to observe microbial motility, and the technical constraints that come with it are challenging. With the advent of single-cell technologies, mimicking the complex environment of microbes and observing their searching behaviour became possible^{97,98,100-110}.

Capillary assays (Fig. 8A) were initially used to estimate chemoattraction in bacteria. A capillary tube containing a chemoattractant is exposed to a bacterial suspension for a given period. Afterwards, the capillary tube is removed, and the attracted bacteria are plated for colony counting^{111,112}. At the same period, the swarming plate technique (Fig. 8B) was developed wherein chemotactic bacteria are inoculated in semisolid agar. The middle of the plate contains a chemoattractant. Attracted bacteria form rings or bands upon metabolizing the chemoattractant. The degree of chemoattraction can be estimated through the relationship of the radius of the ring and the cell density¹¹³. These two techniques can be used to determine the level of attraction towards gradients of specific compounds. However, they cannot provide mechanistic information on chemoattraction. To elucidate individual cell dynamics of amino acid chemotaxis in *Escherichia coli*, Berg¹¹⁴ developed a tracking microscope which can automatically focus on a single motile cell in 3D. The technique allows recording of a complete cell trajectory which is crucial for calculating motility parameters such as speed, angular direction, and run length. In combination with tracking, Berg and Brown¹¹⁵ also utilized the capillary assay to describe the kinematic behaviour of *E. coli* cells towards chemoattractant gradients. Currently, the use of both high-performance microscopy and automated tracking is a common method for analysing motility of microbes^{97,100,102-104,116}. Tracking particles or cells is crucial for motility studies that are often used in combination with microfluidics or micro-particle image velocimetry (micro-PIV)⁹⁷. Most tracking programs have specific algorithms for cell/particle detection, linking between frames, and frequently also visualization and analysis tools for track analysis¹¹⁷ (see Chenouard *et al.*¹¹⁸ and Meijering *et al.*¹¹⁹ for a comprehensive review of available programs). As cell

tracks alone only offers qualitative observations, mathematical and statistical modelling are used to elucidate fine-scale patterns of behaviour in microorganisms^{100,103,104,107,116}. Another technique often used for motility studies is micro-PIV (Fig. 8C) which can give the hydrodynamic signature of a cell based on tracking the fluid movement around it. Tracer particles (0.2–1.0 µm diameter) are seeded into the fluid containing the motile organism, and the movement of the particles are tracked. The speed and direction of the particles provide information to calculate the hydrodynamic signature of moving cells.⁹⁷. For example, *E.coli* has a pusher mechanism for swimming, wherein the flagella push the fluid away from the organism, and then retrieve back from the side¹²⁰. Alternatively, cells can be pullers, wherein the flagella pull the cell as it moves through the fluid. The hydrodynamic signature of microorganisms can affect the viscosity of the fluid medium. In turn, the transportation of chemicals in and out of the cell, as well as the interaction of the moving cell to its physical environment or the cells around it could be affected⁹⁷.

The challenge for microscale behaviour analysis is the integration of realistic environments in experimental assays. At a microscale, most useful resources such as nutrients occur as heterogeneous, patchy, or ephemeral hotspots in dynamic environments. In the marine pelagic environment, this is complicated by the existence of turbulence and physical gradients; thus, motility is a beneficial trait to thrive¹⁰¹. In the last decade, microfluidics as a tool in microbial ecology has emerged. Microfluidics is a technique wherein a set of microchannels are etched in elastic polymeric materials like polydimethylsiloxane (PDMS) (Fig. 8D). The concept is similar to capillary assays, wherein individual channels can contain a chemoattractant source. However, there is a fine control of flow, concentration gradients, and surface chemistry which can aid in mimicking natural environments^{97,121}. A model hotspot for bacterial communities is the phycosphere, an area surrounding an algal cell that is a rich source of DOM and oxygen^{107,122}. Elucidating the role of the phycosphere on bacterial behaviour has been a challenge for microbiologists, oceanographers, and physicists. While capillary assays led to the speculation of a chemotactic behaviour of attracted bacteria towards algal exudates, microfluidics highlighted how cells could sense and actively move towards slowly diffusing DOM patches, and live-cell imaging confirmed the active behaviour towards lysing and living algae. Microfluidics helped in elucidating fine-scale processes such as moving kinematics, which consequently reshaped our understanding of microscale behaviour^{95,103,104,106,107}.

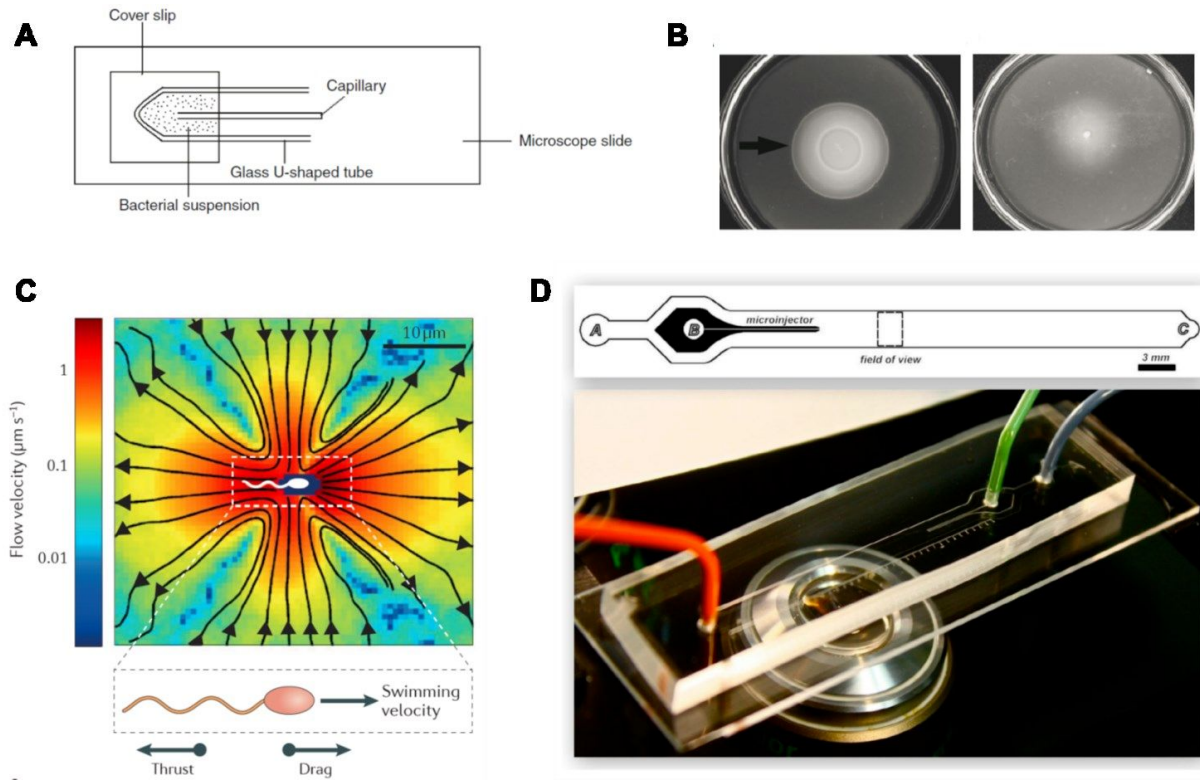


Figure 8. Methods in analysing motility in microbial systems.

(A) The capillary assay is the most traditional set-up for chemotactic assay. The set-up by Adler¹¹² is simple as it only consisted of a microscope slide containing the bacterial community in a liquid medium and covered with a cover slip. The reservoir of the liquid medium is maintained using a glass U-shaped tube. The capillary containing a chemoattractant is loaded inside a capillary tube and placed in the bacteria. The chemoattraction can also be viewed under the microscope. **(B)** The swarming plate assay utilizes soft agar wherein inoculated bacteria can move towards the chemoattractant seeded in the middle of the plate. The arrow on left photo showed the formation of chemotactic rings whereas the right photo showed bacterial growth but no chemotaxis. Figures 8A and 8B are taken from Miller *et al.*¹²³, Copyright License No. 4171411174809. **(C)** The flow field of a swimming *Escherichia coli* generated by micro-particle image velocimetry (micro-PIV). The flow velocities of the particles provide the hydrodynamic signature of a moving cell, whichss could show how cells move. For example, *E. coli* here has a pusher mechanism wherein the flagella can push the surrounding medium while moving. Figure from Son *et al.*⁹⁷, Copyright License No. 4171421096860. **(D)** A microfluidics set-up from Seymour *et al.* 2010. The top panel is the schematic of the bottom panel set-up. Inlet A (blue tubing) injects the microorganism, inlet B (green tubing) injects a chemoattractant, while C is the outlet (orange tubing). Microbial behaviour can be observed under the microscope in the dashed rectangle area. Figure from Seymour *et al.*¹⁰², Copyright License No. 4171460644959.

The effect of microscale behaviour to large-scale processes such as ecosystem dynamics and biogeochemical cycling is often overlooked. A recent study of microbial chemotaxis towards the phycosphere provided a combined approach to connect these processes to a numerical model. The model shows that while non-motile bacteria thrive better in oligotrophic conditions, they can be out-competed by non-motile cells during bloom and collapse events¹⁰³. This study highlighted resource partitioning and competition in a microscale which are significant factors for trophodynamics in the oceans^{103,124}. On the other hand, biogeochemical cycling can be mediated by interactions and heterotrophic consumption of microorganisms. For example, the cycling of sulphur can be affected by the chemoattraction and utilization of a wide range of microorganisms towards dimethylsulfoniopropionate (DMSP). DMSP is produced by planktonic organisms, plants, and corals and has

osmoprotective, cryoprotective, and antioxidative properties for the organism-producer¹²⁵⁻¹²⁷. Pulses of DMSP induce chemotactic behaviour in both bacteria and planktonic algae, highlighting a specific ecological role that this compound has for different microbial groups. The dinoflagellate *Oxyrrhis marina* strongly responded to DMSP pulses compared to the other microbes, and it was inferred that this substance is used as a cue for prey location¹⁰². The foraging behaviour of microbes toward DSMP is a crucial factor for the release of dimethyl sulphide (DMS) which is an essential link between cloud formation and climate^{99,102,128,129}.

In the benthic zone, microscale processes can potentially control the outflux of some nutrients from the sediment to the water column^{45,46,50,86,90,108,110}. However, compared to planktonic environments, the heterogeneity of chemical signals is formed in one-dimension rather than three-dimensions as they extend primarily vertically^{60,96,99} (Fig. 6). Benthic microbes can also actively respond to these gradients through vertical migration. For example, *Thioploca* sp., a giant bacteria (~60 µm long) living in the sediments can exhibit chemotaxis to nitrate and sulphide by migrating between the nitrate-rich overlying water and sulphide-containing sediment¹⁰⁹. It can glide with a speed of 1.5 µm s⁻¹ by forming sheaths of excreted slime trails¹¹⁰. Extensive mats of this chemotactic bacteria can control both nitrogen and sulphur cycling in the sediment¹⁰⁸. While the foraging mechanism of bacteria in the benthos are well-studied, those for diatoms are not. As stated beforehand, most studies on diatom migration are limited to the effect of light, diel, and tidal cycles^{24,25,64,67-69,72-74}, but not on the effect of the patchy distribution of resource gradients, as well as conspecific interactions. The model pennate diatom *Phaeodactylum tricornutum* can sense its environment through Ca²⁺ signalling and allows it to perceive and respond to variability in turbulence, osmotic stress, and dissolved iron levels. Diatoms then can rapidly deal with environmental signals within a matter of seconds¹³⁰. In an environment where there are transient and co-occurring signals, rapid stimuli perception and subsequent behavioural adaptations could aid survival for a benthic diatom. Their collective behaviour could potentially further explain their ability to control nutrient fluxes in the sediment.

2 SCOPE OF THE STUDY

The general aim of this thesis is to provide comprehensive knowledge on how benthic diatoms respond to different chemical and environmental signals, and how they prioritize between co-occurring signals. On this thesis, I focus on two dominant factors over the life phases of diatoms, nutrient and mating partner availability.

Most studies on the effect of nutrient stress focused on the two prominent model diatoms, the centric *Thalassiosira sp.* and pennate *Phaeodactylum tricornutum*, with the latter not having a strict requirement for silicate^{30,131-139}. The use of -omics techniques, which paved ways to understand how cells physiologically respond to such scenarios^{133-136,139,140}. On the other hand, research on benthic biofilms are community-based and concentrates on the effect of nutrient addition, vertical migration due to light and tides, and niche partitioning^{24, 25, 50, 57, 64, 67-70, 73, 74}. It is during the last 20 years where model systems that can be controlled in the laboratory emerged for life cycle studies^{27,31,34-36,92,141-143}. On the other hand, pheromone-mediated sexual behaviour in diatoms is quite new, while there are extensive studies for brown macroalgae with emphasis on pheromone structure, function, and biosynthesis as well as the mechanism of its effect on the motility of gametes¹⁴⁴⁻¹⁴⁷. Although behavioural studies seem to be elementary, only a few studies exist on the external factors that can regulate behaviour in ^{19,20,24-26,32,34,71,130}, and with that, only one focused on resources²⁶ and two on mating in araphid pennates^{32,34}. With the advent of single-cell imaging, there has been a significant influx on behavioural studies of microorganisms and how their collective motility towards specific resources can affect elemental cycling^{97,98,100-110}.

Since benthic diatoms thrive in a complex microhabitat, determining their behaviour could give insights on how they perform in cases where nutrients are limiting, or there is a sexual pressure. The collective microscale behavioural processes of benthic diatoms could potentially explain the spatial and temporal structuring of biofilms. As significant primary producers in the ecosystem, understanding their behaviour could give hints on processes that are often overlooked in biogeochemical models.

Herein, I analyze the behavioural motility across the life cycle of an emerging model benthic raphid, *Seminavis robusta*; consequently, this study provides the first insight on the preferential attraction in different life stages of a microbe. *S. robusta* is chosen as an established pedigree exists³¹, its life cycle and pheromone-mediated mating are well-studied^{33,36,92,141}, and strains in both vegetative and sexual sizes are available. Large-sized vegetative cells (>50 µm) and two sexual states of the cells

with varying sizes (medium: ~40 µm, small: 24–27 µm) are used depending on experimental conditions.

On this work, I use hotspot sources of chemical signals by utilizing specific beads that adsorbed dissolved nutrients (neutral aluminium oxide beads) or the pheromone diproline (hydrophilic-lipophilic balance solid phase extraction beads). Upon medium contact, beads release the stimuli and form steep gradients that could elicit attraction. Attraction assays are done by exposing either nutrient-starved or sexually-induced cells to stimuli beads, and subsequent video monitoring. I develop and optimize cell tracking and statistical modelling procedures to uncover specific movement patterns of *S. robusta*.

Due to the patchy distribution of nutrients, diatoms are continually challenged to locate resources for their growth. I test predominant macronutrients that are often limiting for benthic diatoms – dissolved nitrogen (in NO_3^- and NH_4^+ forms, both termed as dN), phosphate (dP), and silicate (dSi) (**Publications A and C**). I determine their utilization of resources over a growth period, as well as their response to limitation and re-supplementation scenarios. Starved cells are exposed to individual nutrient beads, and cell motility patterns are characterized. I delve more into the specificity of dSi chemoattraction by comparing the response of dSi-starved cells to that of structurally-related dissolved germanium dioxide (dGe). Moreover, I verify the consistency of dSi attraction in different life phases of *S. robusta* and another species of benthic diatom (*Navicula sp.*) (**Publication A**).

I also determine how sexual MT^+ cells locate MT^- cells. I utilize the bioassay developed by Gillard *et al.*³³ by exposing MT^+ to diproline-loaded beads (**Publication B**). The response of the two sizes of sexual stage cells is also evaluated to determine effects of sexual pressure to cell behaviour. Additionally, I verify the prioritization mechanisms of cells through *in silico* comparisons of dSi and diproline attraction (**Publications B and C**).

To experimentally evaluate the decision-making mechanism of cells when faced with co-occurring signals, such as nutrient and mate cues, I design an experimental-set up with varying combinations of dSi starvation and sexual priming. One-bead experiments (dSi or diproline) are performed on cells that recently crossed the sexual size (medium-sized cells) and critically small-sized cells. To further verify the prioritization mechanism of small-sized cells, choice assays between dSi and diproline are done (**Publication C**). The cross-talk between these two signals have significant implications not just for motility control but also for clonal growth and survival in their natural environment.

Finally, an overall discussion of the three publications is provided, together with the description of the possible cascades of this microscale behaviour to the ecology of biofilms and global biogeochemistry. Perspectives for the future direction of research are also provided.

3 PUBLICATIONS

3.1 Publication A

Bondoc, K. G. V., Heuschele, J., Gillard, J., Vyverman, W. & Pohnert, G. Selective silicate-directed motility in diatoms. *Nature Communications* 7, 10540 (2016), doi: 10.1038/ncomms10540.

Summary: Diatoms are ubiquitous microalgae frequently dominating biofilms in intertidal sediments. Ephemeral, local hotspots of nutrients are among the factors affecting the patchy distribution of biofilm communities on a microscale. Dissolved silicate (dSi) is an essential inorganic nutrient for the construction of the diatom's cell wall; hence, dSi limitation of this nutrient can affect ecosystem productivity. In this study, we explored the behaviour and motility patterns of a marine benthic diatom *Seminavis robusta* towards a dSi-loaded bead as a hotspot nutrient source. Motility and speed increased under dSi limitation, and when gradients of this resource are present, a combined tactic and kinetic mechanism towards the source is observed. Our results suggest that the motile behaviour of *S. robusta* increases its chance to detect and benefit from high nutrient micro-environments. The searching behaviour can potentially explain the patchy distribution of biofilms and has further implications for biogeochemical cycling.

Publication equivalents of contributing PhD students as coauthors according to the implementing provision of the doctoral regulations of the Faculty of Chemistry and Earth Sciences of the Friedrich Schiller University Jena

Author 1: Bondoc	
<i>Conception of the work</i>	X
<i>Planning of experiments</i>	X
<i>Data collection</i>	X
<i>Data analysis and interpretation</i>	X
<i>Manuscript writing</i>	X
<i>Proposed publication equivalents</i>	1

The supporting movies of this publication are available via the embedded compact disc.

This is an open access article distributed under the terms of the Creative Commons Attribution License.

ARTICLE

Received 8 Jun 2015 | Accepted 23 Dec 2015 | Published 4 Feb 2016

DOI: 10.1038/ncomms10540

OPEN

Selective silicate-directed motility in diatoms

Karen Grace V. Bondoc^{1,2}, Jan Heuschele^{3,4}, Jeroen Gillard^{5,6}, Wim Vyverman⁵ & Georg Pohnert^{1,2}

Diatoms are highly abundant unicellular algae that often dominate pelagic as well as benthic primary production in the oceans and inland waters. Being strictly dependent on silica to build their biomineralized cell walls, marine diatoms precipitate 240×10^{12} mol Si per year, which makes them the major sink in the global Si cycle. Dissolved silicic acid (dSi) availability frequently limits diatom productivity and influences species composition of communities. We show that benthic diatoms selectively perceive and behaviourally react to gradients of dSi. Cell speed increases under dSi-limited conditions in a chemokinetic response and, if gradients of this resource are present, increased directionality of cell movement promotes chemotaxis. The ability to exploit local and short-lived dSi hotspots using a specific search behaviour likely contributes to micro-scale patch dynamics in biofilm communities. On a global scale this behaviour might affect sediment-water dSi fluxes and biogeochemical cycling.

¹Institute for Inorganic and Analytical Chemistry, Bioorganic Analytics, Department of Chemistry and Earth Sciences, Friedrich-Schiller-Universität Jena, Lessingstrasse 8, D-07743 Jena, Germany. ²Max Planck Institute for Chemical Ecology, Max Planck Fellow, Hans-Knöll-Str. 8, D-07745 Jena, Germany. ³Centre for Ocean Life, National Institute of Aquatic Resources, Technical University of Denmark, Charlottenlund Slot, Jægersborg Allé, DK-2920 Charlottenlund, Denmark. ⁴Department of Biology, Aquatic Ecology Unit, Lund University, SE-22362 Lund, Sweden. ⁵Laboratory of Protistology and Aquatic Ecology, Department of Biology, University Gent, Krijgslaan 281, S8, 9000 Gent, Belgium. ⁶California State University, Department of Biology, 9001 Stockdale Hwy, Bakersfield, California 93311, USA. Correspondence and requests for materials should be addressed to W.V. (email: Wim.Vyverman@ugent.be) or to G.P. (email: Georg.Pohnert@uni-jena.de).

Diatoms contribute about 20% to the global primary production and are key players in marine and freshwater benthic and planktonic communities¹. A hallmark of diatom physiology is their biomineralized cell wall that is formed by template-catalysed precipitation of silicic acid². Given their vast abundance, diatoms are thereby driving the silicate cycle^{3,4}. Dissolved silicic acid (dSi) availability is often the limiting factor controlling diatom growth and thus also shaping species composition in marine communities⁵. While the pelagic zone is often dSi-limited below 1 μM, the benthic zone typically shows strong and steep gradients of this resource with higher dSi concentrations (around 150 μM) in the sediment due to the continuous dissolution of deposited minerals⁶. Because of their high productivity and biomineralization activity, benthic diatom biofilms can influence sediment properties⁷ and alter dSi fluxes within the sediment–water interface, thus regulating dSi concentrations in the oceans⁸. Such processes have implications for the transfer of energy to higher trophic levels, benthopelagic coupling and hence population and ecosystem productivity⁴. Most benthic diatoms belong to the pennates, comprising the youngest (90 Myr old) yet most species-rich clade within the diatoms^{9,10}. Many species evolved a strong capacity for vertical migration in sediments under the control of photoperiod and/or tidal cycles¹¹. However, these processes alone are not fully explaining observed spatiotemporal dynamics of microbial biofilms, and since many years other factors including the direct and indirect influence of herbivory and microbe–microbe interactions are assumed to guide diatom movement^{11–13}. Here we identify an additional guiding factor by showing that diatoms detect and actively move towards dSi sources.

We used the pennate diatom *Seminavis robusta* to explore cell movement and aggregation in response to dSi. Like many other pennate diatoms, this biofilm-forming species moves by gliding through the excretion of extracellular polymeric substances from its raphe, an elongate slit in the cell wall¹⁴. This allows pennate diatoms to move back and forth. Observed turning movements were suggested to result from the action of extracellular polymeric substance-derived pseudopods or stalks. When a pseudopod or stalk is adhering to the substratum resulting torque supports the whole-cell rotation¹⁵. In this contribution, we describe three sets of experiments where we first look at the general influence of dSi concentration on diatom motility, then we observe and analyse diatom behaviour in a dSi gradient and last, we test the specificity of the response by comparing the reaction towards dSi and dGe gradients. These experiments clearly demonstrate that diatoms have means to selectively perceive and orient towards the essential resource dSi. A search behaviour in form of increased cell motility and cell speed is observed when the nutrient dSi is depleted. The unicellular algae are also capable of directional movement towards the sources of dSi gradients, a behaviour that supports foraging in the patchy natural environment of benthic diatoms. The fact that structurally closely related dissolved germanium dioxide (Ge(OH)_4 , dGe) sources are not eliciting attraction suggests a specific receptor-mediated response.

Results

dSi-dependent diatom motility and speed. To determine if dSi availability affects cell behaviour, we counted motile cells in conjunction with dSi depletion in batch cultures. The proportion of motile cells steeply increased along with decreasing dSi availability as cells entered the stationary growth phase (Fig. 1a). Addition of dSi (106 μM) to stationary-phase cultures elicited within 1 h a marked drop in the proportion of motile cells, indicating a reversible reaction controlled by dSi (Fig. 1b). In addition to motility, cell speed is also dependent on dSi

concentration. When stationary-phase *S. robusta* cultures were transferred to artificial sea water without added dSi (low-dSi medium) and were further starved for 3 days, cell movement was more than twice as fast than that of cells transferred to dSi-rich control medium (Fig. 1c). Moreover, cell speed decreased after 1 h of dSi addition while blank addition did not affect the speed. The observed increased proportion of motile cells and higher speed under limiting conditions is a chemokinetic response, that is, a motile response to chemicals. Since dSi is not required for movement, speeding up is an effective mechanism for fast location of this limiting resource during starvation^{16,17}.

Directed movement towards dSi sources. Since steep vertical and horizontal dSi gradients prevail in benthic environments, an additional strategy to exploit this resource would be a directed movement within dSi gradients. Requirements for such a behaviour are the cells' ability to perceive the resource in a quantitative manner, as described above, and a directed movement towards it. Track analysis revealed that *S. robusta* moves in a back and forth manner that enables cells to reverse direction after each stop (Supplementary Movie 1). This behaviour found in many raphid diatoms and in certain bacteria allows for orientation towards higher concentrations in chemical gradients^{18,19}. *S. robusta* thus fulfils both above-mentioned requirements for a directed movement. We therefore verified if it indeed has the capability of chemotaxis that would lead to the accumulation of Si-starved cells at local dSi hotspots. Gradients of dSi were generated from micrometer-sized point sources in form of aluminium oxide (alox) beads that were loaded with dSi in different concentrations. To analyse movement along the dSi concentration gradient, the microscopic observation area was divided into three bins (A–C) of equidistant concentric rings around each observed bead covering a radius of 336 μm (Fig. 2a). Since a directed orientation would likely be most relevant under low dSi concentrations found at the water–sediment interface, we aimed to adjust the local concentration gradient in this range. If 1.4 nmol dSi per microscopic bead were applied, ca. 5% diffused out within the 600 s assay period. In a matter of ~460 s a concentration gradient is established with ~100 μM dSi at the surface of the bead decreasing to ~5 μM dSi at the edges of the microscopic observation field (Supplementary Fig. 1). This concentration gradient mimics conditions at the transition of the pelagic and benthic zones⁶. Si-starved *S. robusta* responded to such dSi gradients with an accumulation of cells around the beads while control beads were not attractive (Fig. 2). This behavioural response is observed in different *S. robusta* isolates (Supplementary Movies 2–5). If the observation period is extended to 1 h, continuous movement of cells towards the bead is observed until ~25 min. After that, chemoattraction becomes less obvious, presumably due to diffusion of dSi. Control beads are not active through the entire assay period (Supplementary Movies 2 and 4). Response to dSi is not limited to *S. robusta*, since *Navicula* sp., another benthic diatom, also accumulated around dSi sources (Supplementary Movie 6). The administered dSi concentration is in the optimum range to elicit a response. Attraction became less pronounced if lower concentrations of dSi were administered, higher concentrations still resulted in a substantial accumulation around the beads but data became noisier, indicating a more erratic search (Supplementary Fig. 2). Such a concentration-dependent response is typical for receptor-mediated interactions, since higher concentrations of dSi on the beads might cause receptor saturation, whereas lower concentrations fall below the detection limit²⁰. The finding capability is thus most efficient in an environmentally relevant concentration range.

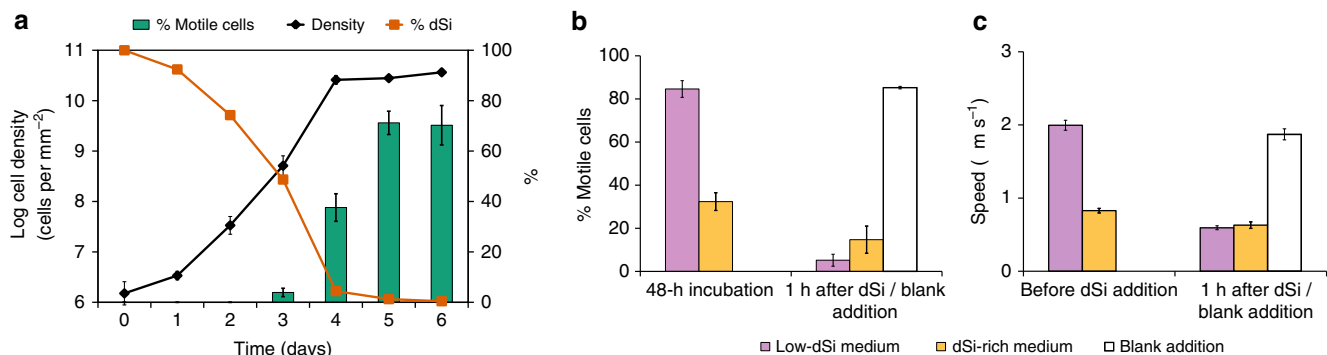


Figure 1 | Seminavis robusta cell motility is modulated by environmental silicic acid concentrations. (a) During silicon (Si)-limited batch culture growth, cell motility increases while dSi (100% dSi = 106 µM) is being depleted and the culture enters stationary phase. Error bars show the s.e.m. of five replicates ($n=300$). (b) There is a higher percentage of motile cells in low-Si medium than Si-rich medium (one-way analysis of variance (ANOVA), $n=5$, $P<0.001$). After addition of dSi (106 µM) to 48-h silicon-starved cultures, cell motility drops within 1h (one-way ANOVA, $n=3$, $P<0.0001$). This is not the case after a blank addition of sea water to such silicon-starved cultures ($P=1.00$). Error bars show s.e.m. of three replicates. (c) The mean cell speed is significantly higher (LME with Tukey's honest significance difference (HSD) test, $n=70\text{--}200$ cells per movie, three movies analysed, $P<0.0001$) in cultures grown in low-dSi medium compared with dSi-rich medium (dSi = 246 µM). One hour after the addition of dSi to starved cultures, cell speed significantly dropped (LME with Tukey's HSD, $n=70\text{--}200$ cells per movie, three movies analysed, $P<0.0001$) while blank addition did not induce any change on cell behaviour (LME with Tukey's HSD, $n=70\text{--}200$ cells per movie, three movies analysed, $P=0.665$). Error bars show s.e.m. of all tracked cells from three 60-s movies.

The fact that starved cells accumulate in the immediate vicinity of the bead suggests that they sense local dSi concentrations and direct their movement up the gradient and ultimately to the source. Surprisingly, the mean swimming speed of cells exposed to a dSi gradient was higher in the close proximity of the beads (Fig. 3a and Supplementary Fig. 3). This only holds true under the influence of the steep dSi gradient in the immediate proximity of the beads and is already not manifested any more in the more distant bin C (Supplementary Fig. 3). While cells generally move faster when starved of dSi (Fig. 1c), it is apparent that an additional response to a steep gradient of dSi is observed. The defined dSi source in an otherwise limited environment causes locally increased speed, which could be the cell's mechanism to avoid diffusion limitation during Si uptake around a dSi hotspot.

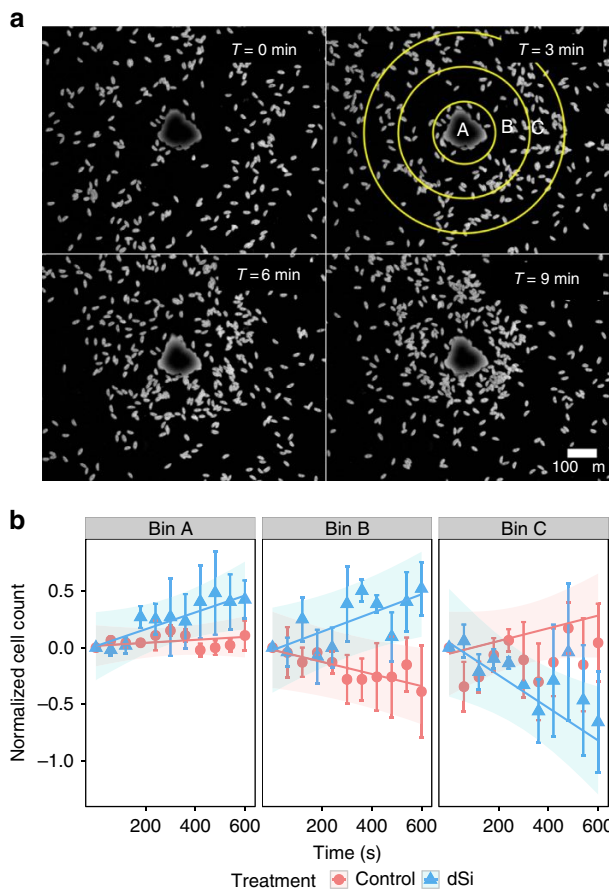
Analysis of movement. The mode of orientation within the dSi gradient was verified in detail by fitting the Taylor's equation²¹ to analyse the swimming characteristics based on tracking individual cell behaviour in response to dSi-loaded and control beads (details in Methods section). *S. robusta* cells have higher directional persistence when perceiving an ascending dSi gradient, as exemplified by longer correlation length and timescales (λ and τ) (Table 1). Cells within the dSi gradient also had on average a 57% higher diffusivity (D) and 81% higher encounter kernel (β) for the dSi beads, showing that they maximize their encounter rate to find dSi beads. Analysis of the angular orientation by monitoring the angle of the vectorized tracks relative to the bead centre did not reveal any differences between control and Si-loaded beads, thereby excluding a directed orientation during reversing events (Fig. 3b). However, cells persistently migrate towards the dSi source as indicated by the change in the sum of distances between bead and all cells over time in the treatment compared with the control (Fig. 3c). The observed behaviour can be explained by a preferential forward movement in an ascending gradient of dSi. This directionality during the chemokinetic response thus promotes chemotaxis. The persistent orientation implies a biased random walk, wherein cells adapt their movement patterns to find a dSi source.

Selectivity of the directed response. To learn more about the selectivity of the response to dissolved minerals we determined

how Si-starved cells react to dGe sources. dGe and dSi share very similar chemical properties. Ge uptake and incorporation instead of Si in diatom frustules inhibits growth and causes morphological aberrations and toxicity^{22,23}. When we administered dGe-loaded beads (1.4 nmol per bead) to dSi-starved cultures, a negative response was elicited as cells in average moved away from the dGe sources. In contrast, dSi-loaded beads were attractive, and near constant cell densities were observed around control treatments (Fig. 4 and Supplementary Fig. 4). *S. robusta* thus discriminates between the two very similar inorganic resources. This remarkably specific behavioural response combined with discrimination of the elements during uptake²⁴ represents an efficient mechanism to protect the cells against Ge toxicity.

Discussion

Our results clearly indicate the specific modulation of foraging behaviour of benthic diatoms in response to silicate. A detailed analysis of movement indicates a chemokinetic response since cell speed changes in dependence of dSi concentrations. In addition the observed attraction of cells within a gradient of dSi indicates a chemotactic search capability. Interestingly this search behaviour is not regulated by directed turns of the cells towards the dSi source but rather by a longer directional persistence within an ascending dSi gradient. This finding mechanism thus differs from the chemoattraction mechanism in brown algae where the pheromone-directed movement is mediated by signal molecule-induced turning events of gametes²⁵. Such orientation towards dSi or any other dissolved mineral has to our knowledge not been observed before in diatoms. The specificity of the attraction is demonstrated by a selective movement towards dSi while the structurally closely related dGe does not stimulate an attraction response. These observations might be explained by a receptor-mediated process²⁰, but until now no candidate receptor mediating a specific recognition of dissolved minerals is known. Since different isolates of *S. robusta* as well as another tested diatom species *Navicula sp.* exhibit this search behaviour, the response might be general for benthic diatoms. The observed dSi-directed movement might thus help to explain the often patchy species composition and structure of marine biofilms.

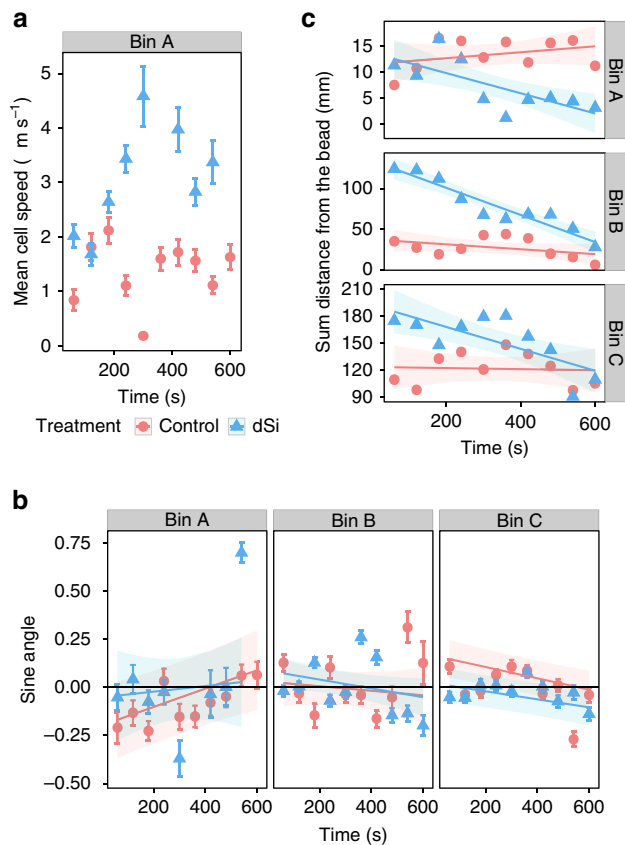


Tactic behaviour towards nutrient sources such as phosphate and different sources of nitrogen has been demonstrated for other algae and bacteria^{26,27}. These responses can provide important adaptive advantage for the organisms due to increased acquisition capability for the resources^{16,17}. The ability of motile diatoms to trace dSi gradients and exploit micro-scale hotspots by changing their foraging behaviour enables them to thrive and dominate phototrophic biofilm communities such as the intertidal microphytobenthos. More general, this capability might be a key factor explaining their explosive radiation in marine and freshwater benthos.

Microbial activity is known to greatly affect global biogeochemical processes involved in the cycling of elements^{28–30}. Several mechanisms have been suggested on how microbial behavioural responses to patchy resources can influence ocean biogeochemistry³¹. The ability of diatoms to track dSi availability in the environment has thus implications on a global scale by affecting dSi fluxes and on a micro-scale by shaping biofilm communities.

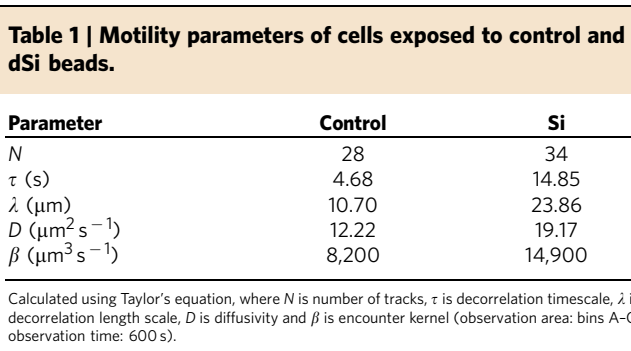
Methods

Cultures. We used the *S. robusta* strains F2-31B and P36 MT⁺ maintained cryopreserved in the BCCM/DCG diatom culture collection at Ghent University



(<http://bccm.belspo.be/about-us/bccm-dcg>)²⁰. *Navicula sp.* was isolated from a mudflat at Solana Beach, California 32° 58' 37.5" N 117° 16' 08.8" W. For both species, cells were grown in batch culture²⁰ either with natural sea water and F/2 medium³² or artificial, buffered sea water (ASW) prepared as described by Maier & Calenberg³³ to avoid overlaying effects of pH changes due to the treatments. In low-dSi treatments no dSi was added while high-dSi treatments were supplemented with 106 µM dSi for F/2 medium and 246 µM dSi for ASW. Experimental cultures were prepared by 10-fold dilution of aliquot of stock cultures using fresh culture medium and then grown in tissue culture flasks with standard caps, Petri or well plates (Greiner Bio-One, Frickenhausen, Germany). Observations, cell culture photography and video recording were done on an Leica DM IL LED inverted light microscope with a Leica DFC 280 camera system (Heerbrugg, Switzerland).

Preparation of dSi- or dGe-loaded aluminium oxide particles. Aluminium oxide (100 mg alox, Merck, Darmstadt, Germany; 90 active neutral; 0.063–0.200 mm particle diameter) was used to adsorb silicate by fully evaporating (overnight at 50–90 °C) 800 µl freshly prepared sodium silicate solution (440 mM Na₂SiO₃ · 9H₂O; Sigma-Aldrich, Deisenhofen, Germany) or germanium dioxide solution (440 mM GeO₂; Alfa Aesar, Karlsruhe, Germany). To determine the most effective concentration of dSi, 50, 800 and 1,270 µl silicate stock were added to 100 mg alox and evaporated, resulting in ~0.088, 1.40 and 2.23 nmol dSi per particle, respectively (Supplementary Fig. 2 and Supplementary Table 7). For all succeeding experiments, the concentration 1.40 nmol per particle was used for both



dSi and dGe treatments. Blank alox particles for control treatments were identically prepared by evaporation of bi-distilled water. The amount of alox particles per unit weight was determined by counting the number of particles within 10 mg alox beads on tissue culture plates. We counted three randomly chosen microscopic fields (area of each field = 5.6 mm^2) from microscopic photographs. On average 2,640 (± 660) particles were present per mg alox.

Determination of dSi diffusing from the bead. To determine the total flux of dSi diffusing from the bead (i), dSi was quantified in water exposed to Si-loaded or control beads after 600 s by standard colorimetric methods³⁴. The steady-state concentration of dSi was calculated from the initial concentration on the particle using the formula¹⁸ $C_{(r)} = i/4\pi\sqrt{rD}$, where i is the total diffusive flux of dSi, r is the radius where dSi diffused, and D is the diffusivity constant for dSi ($10^{-5} \text{ cm}^2 \text{s}^{-1}$)³⁵. Time to steady state was determined as the time $\geq d^2/D$ where d is the diameter of the whole observation area (672 μm). The \sqrt{r} was used to correct the shape of a gradient in a flat chamber³⁶. The i ($1.21^{-13} \pm 1.01^{-14} \text{ mol s}^{-1}$) was substituted in the equation and the steady-state C was calculated based on the distance (radius) from the bead r . A plot showing steady-state concentration of dSi against distance can be found in Supplementary Fig. 1.

Data processing. The open-source software Fiji (<http://fiji.sc/Fiji>)³⁷ with the plugins Cell Counter and TrackMate (<http://fiji.sc/TrackMate>) was used for cell counting and tracking, respectively. All data analyses were done using the open-source statistical and graphic software R version 3.0.3 (<http://www.R-project.org/>)³⁸.

Motility and speed of *S. robusta* controlled by dSi. For the experiment in Fig. 1a, replicate cultures were grown in Petri dishes (Greiner Bio-One; 60 × 15 mm) in F/2 medium as described above. Five cultures were used for density and proportion of motile cells determinations, performed ~9 h after the onset of light. In addition, the medium was collected from one more replicate culture each day, by filtration over a 0.2- μm pore size filter and frozen until analysis for silicate content. Dissolved silicate was measured on a spectrophotometer using the molybdate-silicate method³⁹. For Fig 1b,c, cultures were grown on tissue culture flasks (75 cm^2 growth surface; filter caps) in 20 ml growth medium with three replicates for each condition. Cultures were grown for 3 days in F/2 medium (106 μM dSi, Fig. 1b) and 7 days in dSi-enriched ASW (246 μM dSi, Fig. 1c). For Fig. 1b, at the beginning of the light period on day 4, the supernatant growth medium was replaced by careful aspiration with a Pasteur pipette attached to a water pump, immediately followed by the addition of ASW with 246 μM dSi or without dSi enrichment. Further culturing was performed for 48 h in continuous light to avoid interference of light-dark alterations on cell motility. Proportion of motile cells was assessed by overlaying two photographs taken at a 15-s interval from the same observation field. Cells ($n > 300$) located at the exact same position in both photographs were counted as immotile; others were counted as motile. Cell densities were microscopically estimated by counting cells in at least 35 observation fields with an area of 0.993 mm^2 . The percentage of motile cells was compared before and after addition of dSi (106 μM) or addition of blank artificial sea water without added dSi to cultures grown for 48 h in low-dSi or dSi-rich medium (one-way analysis of variance, Fig. 1b). For Fig. 1c, cell speeds of starved and non-starved cells with addition of bulk dSi (246 μM) or blank addition of artificial sea water without added dSi were assessed by tracking cells from 60-s movies. Differences on treatments were determined by fitting the log + 1-transformed speed to a linear mixed effects (LME) model with unique track ID as random factor and a constant variance function structure (varIdent) for treatment. Multiple pairwise comparisons were done through Tukey's honest significance difference (HSD) test (outcome of statistical analysis is given in Supplementary Table 1).

Movement of Si-starved cells in response to dSi gradients. For all succeeding experiments, *S. robusta* cultures were grown in tissue culture flasks in artificial, buffered sea water with dSi³³ until they reached stationary phase. On the seventh

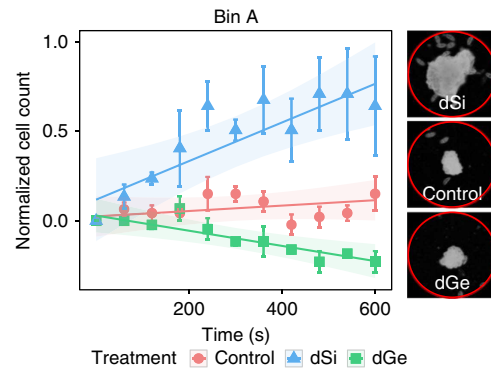


Figure 4 | Substrate-specific response of Si-starved cells to dSi- and dGe-loaded (1.4 nmol per bead), and control beads. Plot of mean normalized cell counts with overlaid LME model demonstrates avoidance of starved cells to dGe (LME, $n=70\text{--}200$ cells per movie, three movies analysed, $P=0.0047$) and attraction to dSi (LME, $n=70\text{--}200$ cells per movie, three movies analysed, $P=0.0088$). Right panels show cells in bin A in selected treatments 600 s after addition of beads (the red circle has a radius of 112 μm).

day, 1 ml of cell suspension was transferred to 12-well tissue culture plates supplemented with 2 ml low-Si medium. Normal light-dark cycle was followed for the 3-day incubation period. Alox particles were carefully administered to each well using a spatula, ensuring that the total number of beads per well does not exceed 30. For obtaining cell count data, photos were taken after exposure to the beads every 60 s for 600 s. Movies for tracking were also recorded for 600 s (1 frame per s). Cell accumulation around the particles was determined from microscopically acquired photographs by counting the number of cells within a circle having an area of 0.300 mm^2 (for Supplementary Fig. 2) or 0.355 mm^2 (Figs 2b and 3). For Figs 2b and 4, the observation area was divided into three concentric rings, called bins (bins A–C), having a Δ radius of 112 μm with the alox bead as the central point (Fig. 2a).

Modelling. A representative movie from dSi and control treatments was chosen and cells were randomly selected to be tracked ($n=29$ for control and 34 for dSi) for 600 s. To analyse the track data, cell density (n), speed ($\mu\text{m s}^{-1}$), angular orientation (sine angle) and distance (μm) of cells relative to the bead were taken as parameters. Mixed models were used to analyse and fit the data to be able to account for the nested and longitudinal design of the study. Linear modelling of sum distance and LME modelling of cell count and angular orientation were done using the R package *nlme*⁴⁰ while general additive mixed modelling of cell speed was done using the R package *mgcv*⁴¹. To correct correlated data between independent variables, a correlation structure, autoregressive order 1 (AR-1) was used. A constant variance function structure (varIdent) was also added to the model for correcting residual spreads. Individual models for each bin were chosen based on the Akaike information criterion. For each model, a Wald test was performed to determine the significance of the fitted estimates on each term. All results are shown in Supplementary Tables 2–6.

Cell counts. Cell counts were standardized according to standard Z-score calculation per treatment: standard score $Z=(X-\mu)/\sigma$, where μ is mean, X is score and σ is s.d. For the starting point to be normalized to 0, we subtracted the standardized cell count on each time point to the value at $T=0$ s. A value of 0 indicates that the cell density is equal to the mean. Positive values indicate a cell density higher than the mean and a negative value the opposite. To compare control and dSi treatments (Fig. 2b and Supplementary Table 2), a model for each bin was fitted using the interaction between treatment and time as independent variables and replicate ID as a random factor. An AR-1 correlation structure for successive measurements within the replicates and a varIdent variance structure for treatment on bins A and B and replicates for bin C were added to the model. For the comparison of substrate specificity (Fig. 4, Supplementary Fig. 4 and Supplementary Table 6), the model for each bin was fitted the same way as described above and a varIdent variance structure for treatment was added for all the bins.

Cell speed. A log + 1 transformation was used to normalize cell speed. The mean speed of the cells every 30 s for each bin was fitted using general additive mixed model (Fig. 3a, Supplementary Table 3 and Supplementary Fig. 3). Data for a time point were excluded when only a single-track data contributed to the mean. The independent variable was fitted with a simple factor smooth and penalized with cubic regression splines of time on each treatment, and track ID (that is, unique

cell ID) was assigned as a random factor. An AR-1 correlation structure between treatment and track ID was added to the model. In addition, a varIdent structure on treatment was used in the model to decrease the Akaike information criterion significantly and for a better fit.

Angular orientation. To determine angular orientation, the sine angle of each coordinate position of the cell relative to the coordinate position of the bead was calculated⁴². A cell is moving towards the bead if it has a positive value and away from it in case of a negative value. Average of the sine angles was determined per bin every 60 s (Fig. 3b and Supplementary Table 4). Data for a time point were excluded when only a single-track data contribute to the mean. Each bin data were fitted via LME using the interaction between treatment and time as independent variables and replicate ID as a random factor. An AR-1 correlation structure was used between treatment and replicate ID as well as a varIdent variance structure for treatment.

Sum distance. The sum of distance from each cell's coordinate position relative to the bead centre was used to determine the migration pattern of cells. Each bin was fitted using a simple linear model (Fig. 3c and Supplementary Table 5) with sum distance as the response variable and the interaction of time and treatment as explanatory variable.

Motility parameters. To determine whether the motility characteristics between the control and dSi treatment were different, we analysed track data from two representative movies. Motility parameters were computed by fitting the root mean square of the net distance as a function of time to Taylor's equation using nonlinear least-squares estimation²¹: root mean square = $[2v^2\tau(t - \tau(1 - e^{-t/\tau}))]^{0.5}$ where v is effective swimming speed, τ is the decorrelation timescale, t is the time and λ is decorrelation length scale: $\lambda = vt$.

The decorrelation length (λ) and timescale (τ) give the distance and time, respectively, wherein there is directional persistence in motility over a period of 600 s.

We also calculated the effective diffusivity of motility ($D = v^2\tau/n$) and encounter kernel ($\beta = 4\pi RD$), where n is number of dimensions and R is radius of the bead. D describes the spread of the cell tracks and β determines the water volume screened by cells within the observation time²¹.

References

- Field, C. B. Primary production of the biosphere: integrating terrestrial and oceanic components. *Science* **281**, 237–240 (1998).
- Kroger, N., Lorenz, S., Brunner, E. & Sumper, M. Self-assembly of highly phosphorylated silaffins and their function in biosilica morphogenesis. *Science* **298**, 584–586 (2002).
- Tréguer, P. J. & De La Rocha, C. L. The world ocean silica cycle. *Annu. Rev. Mar. Sci.* **5**, 477–501 (2013).
- Yool, A. & Tyrrell, T. Role of diatoms in regulating the ocean's silicon cycle. *Global Biogeochem. Cycles* **17**, 1103 (2003).
- Martin-Jezequel, V., Hildebrand, M. & Brzezinski, M. A. Silicon metabolism in diatoms: implications for growth. *J. Phycol.* **36**, 821–840 (2000).
- Leynaert, A., Longphuirt, S. N., Claquin, P., Chauvaud, L. & Ragueneau, O. No limit? The multiphasic uptake of silicic acid by benthic diatoms. *Limnol. Oceanogr.* **54**, 571–576 (2009).
- Ziervogel, K. & Forster, S. Do benthic diatoms influence erosion thresholds of coastal subtidal sediments? *J. Sea Res.* **55**, 43–53 (2006).
- Sigmon, D. E. & Cahoon, L. B. Comparative effects of benthic microalgae and phytoplankton on dissolved silica fluxes. *Aquat. Microb. Ecol.* **13**, 275–284 (1997).
- Bowler, C. *et al.* The *Phaeodactylum* genome reveals the evolutionary history of diatom genomes. *Nature* **456**, 239–244 (2008).
- Cahoon, L. B. in *Oceanography and Marine Biology: An Annual Review* Vol. 37 (eds Ansell, A. D., Gibson, R. N. & Barnes, M.) 47–86 (University College London Press, 1999).
- Consalvey, M., Paterson, D. M. & Underwood, G. J. C. The ups and downs of life in a benthic biofilm: migration of benthic diatoms. *Diatom Res.* **19**, 181–202 (2004).
- Van Collen, C., Underwood, G. J. C., Serôdio, J. & Paterson, D. M. Ecology of intertidal microbial biofilms: mechanisms, patterns and future research needs. *J. Sea Res.* **92**, 2–5 (2014).
- Agogué, H., Mallet, C., Orvain, F., De Crignis, M., Mornet, F. & Dupuy, C. Bacterial dynamics in a microphytobenthic biofilm: a tidal mesocosm approach. *J. Sea Res.* **92**, 36–45 (2014).
- Molino, P. J. & Wetherbee, R. The biology of biofouling diatoms and their role in the development of microbial slimes. *Biofouling* **24**, 365–379 (2008).
- Wang, J., Cao, S., Du, C. & Chen, D. Underwater locomotion strategy by a benthic pennate diatom *Navicula* sp. *Protoplast* **250**, 1203–1212 (2013).
- Amsler, C. D. & Iken, K. B. in *Marine Chemical Ecology* (eds McClintock, J. B. & Baker, B. J.) 413–430 (CRC, 2001).
- Hutz, A., Schubert, K. & Overmann, J. *Thalassospira* sp isolated from the oligotrophic eastern mediterranean sea exhibits chemotaxis toward inorganic phosphate during starvation. *Appl. Environ. Microbiol.* **77**, 4412–4421 (2011).
- Barbara, G. M. & Mitchell, J. G. Marine bacterial organisation around point-like sources of amino acids. *FEMS Microbiol. Ecol.* **43**, 99–109 (2003).
- Witkowski, A., Brehm, U., Palinska, K. A. & Rhiel, E. Swarm-like migratory behaviour in the laboratory of a pennate diatom isolated from North Sea sediments. *Diatom Res.* **27**, 95–100 (2012).
- Gillard, J. *et al.* Metabolomics enables the structure elucidation of a diatom sex pheromone. *Angew. Chem. Int. Ed.* **52**, 854–857 (2013).
- Visser, A. W. & Kiorboe, T. Plankton motility patterns and encounter rates. *Oecologia* **148**, 538–546 (2006).
- Froelich, P. N. & Andreae, M. O. The marine geochemistry of germanium—ekasilicon. *Science* **213**, 205–207 (1981).
- Azam, F., Hemmingsen, B. B. & Voletti, B. E. Germanium incorporation into the silica of diatom cell walls. *Arch. Microbiol.* **92**, 11–20 (1973).
- Sutton, J., Ellwood, M. J., Maher, W. A. & Croot, P. L. Oceanic distribution of inorganic germanium relative to silicon: germanium discrimination by diatoms. *Global Biogeochem. Cycles* **24**, GB2017 (2010).
- Pohnert, G. & Boland, W. The oxylipin chemistry of attraction and defense in brown algae and diatoms. *Nat. Prod. Rep.* **19**, 108–122 (2002).
- Ikegami, S., Imai, I., Kato, J. & Ohtake, H. Chemotaxis toward inorganic phosphate in the red alga *Chattonella antiqua*. *J. Plankton Res.* **17**, 1587–1591 (1995).
- Ermilova, E. V., Nikitin, M. M. & Fernandez, E. Chemotaxis to ammonium/methylammonium in *Chlamydomonas reinhardtii*: the role of transport systems for ammonium/methylammonium. *Planta* **226**, 1323–1332 (2007).
- Azam, F. Microbial control of oceanic carbon flux: the plot thickens. *Science* **280**, 694–696 (1998).
- Seymour, J. R., Marcos & Stocker, R. Resource patch formation and exploitation throughout the marine microbial food web. *Am. Nat.* **173**, E15–E29 (2009).
- Seymour, J. R., Simo, R., Ahmed, T. & Stocker, R. Chemoattraction to dimethylsulfoniopropionate throughout the marine microbial food web. *Science* **329**, 342–345 (2010).
- Stocker, R. Marine microbes see a sea of gradients. *Science* **338**, 628–633 (2012).
- Guillard, R. R. L. in *Culture of Marine Invertebrate Animals*. (eds Smith, L. H. & Chanley, M. H.) 26–60 (Plenum, 1975).
- Maier, I. & Calenberg, M. Effect of extracellular Ca^{2+} and Ca^{2+} -antagonists on the movement and chemoorientation of male gametes of *Ectocarpus siliculosus* (Phaeophyceae). *Bot. Acta* **107**, 451–460 (1994).
- Strickland, J. D. H. & Parson, T. R. *A Practical Handbook of Seawater Analysis* 2nd edn (Fisheries Research Board of Canada, 1978).
- Wollast, R. & Garrels, R. M. Diffusion coefficient of silica in seawater. *Nat. Phys. Sci.* **229**, 94 (1971).
- Blackburn, N., Fenchel, T. & Mitchell, J. Microscale nutrient patches in planktonic habitats shown by chemotactic bacteria. *Science* **282**, 2254–2256 (1998).
- Schindelin, J. *et al.* Fiji: an open-source platform for biological-image analysis. *Nat. Methods* **9**, 676–682 (2012).
- Team, R. C. R Foundation for Statistical Computing www.R-project.org/ (2013).
- Eaton, A. D., Clesceri, L. S., Greenberg, A. E. & Franson, M. A. H. *Standard Methods for the Examination of Water and Wastewater* (American Public Health Association, 1998).
- Pinheiro, J., Bates, D., DebRoy, S., Sarkar, D. & Team, R. C. R nlme: Linear and Nonlinear Mixed Effects Models. R package version 3.1–120 <http://CRAN.R-project.org/package=nlme> (2015).
- Wood, S. N. Fast stable restricted maximum likelihood and marginal likelihood estimation of semiparametric generalized linear models. *J. R. Stat. Soc. Ser. B* **73**, 3–36 (2011).
- Fenchel, T. Orientation in two dimensions: chemosensory motile behaviour of *Euploites vannus*. *Eur. J. Protistol.* **40**, 49–55 (2004).

Acknowledgements

This work was supported by the Volkswagen Foundation, the IMPRS Exploration of Ecological Interactions with Molecular and Chemical Techniques, the Flemish Research foundation project TG.0374.11N and the Ugent research grants 01/04611 and BOF15/GOA/17.

Author contributions

G.P. and W.V. designed the project; K.G.V.B. and J.G. discussed and performed the experiments; K.G.V.B. performed cell tracking; K.G.V.B. and J.H. discussed and performed the modelling; all authors contributed to writing the manuscript.

Additional information

Supplementary Information accompanies this paper at <http://www.nature.com/naturecommunications>

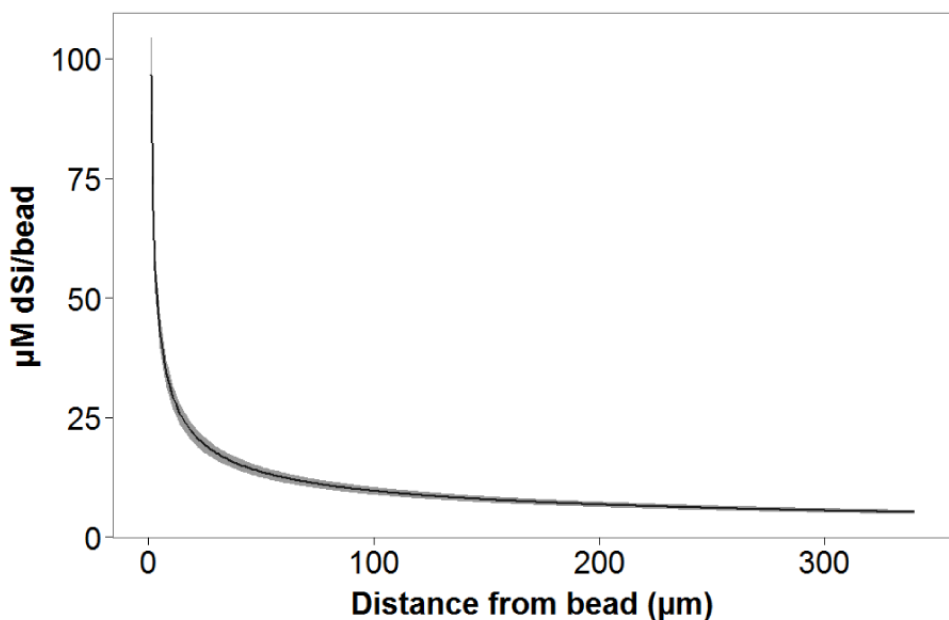
Competing financial interests: The authors declare no competing financial interests.

Reprints and permission information is available online at <http://npg.nature.com/reprintsandpermissions/>

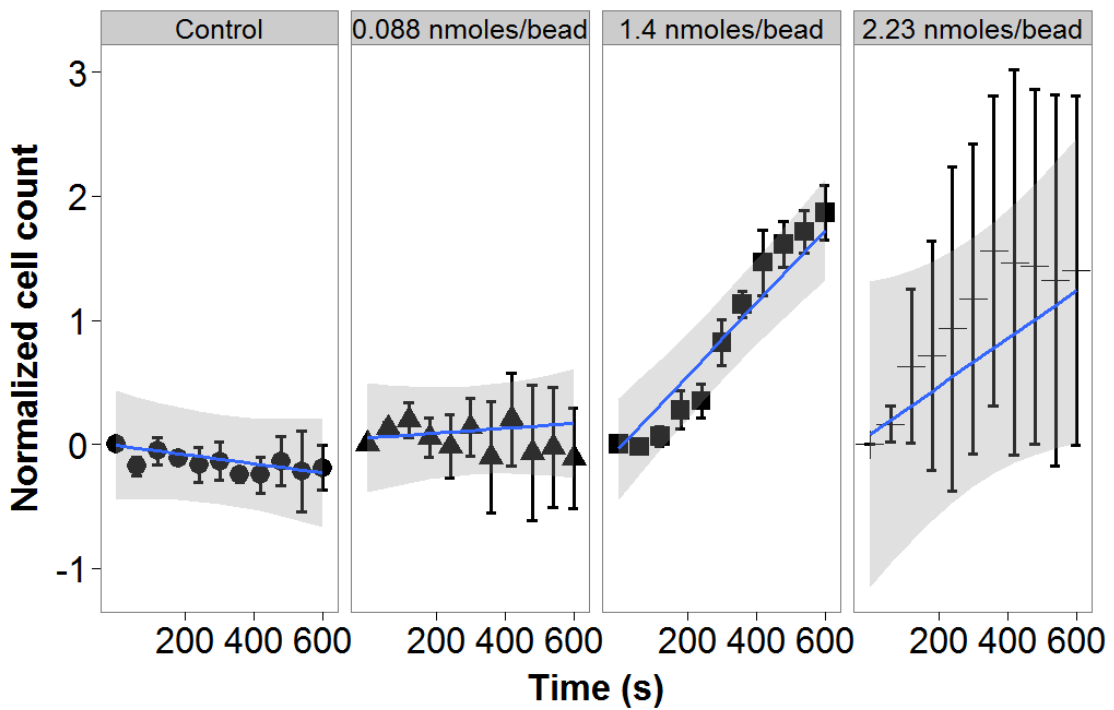
How to cite this article: Bondoc, K. G. V. *et al.*, Selective silica-directed motility in diatoms. 7:10540 doi: 10.1038/ncomms10540 (2016).



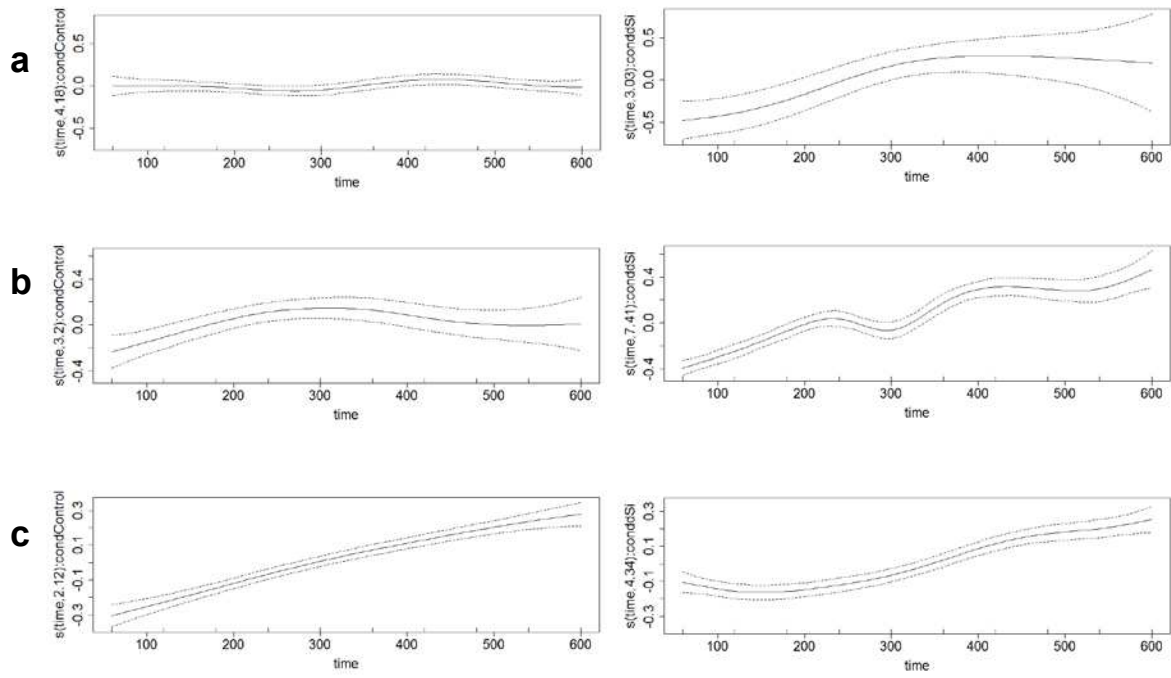
This work is licensed under a Creative Commons Attribution 4.0 International License. The images or other third party material in this article are included in the article's Creative Commons license, unless indicated otherwise in the credit line; if the material is not included under the Creative Commons license, users will need to obtain permission from the license holder to reproduce the material. To view a copy of this license, visit <http://creativecommons.org/licenses/by/4.0/>



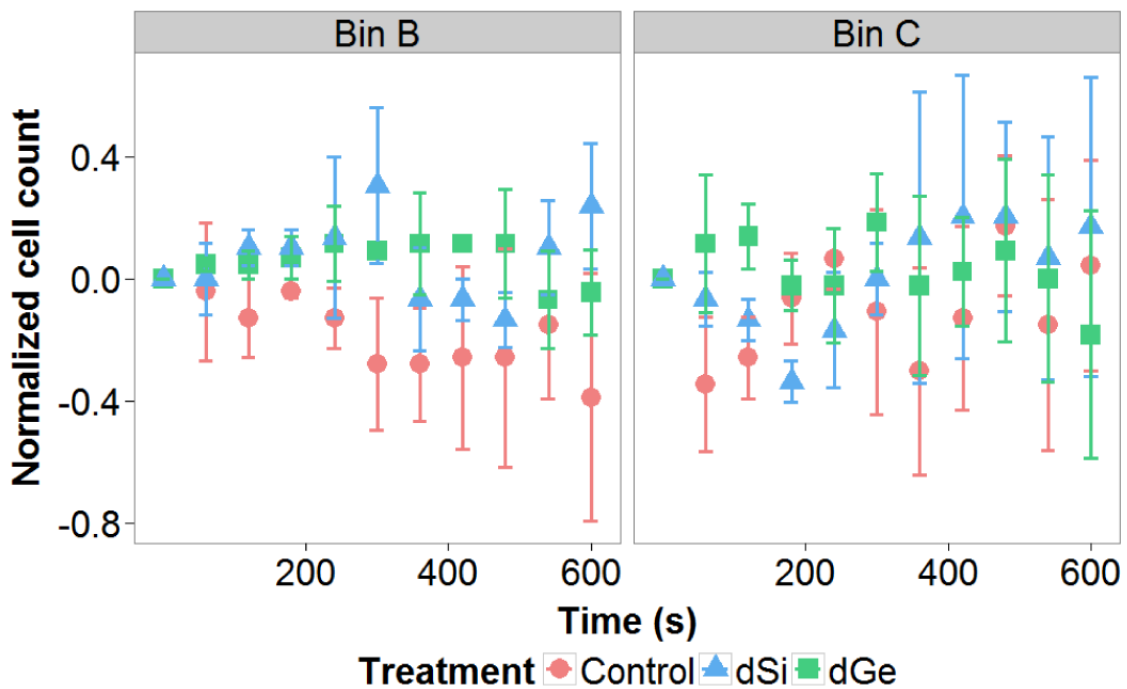
Supplementary Figure 1. Steep dSi concentration gradients that mimic the sediment-water interface are built up around the dSi-alox loaded beads. The gradient depicted here is reached at ~460 s. dSi concentrations in Bin A showed a sudden drop from 97 μM dSi to 9.1 μM while Bins B and C showed a steadier dSi concentration gradient (9-5 μM dSi). dSi was determined in water exposed to Si-loaded or control beads after 600 s on 3 replicates and the concentration depicted here was calculated as described in the methods section. Note: Since beads are not spherical the distance from the bead surface is considered.



Supplementary Figure 2. dSi-starved cells were exposed to different concentrations of dSi and cell density was determined every 60s in an area of 0.3 mm^2 corresponding roughly to the area of bins A-C (0.35 mm^2). Plotted normalized cell counts from every 60s photos were fitted using a linear mixed effects model and an overlay of the model with SE is shown here. For normalization of the starting point to 0, we subtracted the standardized cell count on each time point to the value at $T=0\text{s}$. A value of 0 indicates that the cell density is equal to the mean. Positive values indicate a cell density higher than the mean. A concentration (1.4 nmoles dSi/bead) that elicited the highest chemotaxis as compared to the control and the other two concentrations ($p=<0.0001$, estimate=0.0033, s.e. =0.00059, DF=116, $t=5.62$) was used for further experiments.



Supplementary Figure 3. Fitted cubic splines of cell speed for control (condCon) and dSi (condSi) treatment for bins A-C over T=600s. The data is fitted using smoothing splines which place a knot on each data point over time ($s(\text{time})$). The optimal number of smoothing knots (i.e. the number of connections for each data point) of the fitted model is shown on the y-axis. GAMM models centers the mean of each treatment to 0. **a**, For Bin A, speed of cells exposed to dSi treatment were significantly increasing ($p=8.27^{-8}$) compared to control ($p = 0.176$). The smoothed plots showed that cell speed increased over time in the dSi treatment while a more random pattern mostly centered around 0 could be seen in the control treatment . **b**, For Bin B, both dSi and control gave statistically significant smooth terms with dSi giving a stronger effect ($p=<2^{-16}$) than control ($p=0.00259$). **c**, On the other hand, the trend on Bin C was the same for both control and dSi treatments.



Supplementary Figure 4. Plotted normalized cell counts from every 60 s for Bins B and C of the substrate specificity testing. For normalization of the starting point to 0, we subtracted the standardized cell count on each time point to the value at $T = 0$ s. A value of 0 indicates that the cell density is equal to the mean. Positive values indicate a cell density higher than the mean. We observed no significant differences on both bins.

Supplementary Table 1: Cell speeds of starved and non-starved cells were compared before and after 1h addition of dSi (+dSi) or blank addition. Pairwise comparisons via Tukey's HSD were done after fitting the data with linear mixed effects model. Starved cells significantly move faster than non-starved cells. Addition of dSi to starved cells significantly increased the speed while addition of blank showed no effect. Moreover, when dSi is added to starved cells, the mean speed is almost the same when dSi is added to non-starved cells. Blank addition is significantly different from starved and non-starved cells with dSi addition.

Pair-wise comparisons	Estimate	Std. Error	z value	Pr(> z)
Before dSi addition				
starved – non-starved	0.4036	0.0250	16.165	<1e-04 ***
After dSi addition				
starved+dSi – starved	-0.5223	0.0277	-18.865	<1e-04 ***
starved+blank – starved	0.0452	0.0338	1.338	0.655
starved+dSi - starved+blank	-0.4772	0.0306	-15.60	<1e-04 ***
starved+dSi - non-starved+dSi	-0.0070	0.0201	-0.346	0.997
starved+blank - non-starved+dSi	0.4702	0.0280	16.802	<1e-04 ***
non-starved – starved+blank	0.3584	0.0281	12.753	<1e-04 ***

Signif. codes: 0 `***' 0.001 `**' 0.01 `*' 0.05 `.' 0.1 ` ' 1 (Adjusted p values reported -- single-step method)

Supplementary Table 2. Linear mixed effects model on count data (Control vs. dSi) for individual bins.

	numDF	denDF	F-value	p-value
Bin A				
(Intercept)	1	58	3.706	0.059
treatment	1	4	2.190	0.213
Time	1	58	2.356	0.130
treatment:Time	1	58	1.992	0.164
Bin B				
(Intercept)	1	58	0.0140	0.906
treatment	1	4	3.360	0.141
Time	1	58	0.042	0.838
treatment:Time	1	58	9.363	0.003
Bin C				
(Intercept)	1	58	0.507	0.479
treatment	1	4	5.372	0.081
Time	1	58	0.304	0.584
treatment:Time	1	58	7.571	0.008

Supplementary Table 3. Spline terms of general additive mixed effects model on cell speed (Control vs. dSi) for all bins.

	edf	Ref.df	F	p-value
Bin A				
s(Time):condCon	4.181	4.181	1.756	0.176
s(Time):condSi	3.035	3.035	12.075	8.27^{-8}
Bin B				
s(Time):condCon	3.200	3.200	4.479	0.003
s(Time):condSi	7.413	7.413	26.199	$<2^{-16}$
Bin C				
s(Time):condCon	2.117	2.117	73.50	$<2^{-16}$
s(Time):condSi	4.337	4.337	30.41	$<2^{-16}$

Supplementary Table 4. Linear mixed effects model on sine angle data (Control vs. dSi) for individual bins.

	numDF	denDF	F-value	p-value
Bin A				
(Intercept)	1	2004	0.192	0.662
treatment	1	17	0.140	0.713
Time	1	2004	9.754	0.002
treatment:Time	1	2004	0.702	0.402
Bin B				
(Intercept)	1	6190	0.309	0.578
treatment	1	35	0.268	0.608
Time	1	6190	4.043	0.044
treatment:Time	1	6190	0.261	0.609
Bin C				
(Intercept)	1	9792	0.168	0.682
treatment	1	48	2.887	0.096
Time	1	9792	22.62	<0.0001
treatment:Time	1	9792	0.666	0.414

Supplementary Table 5. Linear mixed model on sum distance (Control vs. dSi) for all bins.

	DF	Sum Sq	Mean Sq	F value	p value
Bin A					
treatment	1	189.98	189.98	17.42	<0.0001
Time	1	28.105	28.105	2.577	0.128
treatment:Time	1	94.442	94.442	8.658	0.010
Bin B					
treatment	1	13460	13460	105.04	1.94 ⁻⁸
Time	1	5804.3	5804.3	45.295	4.88 ⁻⁶
treatment:Time	1	2792.4	2792.4	21.791	<0.001
Bin C					
treatment	1	4691.6	4691.6	10.754	0.005
Time	1	2423.9	2423.9	5.5557	0.031
treatment:Time	1	1987.5	1987.5	4.5556	0.049

Supplementary Table 6. Linear mixed effects model on count data for substrate specificity

(Control vs. dGe vs. dSi).

	numDF	denDF	F-value	p-value
Bin A				
(Intercept)	1	87	0.3857	0.5362
treatment	2	6	26.025	0.0011
Time	1	87	0.6343	0.4279
treatment:Time	2	87	11.745	<.0001
Bin B				
(Intercept)	1	87	0.0726	0.7882
treatment	2	6	1.3802	0.3213
Time	1	87	0.8504	0.3590
treatment:Time	2	87	1.382	0.2566
Bin C				
(Intercept)	1	87	0.004	0.9475
treatment	2	6	0.046	0.9551
Time	1	87	0.025	0.8745
treatment:Time	2	87	0.387	0.6806

Supplementary Table 7. Linear mixed effects model on count data (Control vs. different dSi concentrations).

	numDF	denDF	F-value	p-value
(Intercept)	1	116	9.896	0.0021
treatment	3	8	5.677	0.0221
Time	1	116	19.47	<.0001
treatment:Time	3	116	12.51	<.0001

Supplementary Data Movie legends

Movie 1: The movie shows the characteristic back and forth movement of *Seminavis robusta* (strain F2-31B) synonymous to the run-reverse movement of marine bacteria. Movie was accelerated 10x. Time labels denote min:s.

Movie 2: The movie shows the response of *S. robusta* (strain F2-31B) to a control bead (no dSi). dSi-starved cells move randomly around the area and show no response towards the bead. The video speed was accelerated 50 times and the scale bar indicates 50 μm . Time labels denote min:s.

Movie 3: The movie shows the attraction and accumulation of *S. robusta* (strain F2-31B) to a dSi-loaded bead. dSi-starved cells began to move towards the bead in less than 300s, indicating that they perceived a gradient of dSi diffusing from the bead. The video speed was accelerated 50 times and the scale bar indicates 50 μm . Time labels denote min:s.

Movie 4: The movie shows *S. robusta* (strain P36 MT $^{+}$) starved and exposed to a control bead for 1h. No response towards the bead was observed for the whole observation area. The video speed was accelerated 50 times and the scale bar indicates 100 μm . Time labels denote min:s.

Movie 5: The movie shows *S. robusta* (strain P36 MT $^{+}$) starved and exposed to a dSi-loaded bead for 1h. Attraction towards the bead for the whole observation time was evident indicating that the created diffusion gradient was stable for 1h. Furthermore, cells were observed to stop moving around \sim 25 min which was also observed for dSi-starved cells after bulk addition of dSi. The video speed was accelerated 50 times and the scale bar indicates 100 μm . Time labels denote min:s.

Movie 6: The movie shows the attraction and accumulation of *Navicula sp.* to a dSi-loaded bead for 20 min. Like *S. robusta*, this pennate diatom also has a back and forth movement. dSi-starved cells also accumulated towards the bead in less than 300s. The video speed was accelerated 50 times and the scale bar indicates 100 μm . Time labels denote min:s.

3.2 Publication B

Bondoc, K. G. V., Lembke, C., Vyverman, W. & Pohnert, G. Searching for a mate: Pheromone-directed movement of the benthic diatom *Seminavis robusta*. *Microbial Ecology* **72**, 287-294 (2016), doi: 10.1007/s00248-016-0796-7.

Summary: Diatoms are key players in the aquatic environment as they can affect the global carbon and silica cycles. These species-rich microalgae have a unique life cycle with vegetative cell size reduction followed by size restoration through sexual reproduction of two different mating types (MT⁺ and MT⁻). Mate finding in the marine benthic diatom *Seminavis robusta* is mediated by L-diproline, a pheromone produced by the MT⁻ mating type. Here we show that the MT⁺ mating type employ simultaneous chemotaxis and chemokinesis in response to pheromone gradients produced by L-diproline-loaded beads. Changes in the motile behaviour enable MT⁺ to locate and maximize its encounter rate towards the vicinity of the pheromone. Our results suggest that this active behaviour allows diatoms to be successful in their niche as they can actively search for mating partners.

Publication equivalents of contributing PhD students as coauthors according to the implementing provision of the doctoral regulations of the Faculty of Chemistry and Earth Sciences of the Friedrich Schiller University Jena

	Author 1: Bondoc	Author 2: Lembke
<i>Conception of the work</i>	X	X
<i>Planning of experiments</i>	X	X
<i>Data collection</i>	X	X
<i>Data analysis and interpretation</i>	X	-
<i>Manuscript writing</i>	X	X
<i>Proposed publication equivalents</i>	1	0.75

The supporting movies of this publication are available via the embedded compact disc.

Reproduced with permission from Springer via the Copyright Clearance Center, License number 4158430558280.

Searching for a Mate: Pheromone-Directed Movement of the Benthic Diatom *Seminavis robusta*

Karen Grace V. Bondoc^{1,2} · Christine Lembke¹ · Wim Vyverman³ · Georg Pohnert^{1,2}

Received: 3 April 2016 / Accepted: 25 May 2016 / Published online: 3 June 2016
© Springer Science+Business Media New York 2016

Abstract Diatoms are species-rich microalgae that often have a unique life cycle with vegetative cell size reduction followed by size restoration through sexual reproduction of two mating types (MT^+ and MT^-). In the marine benthic diatom *Seminavis robusta*, mate-finding is mediated by an L-proline-derived diketopiperazine, a pheromone produced by the attracting mating type (MT^-). Here, we investigate the movement patterns of cells of the opposite mating type (MT^+) exposed to a pheromone gradient, using video monitoring and statistical modeling. We report that cells of the migrating mating type (MT^+) respond to pheromone gradients by simultaneous chemotaxis and chemokinesis. Changes in movement behavior enable MT^+ cells to locate the direction of the pheromone source and to maximize their encounter rate towards it.

Keywords Diatoms · Chemoattraction · Pheromone · Chemokinesis · Chemotaxis · Mating success · Modeling

Electronic supplementary material The online version of this article (doi:10.1007/s00248-016-0796-7) contains supplementary material, which is available to authorized users.

✉ Georg Pohnert
Georg.Pohnert@uni-jena.de

¹ Institute for Inorganic and Analytical Chemistry, Bioorganic Analytics, Friedrich-Schiller-Universität Jena, Lessingstrasse 8, D-07743 Jena, Germany

² Max Planck Institute for Chemical Ecology, Hans-Knöll-Str. 8, D-07745 Jena, Germany

³ Laboratory of Protistology and Aquatic Ecology, Department of Biology, University Gent, Krijgslaan 281 S8, 9000 Ghent, Belgium

Introduction

Diatoms are a species-rich group of microeukaryotes contributing to ca. 20 % of global carbon fixation [1] and are important contributors to the ocean carbon pump. Due to the formation of their siliceous cell wall from dissolved silicate, they also affect the global Si-cycle [2]. Although fundamental aspects of diatom physiology have become increasingly well understood [3, 4], our knowledge of their diplontic life cycle is still very limited. Open questions include, for example, cell size-dependent changes in cell physiology and behavior, dormancy, and auxosporulation [5, 6]. In those diatoms for which data are available, relatively long periods of vegetative growth alternate with short episodes of sexual reproduction [5, 7]. During vegetative cell division, one of the two biomineralized halves of the cell wall (thecae) is inherited by each of the daughter cells. The production of the new thecae occurs within the confines of the parental walls, leading to a gradual decrease in the mean cell size of the population [5]. Upon reaching a sexual size threshold (SST), restoration of the original cell size can occur via sexual reproduction, a key process in the life cycle of many diatoms [5]. After mating, a zygote is formed that develops into an auxospore, which upon germination forms a large initial cell that starts again to divide mitotically. Sexual reproduction of pennate diatoms can sometimes be triggered by environmental cues but recent findings show that pheromones play a key role in the control of sexuality [5, 8, 9].

Successful mating requires synchronized behavior between mates that leads to physical encounters [10]. This necessarily implies that one or both mating partners are motile and have the ability to locate their partners. Motile male gametes of the diatoms *Pseudostaurosira trainorii* locate stationary female gametes via pheromone sensing while non-directed random walk is observed in *Tabularia fasciculata* [9, 11]. These two

species are araphid pennate diatoms that exhibit anisogamy wherein the pairing gametes differ behaviorally and morphologically. In contrast, most raphid pennates, including the emerging model species *Seminavis robusta* produce morphologically and physiologically similar isogamous gametes after gametangiogamy [5]. In this species, the induction of the sexual phase as well as the mate-finding under the control of pheromones is confined to gametangial cells. Gamete production only takes place after successful pairing of gametangial MT⁺ and MT⁻ cells. The first diatom pheromone was only recently identified as the L-proline-derived diketopiperazine (in the following abbreviated as diproline) in *S. robusta* using a metabolomics-enabled approach [8]. Diproline is released by the mating type MT⁻ after perceiving chemical signals of the opposite mating type MT⁺ that indicate its presence. Attraction assays showed that MT⁺ cells exhibit a finding behavior towards their mating partner. This behavior can also be observed upon the addition of polymer beads releasing the pheromone diproline as cells accumulate around the pheromone-loaded beads [8]. Diproline is part of a complex signaling system with two other putative pheromones that induce sexualization in the opposite mating types [8, 12].

Raphid pennate diatoms like *S. robusta* move by gliding through adhesive mucilage excreted from elongated slits in the cells' frustules (raphe). The extruded extracellular polysaccharides (EPS) are not only responsible for forward and backward movement but can also form pseudopods or stalks that adhere to the substratum and produce a torque that supports cell rotation. This results in a back and forth movement wherein cells can reverse direction after each stop [13]. Diatoms can utilize directed motility to respond to light [14], monosaccharides [15], and dissolved silicate [16], by biasing their movement towards or away these signals. In this contribution, we record, compare, and analyze the movement of the attracted mating type MT⁺ of *S. robusta* in the presence and absence of diproline gradients generated from diproline-loaded polymeric beads [8]. We show for the first time using a pure pheromone, delivered in defined concentrations how motile diatom cells exhibit a chemotactic and chemokinetic response.

Methods

Strains and Culture Conditions

We used the *S. robusta* strains 85A (MT⁺) and 84A (MT⁻) both below their sexual size threshold (~30 µm). The strains are maintained in the BCCM/DCG diatom culture collection at Ghent University (<http://bccm.belspo.be/about-us/bccm-dcg>). Stock cultures were grown in buffered artificial sea water (ASW) as described by Maier and Calenberg [17]. For tracking experiments, cultures were prepared by inoculating 15 % stock

culture to fresh ASW and kept in standard tissue culture flasks or well plates (Sarstedt, Nümbrecht, Germany). Both were grown at 18 °C in a 12:12 h light:dark regime with cool-white fluorescent lamps at approximately 35 µmol photons m⁻² s⁻¹.

L-Diproline Attraction Assays

The attraction assay methods were modified after Gillard et al. [8]. MT⁺ cells were grown for 2 days in 24-well plates (1.7 mL well⁻¹) and thereafter dark-synchronized for 36 h [18]. MT⁻ cells were grown in culture flasks for 3 days. MT⁺ cells were induced by adding 600 µl of filtered MT⁻ medium into each well, and the plates were kept in the light for 6 h. For bead preparation, aliquots of 0.5 mg HLB-SPE (hydrophilic-lipophilic balanced solid phase extraction, Oasis®, Waters, Eschborn, Germany) material were incubated in 1 ml deionized H₂O with or without synthetic diproline (2 nmol) for 1 h at room temperature. Five micrograms of beads were added into each well of induced MT⁺ culture and immediately afterwards, the swimming behavior of MT⁺ cells was recorded for 600 s. Observations, cell culture photography, and video recording were done on an inverted Leica DM IL LED light microscope (Heerbrugg, Switzerland) mounted with a Nikon DS-Fi2 CCD camera (Tokyo, Japan).

Determination of the Pheromone Gradient

The amount of diproline diffusing from these beads and the concentration gradient this process produced were determined through a combined experimental and calculation approach. Diproline and control beads were prepared as described above. Pheromone-loaded beads (167 µg) were added to 50 mL fresh ASW and after 10 min exposure, the beads were filtered out. The equivalent amount of diproline on the beads (0.668 nmol) was also added to 50 mL fresh ASW to determine the maximum amount that could be adsorbed by the bead. Prior to extraction, 1.5 nmol of caffeine was added to each 50 mL sample as internal standard. The diproline concentration in both experiments was determined after SPE extraction according to an established method by using gas chromatography coupled to mass spectrometry on an ISQ Trace GC-Ultra GC-MS system (Thermo Fisher, Dreieich, Germany) [8].

Based on this concentration, we calculated the total flux of diproline that diffused from the bead (*i*) after 10 min using the formula from Barbara and Mitchell [19]:

$$C = i / 4\pi r D$$

where *C* is the measured concentration that diffused from the bead into the medium, *r* is the radius of the bead (15 µm), and *D* is the diffusion coefficient for small molecules (10⁻⁵ cm² s⁻¹) [20]. From the calculated *i*, we then determined

the steady state concentration $C_{(r)}$ using the same formula mentioned above. To correct for the two dimensionality of the biofilm, we replaced r with the square root of the radius (\sqrt{r}) of the observation area (250 μm) [21]. The time to steady state was determined as the time equal to or greater than d^2/D where d is the diameter of the whole observation area (500 μm).

Video and Statistical Analyses

In total, we recorded five videos for diproline and four for control treatments. On each field of view, 1–7 beads could be used in individual observation fields resulting in a total of 24 beads for diproline and 7 for control. The open-source software Fiji [22] with the plug-ins Cell Counter and TrackMate (<http://fiji.sc/TrackMate>) was used for cell counting and tracking, respectively. All videos were used for cell counting whereas only three videos each from control and treatment were randomly chosen for cell tracking. Movies were taken for 600 s with a frame rate of 100 frames per second. The first 60 s of the movie were excluded from all statistical analyses as cells were disturbed during and shortly after the sinking of the introduced beads. Cell accumulation around the particles was determined from a microscopic picture frame extracted every 30 s from the movies. We determined the number of cells within a circular area with a radius of 50 μm around the beads ($7.85 \times 10^{-3} \text{ mm}^2$). For cell tracking, the circular observation area covered had a radius of 250 μm around the bead (0.196 mm^2). Within this area, 10 randomly selected moving cells were tracked every second using the semi-automatic settings that allow track editing in case of obviously broken trajectories.

From the cell track data recorded for 600 s, parameters such as speed, angular orientation, and sum distance of cells were calculated as follows. All data analyses were done using the open-source statistical and graphic software R version 3.2.1 [23] and the package *ggplot2* [24]. Calculated parameters were fitted either with a linear or a mixed model to account for the nested and longitudinal characteristic of the data. The optimum model was chosen based on the Akaike information criterion (AIC). Linear mixed effects (LME) modeling was done through the package *nlme* [25] and general additive mixed (GAMM) modeling through the package *mgcv* [26]. If needed, correlated data between independent variables were corrected by an autoregressive order 1 (AR-1) correlation structure. A constant variance function structure (varIdent) was also added to the model to correct residual spreads. We also inspected residual plots and verified that the model residuals are not deviating from normality and homoscedasticity. For each optimum model, a Wald test was also performed to determine the significance of the fitted estimates on each term.

Cell Counts

The raw cell count data was normalized according to standard Z-score calculation per treatment.

$$Z = (X - \mu) / \sigma$$

where μ is mean, X is score, and σ is standard deviation. For the starting point to be normalized to 0, we subtracted the standardized cell count on each time point to the value at $T=0$ s. A value of 0 indicates that the cell density is equal to the mean. A positive value indicates that the cell count is above the population mean while a negative value indicates a value below the mean. To compare pheromone and control treatments, normalized cell counts were fitted on a LME model with an interaction term between time and treatment as independent fixed variables and replicate ID as a random factor. Since successive measurements were done on each replicate per treatment, an AR-1 correlation structure was added to the model. A varIdent variance structure on treatment was also added.

Speed

A Wilcoxon rank sum test was performed to compare the overall mean cell speeds from diproline and control treatments. We also determined the effect of time along with treatment on averaged cell speeds in intervals of 30 s of all cell tracks via GAMM. The log +1 transformed speed was fitted to a smoothed factor interaction of time and treatment penalized with cubic regression splines and track ID (i.e., unique cell ID) as random factor. An AR-1 correlation structure between treatment and track ID and a varIdent variance structure on treatment were also added on the model. Additive models connect individual data points by smoothing and setting the population mean of each data set to zero. Computed p values indicate the significance of the smoothing terms and low p values indicate that the fitted model splines used in the function have low likelihood to be zero [26].

Angular Orientation

The angular orientation of the cells towards the gradient was computed by determining the sine angle from vectorized cell tracks. A first vector is defined by the coordinate position of the bead to a cell position at $T=0$ s. A second vector points from this position to the coordinate of the cell at $T=1$ s. The sine angle between these two defined vectors is determined. This procedure is repeated every second for the entire observation period [27]. A cell is moving towards the gradient if the calculated sine angle has a positive value and away from it in the case of a negative value. We performed LME on the mean sine angle over intervals of 30 s with the interaction term of

treatment and time as independent variables and track ID as random factor. The same correlation and variance structure as with the speed model were used.

Sum Distance

Within the observation period, we determined every second the sum distance of cells by taking the sum of the calculated Euclidean distance of each cell coordinate relative to the center of the bead for each treatment. This gives insight into the net migration preference of the cell. The sum distance was fitted into a simple linear model with the interaction of time and treatment as explanatory variables.

Motility Parameters

Motility parameters were determined after a modified protocol described in Bondoc et al. [16]. We computed standard motility parameters using the pooled data tracks from three videos by fitting the root mean square (RMS) of the net distance as a function of time to Taylor's equation [28]

$$RMS = \left[2v^2\tau \left(t - \tau \left(1 - e^{-t/\tau} \right) \right) \right]^{0.5}$$

where v is the effective swimming speed, τ is the decorrelation time scale, and t is the time. From this, we were able to compute the decorrelation time (τ) and length ($\lambda = v\tau$) scale, which corresponds to the time and distance, respectively, wherein there is directional persistence in swimming over the period 60 to 410 s. We also calculated the effective diffusivity of motility ($D = v^2 \times \tau / n$) to describe the spread of the cell tracks, and the encounter kernel ($\beta = 4\pi RD$) to determine the water volume screened by cells within the observation time. We also compared the mean net distance of cells used in the RMS fitting via Wilcoxon rank sum test.

Results

Diproline Release from the Beads

The total diproline administered to each bead was 26.7 ± 9.12 fmol and within the 600-s observation time, 7.40 ± 0.81 fmol diproline diffused out from each bead, corresponding to ~30 % of the loaded amount. The calculated initial flux, i was $6.06^{-18} \pm 6.66^{-19}$ mol s $^{-1}$. This created a steady state gradient after 62.5 s with a concentration of ~5 nM at the surface of the bead and decreasing to 0.30 nM on the edge of the observation area (Fig. 1).

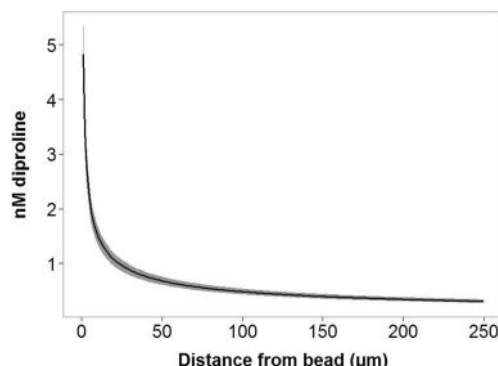


Fig. 1 Concentration gradient produced by the diproline-loaded bead around the observation area, calculated for a distribution within a radius from the bead of 250 μm in the two-dimensional biofilm. This steady state with a steep change of diproline concentration from the surface of the bead to the edge of the observation area is reached after 62.5 s. Shaded area represents the SD of the mean of three replicates

Characterizing Motility Patterns in *S. robusta* MT $^+$

Cells accumulate in the immediate vicinity of diproline-beads confirming chemoattraction towards the pheromone source while no attraction towards control-beads was observed (Fig. 2a; Movies S1 and S2) [8]. Increasing cell density within the observation area over time was found in the diproline treatments while the controls exhibited constant cell counts (LME; $p < 0.0001$, Fig. 2b; Table S1). The overall mean speed of cells under the influence of the diproline gradient was 69.2 ± 22.2 % higher compared to the control (Wilcoxon rank sum test, $p < 0.0001$; Fig. 3a). Increased speed in diproline treatments compared to control was observed from 90 s after addition of pheromone loaded beads with a maximum around ca. 300 s and lasting until 510 s. After this, a mean speed comparable to the control treatment was observed. Cells in the control had a constant mean speed over the entire observation time (GAMM: $p_{\text{control}} = 0.04$, $p_{\text{diproline}} = < 2^{-16}$; Fig. 3b; Table S2). In the statistical test GAMM, each group (control and diproline) has a p -value. It shows the connectedness of each mean speed and compare it over the population mean for that group. In this case, because of random movement of cells that slow down, e.g., when they bump another cell, a statistically relevant p -value is also observed for the control though it is lower compared to the diproline treatment. When the model fit was plotted (Fig. S1), the speed values in the control did not deviate from 0, which is the population mean. On the other hand, the mean speed in the diproline treatment deviated from 0 and even showed an increasing pattern during the first 300 s. This analysis documents the effect of the pheromone on cell speeds. Cells did not have a directed orientation towards the bead as the calculated sine angle did not differ between control and diproline treatments (LME, $p = 0.38$; Fig. 4; Table S3). However, the calculated sum distance traveled by all the tracked cells showed that there is a preferential overall movement over time towards diproline gradients

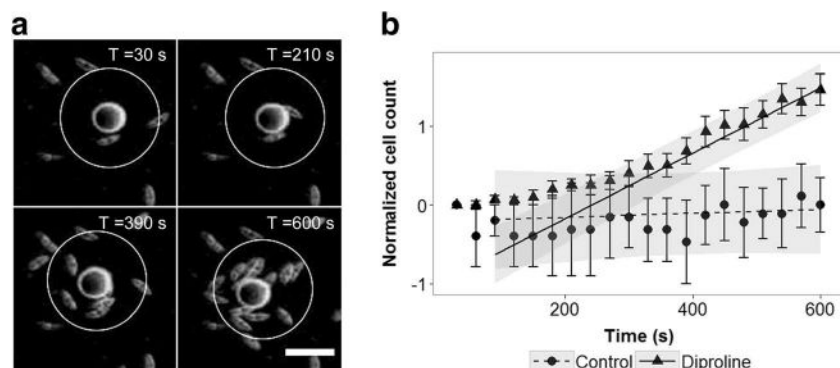


Fig. 2 Chemoattraction of *Seminavis robusta* mating type MT⁺ towards a diproline-loaded bead. **a** MT⁺ cells approach and accumulate around the bead. Scale bar = 50 μ m. **b** Significant increasing normalized cell density recorded every 30 s in the observation area (depicted as the circle in **a**) was observed over time when cells were exposed to diproline compared

(linear model, $p=1.147^{-11}$; Fig. 5; Table S4). This indicates that cells moved closer towards the diproline-bead over time compared to the control and that they bias their back and forth movement towards the pheromone gradient Fig. 6.

Track analysis via RMS fitting showed that cells significantly changed their swimming behavior around diproline-beads. There is a 4800-fold increase in decorrelation time scale (τ) as well as a 150-fold increase in length scale (λ) (Table 1) in the diproline treatment. This higher directional persistence over time also increased the diffusivity (D) and encounter kernel (β) by 6-fold indicating that cells increased their encounter rates for diproline-loaded beads by searching larger areas along the gradient for the pheromone source. The combined increase in cell speed and higher persistence resulted in a higher net distance traveled by cells towards diproline compared to the control (Wilcoxon rank sum test: $p=4.11^{-5}$; Fig. 5a), which was apparent also in the increasing root mean square distance traveled from 60 s until 410 s (Fig. 5b).

As a whole, we observed that cells moved faster with no angular orientation but with a preferred forward movement towards the pheromone source to accumulate around diproline-

beads. Cells also changed their swimming behavior by increasing directional persistence, leading to more frequent encounters with the pheromone-releasing beads compared to control beads.

Discussion

Microphytobenthic communities in intertidal environments and estuaries are primarily composed of raphid pennate diatoms [29] that have the ability to colonize mobile sediments and other niches [30]. Raphe systems emerged after the evolution of gametangiogamy as a life history strategy [30]. Gametangiogamy ensures a high success of pairing and prevents inbreeding in crowded benthic communities [30, 31]. Crucial to this is pairing efficiency that can be supported by species-specific pheromone perception and motility [31]. Thus, the pheromone-mediated mating system of raphid pennates might be one of the factors that helped these microalgae to colonize benthic habitats and to diversify as the youngest lineage of diatoms (90 Myr old) [32].

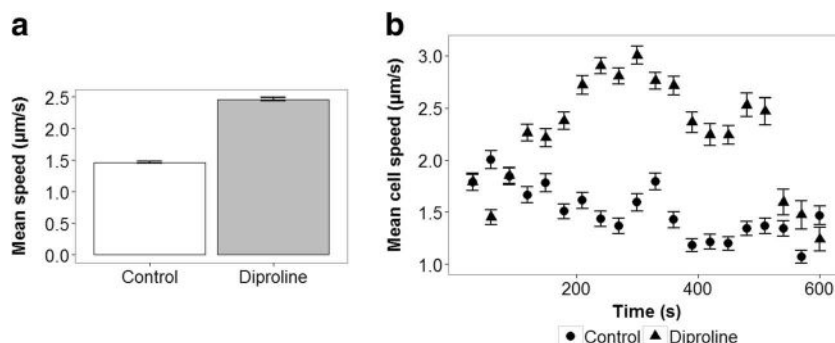


Fig. 3 Speed of MT⁺ cells exposed in the diproline gradient for 600 s. **a** The overall mean speed in the diproline treatment is significantly higher compared to the control (Wilcoxon rank sum test: $p<0.0001$). **b** The mean cell speed over intervals of 30 s from 60 to 600 s was taken and fitted using General additive mixed modeling (GAMM, Table S2,

Fig. S1). Cells moved faster over time when exposed to the pheromone gradient while there was approximately constant speed for cells in the control treatment (GAMM: $p_{\text{control}}=0.04$, $p_{\text{diproline}}=<2^{-16}$). Error bars indicate SE

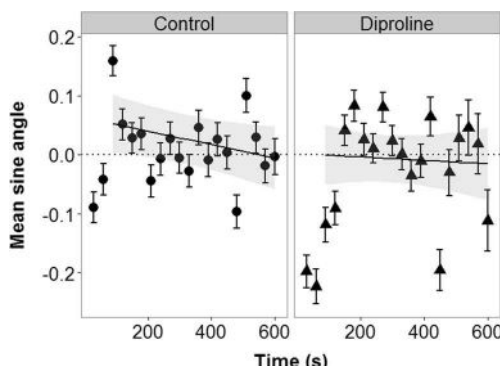


Fig. 4 The mean sine angle values of each cell's coordinate position relative to the position of the bead averaged over intervals of 30 s. A cell moving towards the bead has a positive value while a cell moving away has a negative value. Cells in the diproline treatment did not differ from the cells exposed to a control bead ($LME, p=0.38$). Shaded area represents the LME model fit from 60 to 600 s with 95 % confidence intervals (Table S3) and error bars indicate SE

This study identifies key features of the pheromone-mediated searching behavior of a benthic, raphid pennate diatom. Chemical analytics and organic synthesis allowed us to conduct the studies using a pure, synthetic pheromone. This allows excluding potential overlying effects of other signals as in previous studies where crude preparations were used [8, 33]. We determined that the concentration of diproline in the vicinity of pheromone loaded synthetic beads that elicit an attraction of the migrating *S. robusta* mating type (MT^+) are in the nanomolar range. To characterize how migrating cells respond to diproline, we categorized their movement patterns as taxis or kinesis. These two behavioral responses, chemotaxis and chemokinesis, are two processes that have to be discussed separately, even if they are sometimes interchanged in the literature. Chemotaxis is defined as the directed orientation towards chemical gradients whereas chemokinesis is the change in motility parameters such as turning frequency and speed in response to the presence of signal molecules in

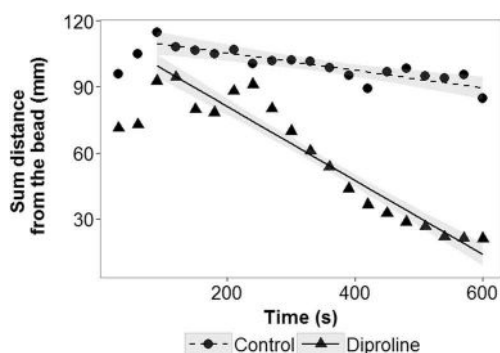


Fig. 5 The sum distance of all cell's coordinate position relative to the position of the bead was averaged over intervals of 30 s. The sum distance of cells in the diproline treatment significantly decreased over time, signifying that cells go nearer the bead compared to the control (linear model, $p=1.147^{-11}$). Shaded area shows the linear model fit from 60 to 600 s with 95 % confidence interval (Table S4) and error bars represent SE

sufficient concentrations [34, 35]. However, both behaviors can lead to accumulation or dispersal of cells in response to signal molecules [35]. The observed preferential migration towards the pheromone source is indicative for chemotaxis whereas changes in cell speed suggest chemokinesis. Successful mating involves pair formation of the opposite mating types. This process is supported by the increased encounter rates with the pheromone source through higher diffusivity (D) and encounter kernel (β) by MT^+ . Although the general concept of pheromone-mediated search behavior has been hypothesized or proven for different diatoms [8, 9, 36], attraction mechanisms seem to be species specific. When stationary female gametes of *T. fasciculata* are in close proximity of searching males, no guided attraction is observed, presumably due to a lack of chemical cue. As a consequence, males search randomly the area as the best strategy to maximize mate encounter [11]. On the other hand, mate-finding in male gametes of *P. trainorii* is pheromone-mediated and characterized by an initial random walk until the gamete is in close-range with the female. Gametes also change their shape from a globular form to an amoeboid one and form pseudopod thread-like extensions that can be used to catch mates [9]. In the case of *S. robusta*, diproline-mediated movement can be characterized as a biased random walk since there is no angular orientation but a clear orientation towards the pheromone source as exemplified by a preferential forward movement. Furthermore, a simultaneous tactic and kinetic mechanism is operative as a searching mechanism in MT^+ . Macroalgal gametes are known to employ either taxis or kinesis but, so far, a combination of both has not been observed [34, 35]. Marine bacteria, on the other hand, are known to employ simultaneous chemotaxis and chemokinesis in response to, e.g., amino acids [19] and coral hosts [37]. Since both marine bacteria and *S. robusta* move via a run-reverse or back and forth mechanism, it might be possible that this type of movement universally enables these cells to utilize taxis and kinesis simultaneously in response to stimulus [16, 37].

We recently reported that *S. robusta* does not only orient towards pheromone sources but that it also has the capability to sense and orient towards the inorganic nutrient dissolved silicic acid (dSi) [16]. Interestingly, the basic behavioral patterns are similar in response to both stimuli. However, when attraction patterns to dSi and diproline are compared, the response to a pheromone-gradient appears more efficient compared to the search for the nutrient. Since the methods employed on creating stimuli gradients and data analyses for the determination of the response towards dSi were similar to those in this study, we can directly compare the data sets (Table S2). In both cases, the *S. robusta* cell size used was below their species-specific sexual size threshold (SST, $51.6 \pm 0.5 \mu\text{m}$). When we compare the degree of change from control to dSi or diproline, a 1600-fold and 75-fold higher decorrelation time (τ) and length (λ) scales, respectively, are

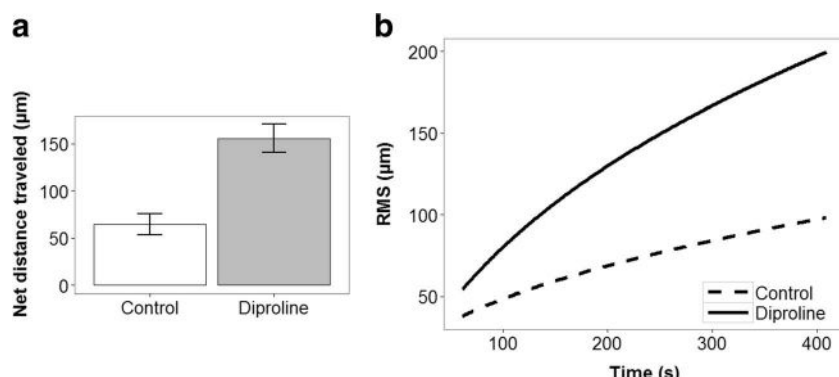


Fig. 6 The difference in the root mean square (RMS) distance traveled between cells in the control and diproline treatment from 60 to 410 s. **a** Cells exposed to the pheromone have 2.4× higher mean net distance

traveled (Wilcoxon rank sum test, $p = 4.11^{-5}$). **b** This is also apparent in the increasing RMS over time

observed when cells are exposed to diproline compared to dSi. Moreover, cells have higher encounter rates to diproline-beads compared to dSi-beads, as indicated by a 3-fold increase on diffusivity (D) and encounter kernel (β). However, such a quantitative comparison might be somewhat oversimplified, since it has to be considered that both responses are dependent on external factors influencing the behavioral response. These factors can include the level of starvation in the case of dSi limitation as well as the cell size or cell cycle stage in the case of pheromone-mediated finding. Cells under the influence of a pheromone gradient have the need to directly encounter the source to facilitate mating. Cell contact with the pheromone-producer is needed to start mate pairing. In contrast, cells exhibiting a foraging behavior for dSi would benefit from a continuous movement within the gradient to avoid diffusion limitation during dSi-uptake.

Dusenberry [38] predicted a cellular diameter of more than 0.6 μm to be a pre-requisite for the successful employment of chemical gradients. Mating *S. robusta* with cellular dimensions of 12–20 μm are clearly above this threshold and thereby fulfill the theoretical requirements for efficient chemotaxis. Our observations show that directed motility strongly increases mate encounters in these diatoms. *S. robusta* was able to detect diproline concentrations of 0.30–5 nM within a

radius of 250 μm . The active radius wherein pheromones can still be perceived has been estimated to 520 μm for aquatic gametes with a size in the micrometer range [39]. At this distance from the pheromone-loaded beads, the calculated steady state concentration is 0.24 nM, a concentration in the range eliciting an attraction response in our experiments (Fig. 1). The threshold concentration for planktonic flagellated brown algal pheromone reception is even lower, 1–1000 pM. This increased sensitivity could be seen as an adaptation to the wider area covered by their flagellated gametes [34, 35, 40, 41]. Initial evidence suggests that diproline is readily degraded after its release [8], which can be seen as a mechanism to avoid misleading information towards aged pheromone sources and to further increase the steepness of the gradient towards the attracting mating type. This additional aspect is not covered in our study using artificial pheromone sources. We also do not take into account that sex-inducing pheromones might synchronize the production of diproline within several cells of the attracting mating type [12]. This might result in additional patchiness of the pheromone landscape encountered by the searching partner. Interestingly, diproline is active in a concentration range over more than three orders of magnitude [8]. Thus, *S. robusta* can respond to diproline over a several hundred micrometer distance to the producer and still perceives the gradient in its immediate vicinity. Thus, only one signal is required for the entire finding process. Attracted cells can orient over this distance along the pheromone gradient by increasing speed and biasing a forward movement. No other signals are required during this mate finding process.

Table 1 Motility parameters of MT⁺ cells exposed to control and diproline-loaded beads

Parameter	Control	Diproline
N	28	29
τ (s)	0.01	47.40
λ (μm)	0.34	51.10
D ($\mu\text{m}^2/\text{s}$)	5.90	27.54
β ($\mu\text{m}^3/\text{s}$)	1112	5191

Calculated using Taylor's equation where N is number of tracks, τ is decorrelation time scale, λ is decorrelation length scale, D is diffusivity, and β is encounter kernel (observation area; 250 μm , observation time; 60–410 s)

Conclusion

Using semi-automated cell tracking as well as statistical modeling, we were able to show that the migrating mating type (MT⁺) of *S. robusta* is orienting towards a source of the pure synthetic pheromone diproline via a biased random walk mediated through simultaneous chemotaxis and chemokinesis.

This could be a characteristic pattern for cells exhibiting a back and forth motility. Cells showed a stronger response to the pheromone diproline compared to the searching behavior in a gradient of the limiting nutrient dSi. However, cells might prioritize one response above another when they are in different need of resources or reproduction. Though sexual reproduction itself is costly, the efficient search behavior explored in this study ensures that this strategy is effective.

Acknowledgments This work was supported by the Deutsche Forschungsgemeinschaft within the framework of the CRC 1127 ChemBioSys, the IMPRS Exploration of Ecological Interactions with Molecular and Chemical Techniques, the International Leibniz Research School for Microbial and Biomolecular Interactions, the Flemish Research foundation project TG.0374.11 N, and the Ugent research grants 01/04611 and BOF15/GOA/17.

References

- Field CB, Behrenfeld MJ, Randerson JT et al (1998) Primary production of the biosphere: integrating terrestrial and oceanic components. *Science* 281:237–240
- Yool A, Tyrrell T (2003) Role of diatoms in regulating the ocean's silicon cycle. *Global Biogeochem Cy* 17, GB1103
- Armbrust EV (2009) The life of diatoms in the world's oceans. *Nature* 459:185–192
- Sarthou G, Timmermans KR, Blain S et al (2005) Growth physiology and fate of diatoms in the ocean: a review. *J Sea Res* 53:25–42
- Chepurnov VA, Mann DG, Sabbe K et al (2004) Experimental studies on sexual reproduction in diatoms. *Int Rev Cytol* 237:91–154
- von Dassow P, Montresor M (2010) Unveiling the mysteries of phytoplankton life cycles: patterns and opportunities behind complexity. *J Plankton Res* 33:3–12
- Frenkel J, Vyverman W, Pohnert G (2014) Pheromone signaling during sexual reproduction in algae. *Plant J* 79:632–644
- Gillard J, Frenkel J, Devos V et al (2013) Metabolomics enables the structure elucidation of a diatom sex pheromone. *Angew Chem Int Ed Engl* 52:854–857
- Sato S, Beakes G, Idei M et al (2011) Novel sex cells and evidence for sex pheromones in diatoms. *PLoS One* 6, e26923
- Johansson BG, Jones TM (2007) The role of chemical communication in mate choice. *Biol Rev Camb Philos Soc* 82:265–289
- Edgar R, Drolet D, Ehrman JM et al (2014) Motile male gametes of the araphid diatom *Tabularia fasciculata* search randomly for mates. *PLoS One* 9, e101767
- Moeyns S, Frenkel J, Lembke C et al (2016) A sex-inducing pheromone triggers cell cycle arrest and mate attraction in the diatom *Seminavis robusta*. *Sci Rep* 6:19252
- Wang J, Cao S, Du C et al (2013) Underwater locomotion strategy by a benthic pennate diatom *Navicula* sp. *Protoplasma* 250:1203–1212
- Cohn SA, Halpin D, Hawley N et al (2015) Comparative analysis of light-stimulated motility responses in three diatom species. *Diatom Res* 30:213–225
- Cooksey B, Cooksey KE (1988) Chemical signal-response in diatoms of the Genus *Amphora*. *J Cell Sci* 91:523–529
- Bondoc KGV, Heuschele J, Gillard J et al (2016) Selective silicate-directed motility in diatoms. *Nat Commun* 7:10540
- Maier I, Calenberg M (1994) Effect of Extracellular Ca^{2+} and Ca^{2+} -antagonists on the movement and chemoorientation of male gametes of *Ectocarpus siliculosus* (Phaeophyceae). *Bot Acta* 107:451–460
- Gillard J, Devos V, Huysman MJ et al (2008) Physiological and transcriptomic evidence for a close coupling between chloroplast ontogeny and cell cycle progression in the pennate diatom *Seminavis robusta*. *Plant Physiol* 148:1394–1411
- Barbara GM, Mitchell JG (2003) Marine bacterial organisation around point-like sources of amino acids. *FEMS Microbiol Ecol* 43:99–109
- Berg HC (1993) Random walks in biology. Princeton University Press, Princeton
- Blackburn N, Fenchel T, Mitchell J (1998) Microscale nutrient patches in planktonic habitats shown by chemotactic bacteria. *Science* 282:2254–2256
- Schindelin J, Arganda-Carreras I, Frise E et al (2012) Fiji: an open-source platform for biological-image analysis. *Nat Methods* 9:676–682
- R Core Team (2015) R: a language and environment for statistical computing. R Foundation for Statistical Computing, Vienna
- Wickham H (2009) ggplot2: elegant graphics for data analysis. Springer Science & Business Media
- Pinheiro J, Bates D, DebRoy S et al (2015) *nlme*: linear and non-linear mixed effects models. vol R package version 3.1-121
- Wood SN (2011) Fast stable restricted maximum likelihood and marginal likelihood estimation of semiparametric generalized linear models. *J Roy Stat Soc B* 73:3–36
- Fenchel T (2004) Orientation in two dimensions: chemosensory motile behaviour of *Euploites vannus*. *Eur J Protistol* 40:49–55
- Visser AW, Kiorboe T (2006) Plankton motility patterns and encounter rates. *Oecologia* 148:538–546
- Underwood GJC, Kromkamp J (1999) Primary production by phytoplankton and microphytobenthos in estuaries. *Adv Ecol Res* 29: 93–153
- Sims PA, Mann DG, Medlin LK (2006) Evolution of the diatoms: insights from fossil, biological and molecular data. *Phycologia* 45: 361–402
- Edlund MB, Stoermer EF (1997) Ecological, evolutionary, and systematic significance of diatom life histories. *J Phycol* 33:897–918
- Bowler C, Allen AE, Badger JH et al (2008) The *Phaeodactylum* genome reveals the evolutionary history of diatom genomes. *Nature* 456:239–244
- Frenkel J, Wess C, Vyverman W et al (2014) Chiral separation of a diketopiperazine pheromone from marine diatoms using supercritical fluid chromatography. *J Chromatogr B Anal Technol Biomed Life Sci* 951–952:58–61
- Amsler CD, Iken KB (2001) Chemokinesis and chemotaxis in marine bacteria and algae. In: McClintock J. B. BBJ (ed) *Marine Chemical Ecology*. CRC Press, p 413–430
- Maier I (1993) Gamete orientation and induction of gametogenesis by pheromones in algae and plants. *Plant Cell Environ* 16:891–907
- Scalco E, Stec K, Iudicone D et al (2014) The dynamics of sexual phase in the marine diatom *Pseudo-nitzschia multiseries* (Bacillariophyceae). *J Phycol* 50:817–828
- Garren M, Son K, Raina JB et al (2014) A bacterial pathogen uses dimethylsulfoniopropionate as a cue to target heat-stressed corals. *ISME J* 8:999–1007
- Dusenberry DB (1997) Minimum size limit for useful locomotion by free-swimming microbes. *Proc Natl Acad Sci* 94:10949–10954
- Dusenberry DB (2000) Selection for high gamete encounter rates explains the success of male and female mating types. *J Theor Biol* 202:1–10
- Pohnert G, Boland W (2002) The oxylipin chemistry of attraction and defense in brown algae and diatoms. *Nat Prod Rep* 19:108–122
- Boland W, Pohnert G, Maier I (1995) Pericyclic reactions in nature: spontaneous Cope rearrangement inactivates alga pheromones. *Angew Chem Int Ed Engl* 34:1602–1604

Electronic Supplementary Material

Searching for a mate: pheromone-directed movement of the benthic diatom *Seminavis robusta*

Karen Grace V. Bondoc^{1,2}, Christine Lembke¹, Wim Vyverman³, Georg Pohnert^{1,2,*}

¹Institute for Inorganic and Analytical Chemistry, Bioorganic Analytics, Friedrich-Schiller-Universität Jena, Lessingstrasse 8, D-07743 Jena, Germany

²Max Planck Institute for Chemical Ecology, Hans-Knöll-Str. 8, D-07745 Jena

³Laboratory of Protistology and Aquatic Ecology, Department of Biology, University Gent, Krijgslaan 281 S8, 9000 Gent, Belgium

*For correspondence: Georg.Pohnert@uni-jena.de, Tel. +49 3641 948170

Supplementary Tables

Table S1 Results of Wald test on the linear mixed effects model (LME) fitted on cell count data (Control vs. Diprolime).

	numDF	denDF	F-value	p-value
(Intercept)	1	377	18.445	<0.0001
Treatment	1	29	7.7834	0.0092
Time	1	377	101.545	<0.0001
Treatment:Time	1	377	31.7424	<0.0001

Table S2 Approximate significant of smooth terms from the general additive mixed effects model on cell speed (Control vs. Diprolime).

	edf	Ref.df	F	p-value
s(Time):Control	6.444	6.444	2.321	0.0423
s(Time):Diprolime	6.245	6.245	24.550	<2.11 ⁻¹⁶

Table S3 Results of Wald test on the linear mixed effects model (LME) fitted on sine angle data (Control vs. Diproline).

	numDF	denDF	F-value	p-value
(Intercept)	1	20975	0.4180	0.5179
Treatment	1	58	1.280	0.2624
Time	1	20975	3.193	0.0739
Treatment:Time	1	20975	0.7635	0.3822

Table S4 Results of Wald test on the linear model (LM) fitted on sum distance (Control vs. Diproline).

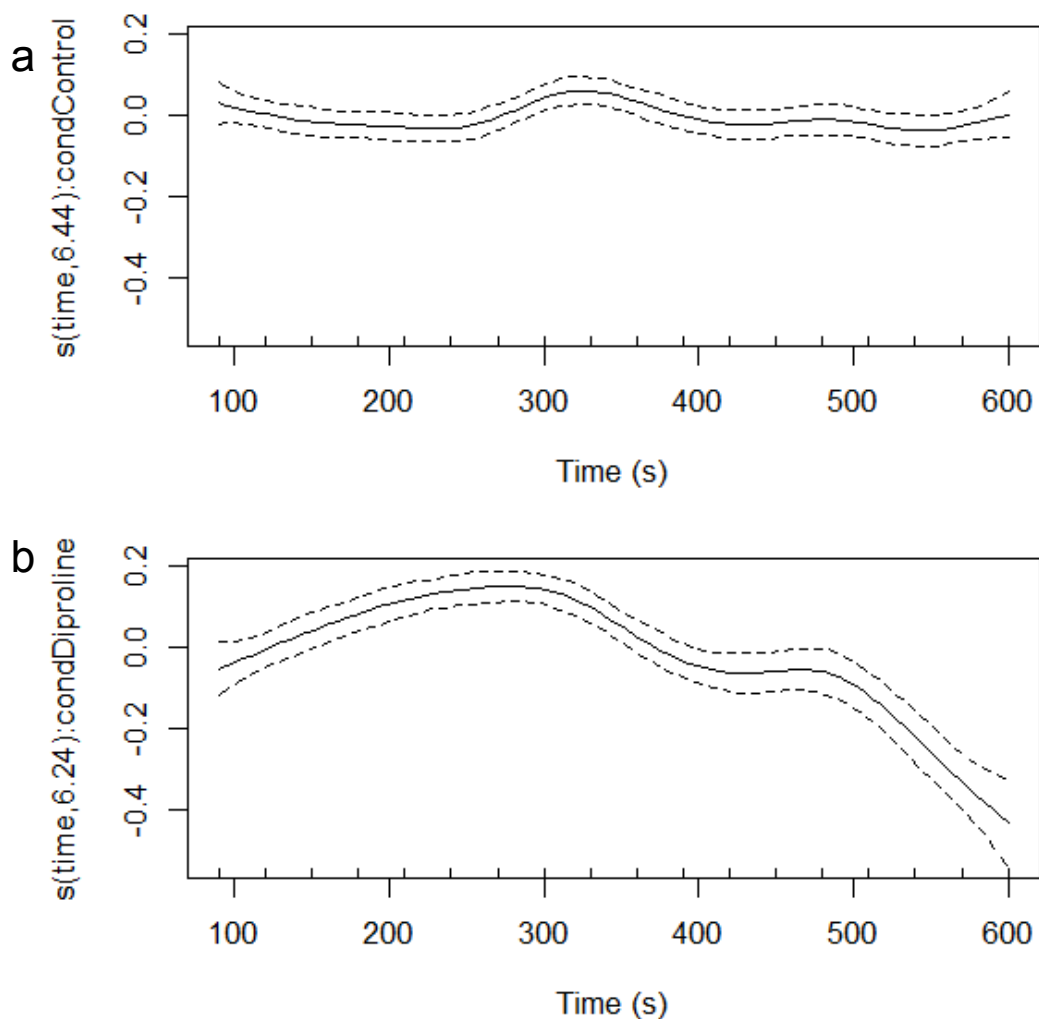
	DF	Sum Sq	Mean Sq	F value	p Value
Treatment	1	9403.1	9403.1	277.39	$<2.2^{-16}$
Time	1	16597.1	16597.1	489.62	$<2.2^{-16}$
Treatment:Time	1	3582.7	3582.7	105.69	1.147^{-11}
Residuals	32	1084.7	33.9		

Table S5 Motility parameters of cells exposed to control and dSi beads from Bondoc *et al.* [16]. Calculated using Taylor's equation where N is number of tracks, τ is decorrelation time scale, λ is decorrelation length scale, D is diffusivity and β is encounter kernel (observation area: 336 μm , observation time: 600 s).

Parameter	Control	Si
N	28	34
τ (s)	4.68	14.85
λ (μm)	10.70	23.86
D ($\mu\text{m}^2 \text{s}^{-1}$)	12.22	19.17
β ($\mu\text{m}^3 \text{s}^{-1}$)	8200	14900

Supplementary Figures

Fig. S1 Fitted cubic splines for speed data of control (condControl) and diproline (conDiproline) treatments over Time (60-600 s). The y-axis shows the optimal smoothing knot values (i.e. the number of connections of data point needed to explain the model) computed from the fitted model. GAMM models centers the mean of each treatment to 0.



Supplementary Movies

Movie S1 The movie shows the attraction and accumulation of *Seminavis robusta* MT⁺ cells towards the diproline-loaded bead. Cells repeatedly touch the bead as an attempt to pair. The movie was accelerated 50 times and the scale bar indicates 50 μm.

Movie S2 The movie shows that a control bead did not induce any reaction from *S. robusta* MT⁺ cells. The movie was accelerated 50 times and the scale bar indicates 50 μm.

3.3 Publication C

Bondoc, K.G.V., Lembke, C., J., Vyverman, W. & Pohnert, G. Food or Sex? Microbial decision-making by diatoms searching for nutrients and pheromones, Submitted at Proceedings of the National Academy of Sciences, Aug 2017.

Summary: Microorganisms encounter diverse and co-occurring stimuli in their environment. However, the factors affecting the decision-making of cells are rarely known. In this study, we focused on multiple stimuli which can trigger specific cell migration of benthic diatoms in biofilm communities. Their search behaviour under a nutrient limitation or sexual pressure is an excellent system to evaluate prioritisation mechanisms of microbes. Starved foraging cells can locate hotspot sources of silicate and phosphate, but not nitrate, through a simultaneous tactic and kinetic approach. We also observed a behavioural prioritization between silicate acquisition and mating on sexual cells, particularly when sexual pressure is high. Critically small-sized cells exhibit auto-induction, which could be a method to circumvent programmed cell death. Moreover, trace amounts of silicate were needed for pheromone attraction. Under different physiological conditions and life phase, the interplay between nutrient foraging and mate locating triggers specific motility patterns. The on-off switch for chemoattraction can potentially allow diatoms to exploit heterogeneous chemical signals to increase their ecological success, and explain the structuring of benthic biofilms.

Publication equivalents of contributing PhD students as coauthors according to the implementing provision of the doctoral regulations of the Faculty of Chemistry and Earth Sciences of the Friedrich Schiller University Jena

	Author 1: Bondoc	Author 2: Lembke
<i>Conception of the work</i>	X	X
<i>Planning of experiments</i>	X	X
<i>Data collection</i>	X	X
<i>Data analysis and interpretation</i>	X	X
<i>Manuscript writing</i>	X	X
<i>Proposed publication equivalents</i>	1	1

The supporting movies of this publication are available via the embedded compact disc.

Manuscript Approved (2017-15110).

Home Page for Georg Pohnert

Author Tasks

- [Instructions for Authors](#)
- [Submit Manuscript](#)
- [Check Manuscript Length Pre-Submission](#)
- [Live Manuscripts \(1\)](#)
- [Published Articles \(View usage and citation data\) \(1\)](#)

General Tasks

- [Modify Unavailability Dates](#)
- [Modify Profile/Password](#)
- [Logout](#)

Detailed Status Information

Manuscript #	2017-15110
Current Revision #	0
Submission Date	2017-08-25
Manuscript Title	Food or Sex? Microbial decision-making by diatoms searching for nutrients and pheromones
Manuscript Type	Direct Submission
Special Features and Colloquia	N/A
Classification	Biological Sciences/Ecology
Database deposition	
Comments for Editorial Staff	We would like to suggest Dr. Jerry Meinwald as handling editor since this manuscript deals with central aspects in Chemical Ecology - he is an expert.
Corresponding Author	Georg Pohnert (Friedrich Schiller University of Jena)
Co-Authors	Karen GV Bondoc , Christine Lembke , Wim Vyverman , Georg Pohnert (corr-auth)
Abstract	Microbes encounter diverse chemical stimuli in their environment that trigger individual responses. Microbial behaviour under the influence of multiple chemical signals is, however, poorly understood ... View full abstract
Significance Statement	Benthic diatoms are unicellular algae that dominate primary production in coastal biofilms worldwide. These biofilms represent highly complex environments in which cells encounter multiple stimuli. ... View full Significance Statement
Suggested Editorial Board Member	Jerrold Meinwald (Cornell University)
Suggested Editor	Jerrold Meinwald (Cornell University) -BOARD
Author Conflict of Interest	
Funding Body Archiving Mandates	No Funders
Preprint Server	Please let us know whether you have posted a version of your submission to a preprint server: No

Stage	Start Date
Quality Control Review Started	2017-08-25
Author Approved Submission	2017-08-25
Waiting for Author Approval of Converted Files	2017-08-25
Waiting for File Conversion	2017-08-25



FRIEDRICH-SCHILLER-
UNIVERSITÄT
JENA

Institut für Anorganische und
Analytische Chemie

Universität Jena · Institut für Anorganische und Analytische Chemie · 07737 Jena

Prof. Dr. Georg Pohnert
Institutsdirektor

Lessingstraße 8
07743 Jena

Telefon: 0 36 41 9-481 70
Telefax: 0 36 41 9-481 72
E-Mail: georg.pohnert@uni-jena.de

Jena, 25. August 2017

Dear Dr. Meinwald,

Please find enclosed our manuscript entitled “Food or Sex? Microbial decision-making by diatoms searching for nutrients and pheromones” where we use the unique opportunity offered by the unicellular microalga *Seminavis robusta* to study decision making and preferential motility of microorganisms. The ability of *S. robusta* to detect and orient towards multiple stimuli, such as sex pheromones and different nutrients, requires privileged responses. In our study we untangle at which state in their life cycle cells switch from foraging to mate locating behaviour and how this switch is dependent on the current requirements for nutrients and sexual reproduction. We develop a picture of cells that can find their way according to their needs within a complex environment structured by chemical signals. This study reveals an unprecedented complexity of microbial behaviour and demonstrates a surprising plasticity of the diatoms□ response. It thereby contributes substantially to our understanding of biofilm organisation.

Best regards,

Georg Pohnert

(on behalf of all co-authors)

1 **Food or Sex? Microbial decision-making by diatoms searching for nutrients and pheromones**

2

3 Karen Grace Verbo Bondoc^{1, 2, 4,*}, Christine Lembke^{1, 4}, Wim Vyverman³, Georg Pohnert^{1, 2, *}

4

5 ¹Institute for Inorganic and Analytical Chemistry, Bioorganic Analytics, Friedrich-Schiller-Universität
6 Jena, Lessingstrasse 8, D-07743 Jena, Germany

7 ²Max Planck Institute for Chemical Ecology, Hans-Knöll-Str. 8, D-07745 Jena

8 ³Laboratory of Protistology and Aquatic Ecology, Department of Biology, University Gent, Krijgslaan
9 281 S8, 9000 Gent, Belgium

10 ⁴ Co-first author

11 * Correspondence: karen.bondoc@gmail.com (K.G.V.B.); Georg.Pohnert@uni-jena.de (G.P.)

12

13 **Author contributions**

14 Conceptualization, K.G.V.B., C.L., W.V. and G.P.; Methodology, K.G.V.B. and C.L.; Formal
15 Analysis, K.G.V.B.; Investigation, K.G.V.B. and C.L.; Resources, G.P. and W.V.; Data Curation,
16 K.G.V.B. and G.P.; Writing - Original Draft, K.G.V.B., C.L., and G.P., Writing - Review & Editing,
17 K.G.V.B., C.L., W.V., and G.P.: Visualization, K.G.V.B. and C.L.; Supervision, G.P.

18

19

20 **Abstract**

21 Microbes encounter diverse chemical stimuli in their environment that trigger individual responses.
22 Microbial behaviour under the influence of multiple chemical signals is, however, poorly understood
23 and our information about microbial decision-making is limited. Particularly in biofilms, stimuli that
24 are highly variable in time and space require prioritizing. Benthic marine diatoms that react to sexual
25 attractants during part of their life cycle as well as to nutrient gradients face such complex scenarios.

26 Here, we document behavioural complexity and context-sensitive responses to sex pheromones and
27 nutrients of the motile unicellular model diatom *Seminavis robusta*. Throughout the life cycle, nutrient-
28 starved cells localize sources of silicate and phosphate, but not nitrate, by combined chemokinetic and
29 chemotactic motility. However, with increasing need for sexual reproduction, behavioural prioritisation
30 takes place, favouring the attraction pheromone-guided search for a mating partner above the search for
31 nutrients. In times of utmost requisite for sexual reproduction safeguard mechanisms, controlled by
32 synchronizing pheromones are abandoned and cells prioritize the orientation towards mating partners
33 above all. Such finely tuned selection processes help to explain biofilm organization and to understand
34 species interactions in these complex communities.

35

36 **Keywords:** diatoms, chemoattraction, nutrient acquisition, pheromones, biofilm

37

38 **Significance**

39 Benthic diatoms are unicellular algae that dominate primary production in coastal biofilms worldwide.
40 These biofilms represent highly complex environments in which cells encounter multiple stimuli. Here
41 we show that even a unicellular organism can make decisions and adjust its behavior under such
42 variable physical and physiological constraints. The motile diatom *Seminavis robusta* modifies its
43 behavior and prioritizes responses according to prevailing needs. If starved, the diatoms follow
44 gradients of the essential nutrients silicic acid and phosphate thereby locating optimum environments
45 for growth. However, once the cells are in need for sexual reproduction they shift their priorities and
46 respond to sexual stimuli. This study demonstrates a surprisingly complex microbial decision making
47 and helps to explain the often observed patchiness of biofilms.

48

49

50 **Introduction**

51 Diatoms are a species-rich group of silicifying microalgae responsible for about 20% of global carbon
52 fixation (1). As major primary producers in marine and freshwater ecosystems, they shape the aquatic
53 and global carbon and silicon biogeochemical cycles (2, 3). Pennate diatoms often dominate the soft
54 sediment substrata of aquatic habitats, forming benthic biofilms which can contribute substantially to
55 ecosystem productivity (4). These phototrophic biofilms typically represent a spatially heterogeneous
56 and dynamic environment and are characterized by strong and fluctuating gradients in physical
57 conditions and resource availability. Consequently, it can be hypothesised that diatoms populating
58 biofilms have evolved multiple strategies to maximize their fitness under such variable constraints (5,
59 6). Motile species, in particular, can rapidly respond to external cues, possibly contributing to
60 patchiness within biofilms (7, 8). Directional responses in many raphid pennate diatoms are enabled by
61 a characteristic forward and backward movement that is mediated by the excretion of adhesive
62 extracellular polymeric substances (9). Additionally, cells can undergo turning movements mediated by
63 pseudopod-like structures that temporary attach on the substrate (10).

64 The directed movement of gametangial cells is essential in the mating behaviour of motile diatoms
65 once they have entered the sexual phase of their life history (11). In brief, during cell division of
66 diatoms, each daughter cell inherits one part of the parental biomimeticized cell wall (theca) and forms
67 a new theca by precipitation of incorporated dSi. Since the formation of new thecae is occurring within
68 the parental cell, a gradual decrease in cell size of the diatom population is observed over time. When a
69 certain sexual size threshold (SST) is reached, cells of opposite mating types can pair and reproduce
70 sexually, resulting in auxospore formation, and subsequently in the development of large initial cells
71 that can again undergo repeated mitotic cell divisions (11-13). If sexual reproduction is not possible
72 (e.g. due to the absence of a mating partner), cells will typically die once below a critical minimal cell
73 size (13, 14). Whereas sexual reproduction is mainly triggered by environmental signals in centric
74 diatoms (13), pennate species employ elaborate pheromone systems to synchronize sexuality and to

75 attract mating partners (12, 15). Recently, a first diatom pheromone was identified as the L-proline-
76 derived diketopiperazine (in the following abbreviated as diproline) in *Seminavis robusta* (16). It
77 mediates the chemoattraction of cells of the Mating Type⁺ (MT⁺) to the corresponding diproline-
78 producing Mating Type⁻ (MT⁻) cells. Analysis of the attraction of *S. robusta* towards diproline sources
79 revealed that the cells use a chemotactic and chemokinetic movement to approach a pheromone source
80 (17). Diproline production and perception capabilities are synchronized by Sex-Inducing Pheromones
81 (SIP) that are released by the respective mating types once they reach the SST (16, 18). Whereas
82 motility aids in the location of mating partners, it can also be induced by other environmental cues. A
83 significant body of research has demonstrated the role of motility in the response of biofilm-forming
84 diatoms to photoperiod, light quality and tidal cycles (19, 20).

85 Nutrients including nitrogen, phosphorous can limit the growth of diatoms in benthic biofilms (21-23).
86 However, also dissolved silicate (dSi), a resource for the formation of the biomineralized cell walls of
87 diatoms, is a common limiting factor for diatom growth (13, 24). While the general effect of nutrient
88 limitation on diatom growth and metabolism has been intensively studied, little is known about their
89 behavioural response towards gradients of such resources. Recently we could show that in addition to
90 the orientation towards sexual stimuli, *S. robusta* is also attracted to point sources of dissolved silicate
91 (dSi). Interestingly, both search behaviours follow similar chemotactic and chemokinetic patterns (25).
92 In this contribution, we explore for the first time how diatoms respond to multiple chemical cues. We
93 studied the behavioural response of *S. robusta* to localized sources of other essential nutrients,
94 including dissolved nitrogen in the form of nitrate or ammonium (dN) and dissolved phosphate (dP) to
95 investigate their general capability to locate nutrient hotspots. We then set out to examine how
96 responses towards dSi and the attraction pheromone are manifested under different environmental and
97 physiological constraints to elucidate the process of microbial decision making. Diatoms prioritize the
98 search for pheromones above that for dSi in cases where cell size was close to the critical size required
99 for survival. In contrast, cells that just recently crossed SST preferred dSi over pheromones. Our data

100 provide new insights into biofilm organization and function and suggests that searching behaviour
101 depends on life cycle state, induction by SIPs, as well as on the strength and nature of competing
102 attractors.

103

104 **Results**

105 ***Cell growth and nutrient limitation***

106 For the systematic comparison of the effects of nutrient limitation, growth and nutrient usage of *S.*
107 *robusta* was analysed (Figure S1). We followed *S. robusta* batch cultures of small-sized cells (24-27
108 µm, strain PONTON 36) in artificial seawater (ASW) medium and documented their nutrient use (dSi,
109 dP, and dN in NO₃⁻ form) over seven days. Nutrient analysis revealed that the limiting factor was dSi,
110 which was below the 1 µM detection limit during the stationary phase. In contrast, dN and dP
111 concentrations were not limiting (in stationary phase dN remained present at ~60% of the initial 621
112 µM concentration and dP ~40% of the initial 15 µM concentration) (Figure S1A). To elucidate the
113 effects of limitation, we performed studies using the same ASW medium but without the addition of
114 the particular nutrient under investigation. Cells starved in dSi did not grow even in the presence of
115 excess dN and dP while cells in dP depleted medium continued to divide for four days. Cells in dN-
116 starved cultures also increased in cell density, albeit, at a lower rate than dP-starved and control
117 treatments (Figure S1B, Table S2). To fully deplete cellular nutrient stores from the cells, medium from
118 batch cultures was exchanged with fresh medium supplemented with all nutrients except for the
119 limiting one every other day. The treatment was repeated until no further growth was observed after 3,
120 5, and 12 days of starvation for dSi, dP and dN, respectively. Aliquots of these cultures were
121 transferred to artificial sea water containing the full amount of nutrients (ASW) and growth was
122 monitored to determine cell recovery. Within seven days, cell densities increased 100-, 12-, and 6-fold
123 after addition of dSi, dP, and dN, respectively, highlighting survival and recovery capabilities (Figure
124 S1C, Table S2).

125

126 ***Attraction of starved cells within nutrient gradients***

127 We tested if nutrient-starved cells can locate hotspot sources in attraction assays. Therefore aluminium
128 oxide (alox) particles that do not elicit any response in the diatoms (25) were loaded with the particular
129 nutrient. Nutrient loading was achieved by evaporating a solution of the individual nutrients in the
130 presence of a pre-determined amount of beads as explained in the materials and methods section. These
131 beads release nutrients generating a steep gradient in their vicinity. As with prior experiments (25), dSi-
132 starved cells were attracted to dSi-loaded beads within a 10 min observation time (Figure 1, Movie S1).
133 Using the same methods, we tested the attraction of dP and dN-starved cells to beads loaded with
134 phosphate, nitrate, or ammonium. While dP-starved cells were attracted to dP-loaded beads (0.72 nmol
135 dP per bead) within ~20 min (Figure 2, Movie S2), dN-starved cells did not orient towards dN-loaded
136 beads (0.54 nmol dN per bead) (Figure 1), regardless of the dN form (NO_3^- , NH_4^+) used (Movies S3
137 and S4).

138

139 ***Characterization of chemoattraction to dP-loaded beads***

140 To characterize the response of *S. robusta* to dP, we first determined if cell motility is regulated by dP
141 availability (Figure 2A). After five days of dP starvation, cell speed increased 3-fold compared to non-
142 starved cells. Clearly, this change in motility is resource-dependent since one hour after addition of dP
143 to such starved cultures, cell motility significantly decreased to levels comparable to non-starved
144 cultures. The control treatment with the addition of dP-deplete medium did not significantly alter cell
145 speed (Figure 2A, Table S3). This marked change in speed in response to dP is a hallmark of
146 orthokinesis, wherein the speed is regulated by the concentration of the chemical cue that the organism
147 encounters (26). To characterize the response to dP-gradients, we analysed the movement of dP-starved
148 cells and their orientation towards dP loaded beads using video monitoring. The experimental set-up
149 and data collection permit a systematic comparison with the orientation within dSi or pheromone

150 gradients (17, 25). Tracking data of dP starved cells exposed to dP-loaded (Movie S2) and control
151 (Movie S5) beads were recorded over 1 h. To analyse cell behaviour in dP gradients, the observation
152 area (total radius: 336 μm) was divided into three equidistant concentric circles called bins A-C with
153 the bead in the middle (Figure 1). Within ca. 7 min, the dP-loaded bead generated a gradient with a
154 local concentration of 45 μM at the surface of the bead to 3 μM at the limit of the observation area
155 (Figure S2). Increased accumulation around the bead was evident after \sim 20 min exposure (Figure 2b,
156 Table S4). Compared to the control, an increasing cell density over the entire observation time was
157 observed for Bin A. In Bin B, cell density increased as well during the first 30 min and later a plateau-
158 phase was reached (30-60 min). In Bin C, cell density did not statistically differ from the control. These
159 data indicate an overall migration of cells into the observation area over the entire experiment.
160 Additionally, the mean distance relative to the bead of cells in Bins B and C decreased, confirming that
161 exposure to dP triggers an approach indicative for a tactic mechanism (Figure 2D, Table S6). Cells in
162 proximity to dP-loaded beads increased their motility, more than doubling their speed after 45 min
163 exposure. Meanwhile, cell speeds in the control treatment were variable and overall lower with no
164 distinct pattern throughout the observation period (Figure 2C, Figure S3, Table S5). The observed
165 behaviour implies that cells adapt towards a dP source by regulating their speed and by directing their
166 movement towards it through simultaneous taxis and kinesis.

167

168 ***On/off switch of nutrient and mate searching behaviour***

169 Once below the sexual size threshold, *S. robusta* MT⁺ cells can also exhibit a searching behaviour
170 towards the sex pheromone diproline (16, 17). Given the constraints of the need for nutrients and the
171 finding of sexual partners, diatoms are challenged to locate different chemical signals in a patchy
172 environment. We hypothesized that diatoms could prioritize between different stimuli depending on
173 their nutrient requirements and readiness for sexual reproduction. To test this hypothesis, we focused
174 on the two most prominent behavioural responses towards pheromones and dSi. In previous

175 experiments, a clear priority of large-sized cells was observed, which are attracted to dSi once starved
176 (Figure S4, Table S10) but do not respond to pheromones even when treated with SIP (16).
177 Prioritization of responses of cells below the sexual size threshold was more complex than vegetative
178 cells. Thus, cell size, the state of SIP-mediated sex-induction as well as the degree of starvation has to
179 be taken into account. Therefore, we tested all possible combinations of starvation and induction in
180 small and intermediate-sized cells. Diproline or dSi releasing beads were applied to these cells, and
181 attraction was monitored by determining the cell density for 10 min within a radius of 115 µm around
182 the beads (Figure 4).

183 Medium-sized MT⁺ cells only accumulated around diproline beads if the two conditions nutrient
184 repletion and SIP induction were fulfilled. Under dSi limitation, no response to the attraction
185 pheromone was observed even if cells were induced with SIP. Conversely, SIP-induced medium-sized
186 MT⁺ cells were not attracted to dSi beads when dSi-starved (Figure 4A, Table S7). This underlines that
187 dSi starvation could interfere with mate searching behaviour.

188 Small-sized cells have a more pronounced response to diproline. If grown under dSi replete conditions,
189 accumulation around diproline-loaded beads was evident even when cells were not induced by the SIP
190 (Figure 3B, Table S8). This auto-induction of small-sized cells suggests an additional cell size-
191 dependent switch towards a mate searching behaviour once a critical minimal cell size is reached. In
192 contrast to the medium-sized cells, attraction towards diproline was also evident when small cells were
193 dSi starved. However, this behaviour was only observed when cells were induced with SIP. Only under
194 the combination of adverse conditions, dSi starvation and a lack of SIP induction, no response to
195 diproline was observed. It should be noted that small amounts of dSi (~ 50 µM) were carried over
196 during SIP induction, as this had to be done through the addition of spent medium from exponentially
197 growing cultures of the opposite mating type. However, since cells slowed down but remained motile
198 in the treatment, no substantial interference with the assay can be expected (Figure S5, Table S11).

199 **Choice assays**

200 To investigate potential selection behaviour, we performed choice experiments with dSi-starved small
201 cells that were either induced or non-induced with SIP. Both dSi and diproline-loaded beads were
202 applied simultaneously to each well, and the accumulation around the beads, as well as movement
203 patterns from track data, were analysed. Consistent with our one-bead experiments, starved cells were
204 attracted towards diproline beads when induced and to dSi beads when not induced after both point
205 sources were applied (Figure 3B, Figure 4A, Movies S6 and S7, Table S8). Within the 10 minute
206 observation period, no switch towards mate finding could be observed. We determined the mean cell
207 speed around the beads and outside the bead area. Cells moved significantly faster when they were
208 around the stimuli that they were attracted to, increasing their speed two-fold (Figure 4B, Table S9),
209 indicative of an orthokinetic response (17).

210

211 **Discussion**

212 Microorganisms are known to contribute to micro-scale community structure by selecting suitable
213 microhabitats and by exploiting ephemeral and spatially varying nutrient sources. Additionally, the
214 location of mating partners or avoidance of competitors can be guided by the perception of chemical
215 stimuli (7, 8). Migration towards chemical attractors is an important mechanism underlying many of
216 these strategies. This searching behaviour can be mediated by either taxis or kinesis. In the former, a
217 directed movement is observed, whereas, in the latter, distinct changes in the motility patterns such as
218 speed or turning frequency are evident (26). While movement patterns in response to single chemical
219 factors are well understood, we know little about the behaviour of microorganisms under the influence
220 of multiple stimuli. We introduce here the benthic diatom *S. robusta* as a model for behavioural studies
221 in microorganisms since its response towards nutrients and pheromones can be triggered independently
222 and easily monitored. Here, movement patterns of vegetative and sexual cells of different sizes and
223 degrees of induction were monitored under the influence of macronutrients (dSi, dP, and dN), and the

224 attraction pheromone diproline. Our results offer a first insight into the behavioural response of this
225 species to multiple chemical signals and nutrient gradients throughout its life cycle.

226 We have previously shown that small dSi-starved *S. robusta* cells exhibit an active searching behaviour
227 to gradients of this mineral acid (25). In this study, this type of behaviour was also observed in
228 medium- and large-sized cells (Figure 3, Figure S4) indicating a universal response of cells towards
229 this stimulus throughout the life cycle (27). We also determined if dP and dN-starved cell exhibit
230 finding behaviour as well, when exposed to hotspot sources of the particular nutrients. While *S. robusta*
231 was insensitive to dN gradients, a clear searching behaviour towards dP sources could be observed
232 (Figures 1 and 2). This might be interpreted in light of the fact, that both, dSi as well as dP are released
233 from mineral sources in the sediment and will thus occur as patchy resources (28). Since diatoms can
234 be outcompeted by bacteria in taking up dP, the observed directed dP-foraging mechanism might allow
235 them to compensate for this disadvantage by the location of hotspots (29). To date, chemotaxis to dP
236 sources has only been observed for the planktonic dinoflagellate *Chattonella antiqua* (30) and the
237 planktonic bacterium *Thalassospira sp.* (31). The speed of dP starved *S. robusta* is under the influence
238 of bulk amounts or diffusing gradients of this resource. The increased motility in dP depleted medium
239 might be explained as an increased readiness to relocate under adverse conditions, as it was also
240 observed in the case of dSi depletion (25). In a dP gradient, movement during the finding process is
241 adjusted by increasing speed, as well as by taking more or longer forward steps towards the dP-loaded
242 bead as compared to the control. While universally favourable conditions simulated by the addition of
243 bulk amounts of dP lead to an overall lower motility, gradients of the resource trigger an increased
244 motility and search behaviour. The observed combined chemokinesis and chemoattraction enable dP-
245 starved cells to locate dP sources efficiently. Although the general patterns of the behavioural response
246 of *S. robusta* to dP, dSi, and diproline are similar, the response to dP was slower, with chemoattraction
247 starting only after ~20 min exposure, as compared to the fast attraction to dSi within ~5 min (17). Since

248 the diffusibility of dP, as well as dSi, is similar, this variable response time could be due to differences
249 in nutrient sensing and uptake mechanisms and how this activates motility in the cells under limitation.
250 The lack of attraction to dN is surprising since this resource is occurring in steep vertical concentration
251 gradients in the environment of *S. robusta* (32). Capabilities for dN resource location has been reported
252 for other algae. The flagellated planktonic chlorophytic alga *Dunaliella tertiolecta* is attracted to NH₄⁺
253 ions (33) and vegetative pre-gametes of *Chlamydomonas reinhardtii* exhibit chemotaxis towards NH₄⁺
254 (34, 35), NO₃⁻ (36), and NO₂⁻ (37). However, since diatoms and green algae respond fundamentally
255 different to dN starvation, the situation might not be comparable. Under nitrogen limitation, green
256 algae increase their carbon stores to produce lipids while diatoms remobilize carbon sources (38-41).
257 Since diatom movement is mediated by the excretion of mucus, such metabolic reprogramming might
258 reduce the tendency for displacement and explain the lack of dN responsiveness.

259 The finding behaviour within a gradient of the pheromone diproline is strongly dependent on cell size
260 and priming by SIP. Large cells above the SST do not respond to diproline even under the influence of
261 SIP, while cells that crossed the SST are attracted to this pheromone (16). Comparison of two
262 independent data sets led to the speculation that *S. robusta* has greater behavioural adaptation to the
263 pheromone gradient as compared to dSi (17). Here, we systematically addressed the influence of cell
264 size, induction, and nutrient limitation on the response of diatoms to different stimuli to evaluate if and
265 how cells select for specific responses. In cells just below the SST, only under favourable conditions
266 (nutrient availability and priming by a sex inducing factor), a search behaviour for partners is initiated.
267 This changes when small cells near the minimal critical size are considered. These cells would die if no
268 cell size restoration by sexual reproduction would occur and further mitotic cell divisions would reduce
269 their size (42). Under nutrient replete conditions, these cells do not require induction by SIP to orient
270 towards the attraction pheromone diproline, thereby exhibiting a self-priming behaviour. The observed
271 increased readiness for mating behaviour might explain that a reduced cell size is correlated with a
272 higher reproduction success in mating *S. robusta* (43). The auto-induction mechanism represents a

273 breach in the highly orchestrated synchronization of sexual reproduction in *S. robusta* and might be
274 considered as an emergency mechanism to prime sexuality in the face of clonal death.

275 In the case where *S. robusta* faces more than one constraint, again a shift in the responsive behaviour is
276 observed. Under dSi starvation, self-induction of the diproline-searching behaviour of small cells is not
277 initiated. Since cell proliferation only occurs when dSi is available (Figure S1), guidance to a mating
278 partner might not be efficient since no resource for the formation of the novel cell wall after pairing
279 would be available. Instead, priority for dSi acquisition would be a logical consequence. This priority is
280 also supported in the choice experiment where dSi-starved, not induced small cells still responded to
281 dSi beads and not to diproline within a 10 min observation time.

282 Multiple stimuli integration is not unknown for microorganisms but has till now been reported to occur
283 on a transcriptomic and not a behavioural level. In the case of the yeast *Saccharomyces cerevisiae*, for
284 example, a mating response pathway can only be induced by a hormone under nutrient repletion⁴². In a
285 recent study on the transcriptomic changes of the diatom *Pseudo-nitzschia multiseries*, nutrient
286 transporters and cyclins involved in sensing the nutritional status were downregulated during sexual
287 reproduction, suggesting the existence of a complex interplay between nutrient uptake and sexual
288 response (44). In contrast, our choice assays in *S. robusta* show an immediate response that requires
289 different reception processes for the respective stimuli and the ability to respond in a directed
290 orientation. If also here a signalling pathway crosstalk between dSi-sensing and mating on a
291 transcriptome level is involved has to be further explored. Initial evidence for such a process is
292 emerging from the observation that both dSi limitation and SIP induction can arrest the cell cycle in the
293 G1/S phase (18) and that secondary messenger cyclic nucleotides (cAMP or cGMP) may play a role in
294 both pheromone perception and motility (44, 45). Future research should thus focus on the regulatory
295 signalling pathways within the diatom cell and how they interact to maximize survival and fitness in a
296 heterogeneous environment and during interaction with other species.

297 Our work provides first insights into the behaviour of pennate diatoms across their life cycle and
298 underscores the adaptations to exploit small-scale nutrient and pheromone gradients in their benthic
299 habitat. This active directed motility may have been a major mechanism underlying the rapid
300 diversification and ecological success of pennate diatoms.

301

302 Materials and Methods

303 *Strains, maintenance of stock cultures, and microscopy*

304 We used the *Seminavis robusta* strains MT⁺ (85A and PONTON36) and MT⁻ (84A), which are
305 maintained in the BCCM/DCG diatom culture collection at Ghent University
306 (<http://bccm.belspo.be/about-us/bccm-dcg>). The strains used had different cell sizes in apical length
307 below and above the sexual size threshold (SST, ~ 50 µm)(16). We classified them as small- (24-27
308 µm), medium- (~ 40 µm), and large-sized cells (>50 µm). For microscopic observations, photography
309 and video recording an inverted Leica DM IL LED microscope (Heerbrugg, Switzerland) mounted with
310 a Nikon DS-Fi2 CCD camera (Tokyo, Japan) recording 100 fps was used. Additional information is
311 given in *SI Materials and Methods*.

312

313 *dP, dN and dSi starvation*

314 Small sized MT⁺ (PONTON36) stock cultures were inoculated (1/10 v/v) into 25 ml ASW
315 where no dSi, dN, or dP was added but which was supplemented with all other nutrients. Every second
316 day, dN or dP-depleted medium was exchanged to avoid that other nutrients become limited. Due to
317 slow growth, this exchange was not required for the dSi-limited cultures. After culturing under limited
318 condition (3 days for dSi limitation, 5 days for dP limitation, or 12 days for dN limitation), cells were
319 used for motility and attraction studies. Cells grown in ASW served as a control. 24 h before video
320 monitoring cells were scraped off from the culture flask and aliquots of 2 ml were transferred into 12-
321 well plates (Sarstedt, Nümbrecht, Germany).

322

323 ***Monitoring of motility under the influence of dP***

324 dP-limited cells in 12 well plates were grown for 24 hours, and the medium was exchanged
325 with either dP-depleted or full ASW medium. As a control, non-starved cells were used. Motility of the
326 cells was monitored before and 1 h after medium exchange by taking 60 s movies per well.

327

328 ***Bead preparation and monitoring of diatom motility and chemoattraction***

329 For nutrient limitation experiments, bead preparation and attraction assays were modified after
330 Bondoc et al.(25). To 100 mg aluminium oxide beads (Merck, Darmstadt, Germany; 90 active neutral;
331 0.063-0.200 mm) either 800 µl of 440 mM Na₂SiO₃ · 9 H₂O, 200 µl of 670 mM NaNO₃ or NH₄Cl, or
332 800 µl of 225 mM KH₂PO₄ were added and dried overnight at 60 °C, resulting in 1.40 nmol dSi, 0.54
333 nmol dN, and 0.72 nmol dP per bead, respectively. Control beads were correspondingly prepared using
334 water. Loading success and release rates were monitored as described in the supporting information.
335 Aliquots of beads (~30 beads per well) were carefully introduced using a spatula to cells starved with
336 dSi, dN, or dP for 3, 5, and 12 days, respectively, and attraction was monitored for 1 h.

337

338 ***Attraction and choice assays with dSi- and L-diproline-loaded beads***

339 L-diproline-loaded beads were prepared modified after Gillard et al.(16). Onto 10 mg HLB
340 cartridges (Oasis®, Waters, Eschborn, Germany), 2 ml of 20 µM L-diproline in deionized water was
341 loaded according to the user's manual. The material was rinsed with 1 ml ddH₂O, the cartridge was
342 opened by removing the top plate with a needle, and the material was washed out of the cartridge with
343 2 ml ddH₂O, yielding a suspension of 5 mg beads per ml and 4 nmol L-diproline per mg bead.

344 Attraction assays were modified from previous studies(16, 17). One ml aliquots of small- and
345 medium-sized 7-day old stock cultures of 85A (MT⁺) were transferred into 12-well plates, and 2 ml of
346 either fresh ASW or dSi-depleted medium was added. Cells were grown for 2 days before cell-cycle

347 synchronization by prolonging the dark period to 36 h(46). For induction, 1 ml of SIP-containing
348 medium (prepared from 84A (MT⁻) cultures that were sterile-filtered during the late exponential growth
349 phase) was added into each well of MT⁺ culture before illumination. The attraction and choice assays
350 were carried out 6 and 8 hours after the onset of illumination for small- and medium-sized cells,
351 respectively. Aliquots of <30 dSi beads or 5 µg of L-diproline-loaded beads were added to each well
352 and the movement of the cells was monitored for 10 min. For choice assays, both beads were applied
353 simultaneously.

354

355 ***Video and Statistical Analyses***

356 Movies for counting and tracking were re-processed from 100 fps to 1fps using VirtualDub
357 (<http://virtualdub.org/>) and Fiji. The open-source tracking plug-in, TrackMate
358 (<http://fiji.sc/TrackMate>)(47) was used in automatic mode for all experimental sets except for dP
359 attraction, wherein a semi-automatic tracking with spot checking and track correction was done to
360 precisely determine distinct movement patterns. Automatic tracking parameters of the simple LAP
361 tracker were first optimized on an individual movie before using it for the whole experimental data set.
362 All data analyses were done under the open-source statistical program R v. 3.3.1(48) with the packages
363 ggplot2(49) for plotting, nlme(50) for linear mixed effects (LME) modelling, and mgcv(51) for general
364 additive mixed modelling (GAMM). Additional information is given in *SI Materials and Methods*.

365

366 **Acknowledgements**

367 This work was supported by the Volkswagen Foundation, the Max Planck Institute for Chemical
368 Ecology, the IMPRS Exploration of Ecological Interactions with Molecular and Chemical Techniques,
369 the Richard-Winter-Stiftung, the International Leibniz Research School for Microbial and
370 Biomolecular Interactions, the CRC1127 ChemBioSys, the Flemish Research foundation project

371 TG.0374.11N and the Ugent research grants 01/04611 and BOF15/GOA/17. We thank Emilio Cirri for
372 providing and maintaining some of our diatom cultures.

373

374 **References**

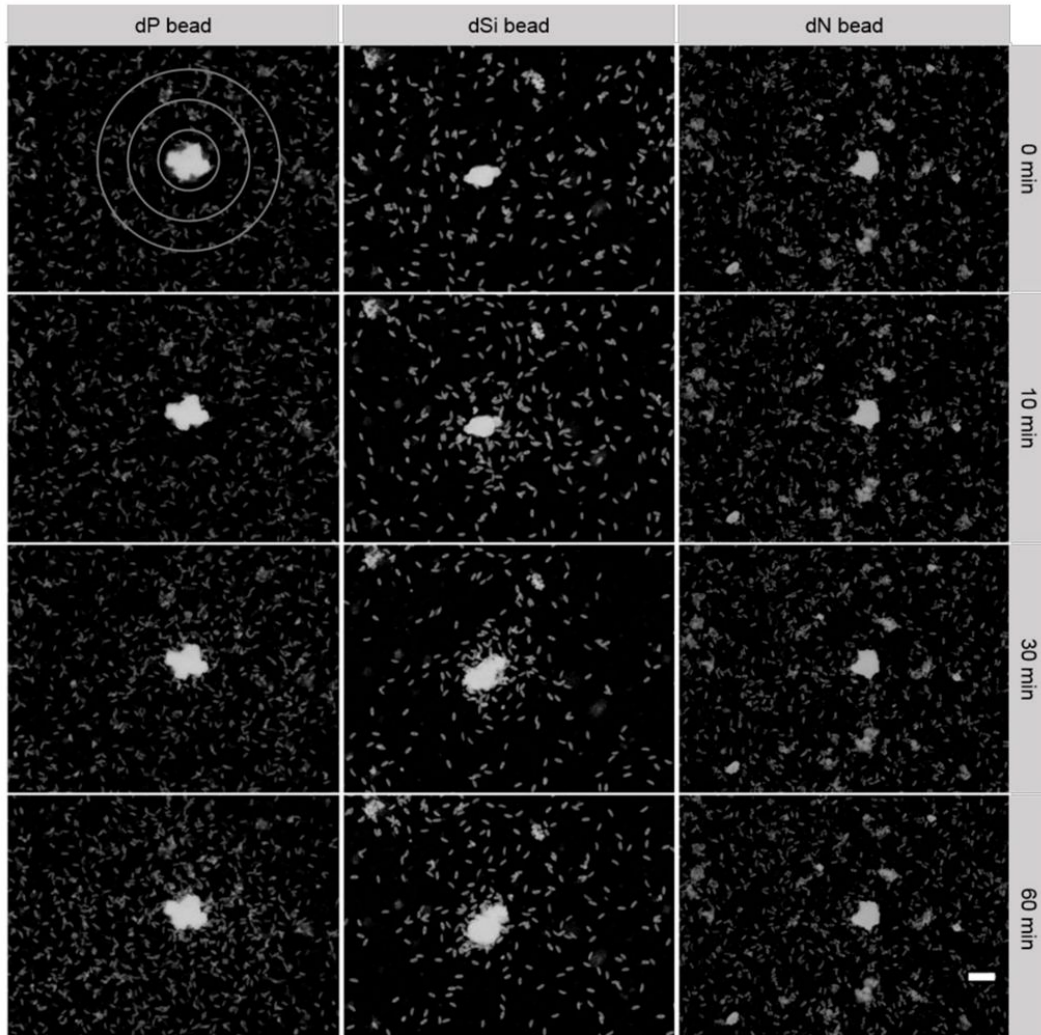
- 375 1. Field CB, Behrenfeld MJ, Randerson JT, Falkowski P (1998) Primary production of the
376 biosphere: Integrating terrestrial and oceanic components. *Science* 281(5374):237-240.
- 377 2. Treguer PJ, De La Rocha CL (2013) The world ocean silica cycle. *Annu Rev Mar Sci* 5:477-501.
- 378 3. Wang BL, Liu CQ, Maberly SC, Wang FS, Hartmann J (2016) Coupling of carbon and silicon
379 geochemical cycles in rivers and lakes. *Sci Rep* 6, 35832.
- 380 4. Underwood GJC, Kromkamp J (1999) Primary production by phytoplankton and
381 microphytobenthos in estuaries. *Adv Ecol Res* 29:93-153.
- 382 5. Barnett A, *et al.* (2015) Growth form defines physiological photoprotective capacity in
383 intertidal benthic diatoms. *ISME J* 9(1):32-45.
- 384 6. Magni P, Montani S (2006) Seasonal patterns of pore-water nutrients, benthic chlorophyll a and
385 sedimentary AVS in a macrobenthos-rich tidal flat. *Hydrobiologia* 571:297-311.
- 386 7. Seymour J, Marcos, Stocker R (2008) Resource patch formation and exploitation throughout the
387 marine microbial food web. *Am Nat* 173(1):E15-E29.
- 388 8. Stocker R (2012) Marine microbes see a sea of gradients. *Science* 338(6107):628-633.
- 389 9. Molino PJ, Wetherbee R (2008) The biology of biofouling diatoms and their role in the
390 development of microbial slimes. *Biofouling* 24(5):365-379.
- 391 10. Wang JD, Cao S, Du C, Chen DR (2013) Underwater locomotion strategy by a benthic pennate
392 diatom *Navicula sp.* *Protoplasma* 250(5):1203-1212.
- 393 11. Chepurnov VA, *et al.* (2008) In search of new tractable diatoms for experimental biology.
394 *Bioessays* 30(7):692-702.

- 395 12. Frenkel J, Vyverman W, Pohnert G (2014) Pheromone signaling during sexual reproduction in
396 algae. *Plant J* 79(4):632-644.
- 397 13. Chepurnov VA, Mann DG, Sabbe K, Vyverman W (2004) Experimental studies on sexual
398 reproduction in diatoms. *Int Rev Cytol* 237:91-154.
- 399 14. Geitler L (1932) Der Formwechsel der pennaten Diatomeen. *Arch Protistenkd* 78:1-226.
- 400 15. Sato S, Beakes G, Idei M, Nagumo T, Mann DG (2011) Novel sex cells and evidence for sex
401 pheromones in diatoms. *PloS one* 6(10):e26923.
- 402 16. Gillard J, *et al.* (2013) Metabolomics enables the structure elucidation of a diatom sex
403 pheromone. *Angew Chem Int Ed* 52(3):854-857.
- 404 17. Bondoc KGV, Lembke C, Vyverman W, Pohnert G (2016) Searching for a mate: pheromone-
405 directed movement of the benthic diatom *Seminavis robusta*. *Microb Ecol* 72(2):287-294.
- 406 18. Moeys S, *et al.* (2016) A sex-inducing pheromone triggers cell cycle arrest and mate attraction
407 in the diatom *Seminavis robusta*. *Sci Rep* 6:19252.
- 408 19. Consalvey M, Paterson D, M., Underwood G, J.C. (2004) The ups and downs of life in a
409 benthic biofilm: Migration of benthic diatoms. *Diatom Res* 19(2):181–202.
- 410 20. Blommaert L, Huysman MJJ, Vyverman W, Lavaud J, Sabbe K (2017) Contrasting NPQ
411 dynamics and xanthophyll cycling in a motile and a non-motile intertidal benthic diatom.
412 *Limnol Oceanogr* 62:1466-1479.
- 413 21. Moore CM, *et al.* (2008) Relative influence of nitrogen and phosphorous availability on
414 phytoplankton physiology and productivity in the oligotrophic sub-tropical North Atlantic
415 Ocean. *Limnol Oceanogr* 53(1):291-305.
- 416 22. Paytan A, McLaughlin K (2007) The Oceanic Phosphorus Cycle. *Chem Rev* 107(2):563-576.
- 417 23. Lin SJ, Litaker RW, Sunda WG (2016) Phosphorus physiological ecology and molecular
418 mechanisms in marine phytoplankton. *J Phycol* 52(1):10-36.

- 419 24. Martin-Jézéquel V, Hildebrand M, Brzezinski MA (2000) Silicon metabolism in diatoms:
420 Implications for growth. *J Phycol* 36(5):821-840.
- 421 25. Bondoc KGV, Heuschele J, Gillard J, Vyverman W, Pohnert G (2016) Selective silicate-
422 directed motility in diatoms. *Nat Commun* 7:10540.
- 423 26. Amsler CD, Iken KB (2001) Chemokinesis and chemotaxis in marine bacteria and algae.
424 *Marine Chemical Ecology*, ed McClintock J. B. BBJ (CRC Press), pp 413-430.
- 425 27. Kiørboe T (2008) *A mechanistic approach to plankton ecology* (Princeton University Press).
- 426 28. Karl DM (2014) Microbially mediated transformations of phosphorus in the sea: New views of
427 an old cycle. *Annu Rev Mar Sci* 6:279-337.
- 428 29. Thingstad TF, Skjoldal EF, Bohne RA (1993) Phosphorous cycling and algal-bacterial
429 competition in Sandsfjord, Western Norway. *Mar Ecol Prog Ser* 99:239-259.
- 430 30. Ikegami S, Imai I, Kato J, Ohtake H (1995) Chemotaxis toward inorganic phosphate in the red
431 tide alga *Chatonella antiqua*. *J Plankton Res* 17:1587-1591.
- 432 31. Huetz A, Schubert K, Overmann J (2011) Thalassospira sp Isolated from the Oligotrophic
433 Eastern Mediterranean Sea Exhibits Chemotaxis toward Inorganic Phosphate during Starvation.
434 *Appl Environ Microbiol* 77:4412-4421.
- 435 32. Longphuirt SN, et al. (2009) Dissolved inorganic nitrogen uptake by intertidal
436 microphytobenthos: nutrient concentrations, light availability and migration. *Mar Ecol Prog Ser*
437 379:33-44.
- 438 33. Sjoblad RD, Chet I, Mitchell R (1978) Chemoreception in the green alga *Dunaliella tertiolecta*
439 *Curr Microbiol* 1(5):305-307.
- 440 34. Ermilova EV, Zalutskaya ZM, Lapina TV, Nikitin MM (2003) Chemotactic behavior of
441 *Chlamydomonas reinhardtii* is altered during gametogenesis. *Curr Microbiol* 46(4):261-264.
- 442 35. Sjoblad RD, Frederikse PH (1981) Chemotactic responses of *Chlamydomonas reinhardtii*.
443 *Mol Cell Biol* 1:1057-1060.

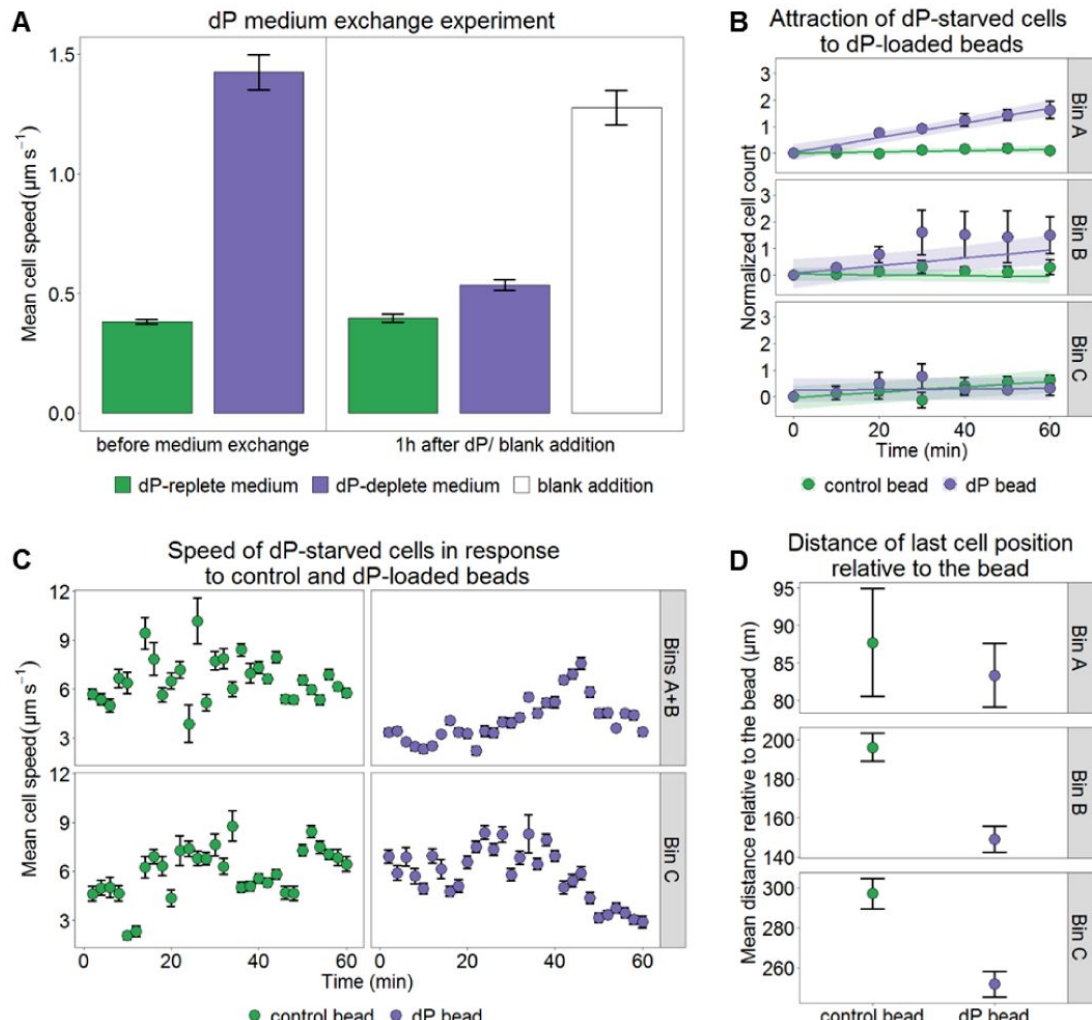
- 444 36. Ermilova EV, Zalutskaya ZM, Lapina TV (2009) Chemotaxis of *Chlamydomonas reinhardtii* to
445 nitrate is changed during gametogenesis. *Protistology* 6:79-84.
- 446 37. Ermilova E, Zalutskaya Z (2014) Regulation by Light of Chemotaxis to Nitrite during the
447 Sexual Life Cycle in *Chlamydomonas reinhardtii*. *Plants* 3:113-127.
- 448 38. Hockin NL, Mock T, Mulholland F, Kopriva S, Malin G (2012) The response of diatom central
449 carbon metabolism to nitrogen starvation is different from that of green algae and higher plants.
450 *Plant Physiol* 158(1):299-312.
- 451 39. Alcoverro T, Conte E, Mazzella L (2000) Production of mucilage by the Adriatic epipelagic
452 diatom *Cylindrotheca closterium* (Bacillariophyceae) under nutrient limitation. *J Phycol*
453 36(6):1087-1095.
- 454 40. Daglio Y, Maidana NI, Matulewicz MC, Rodriguez MC (2016) Changes in motility and
455 induction of enzymatic activity by nitrogen and phosphate deficiency in benthic *Halimphora*
456 *luciae* (Bacillariophyceae) from Argentina. *Phycologia* 55(5):493-505.
- 457 41. Guerrini F, Cangini M, Boni L, Trost P, Pistocchi R (2000) Metabolic responses of the diatom
458 *Achnanthes brevipes* (Bacillariophyceae) to nutrient limitation. *J Phycol* 36(5):882-890.
- 459 42. von Dassow P, Montresor M (2010) Unveiling the mysteries of phytoplankton life cycles:
460 patterns and opportunities behind complexity. *J Plankton Res* 33(1):3-12.
- 461 43. Chepurnov VA, Mann DG, Vyverman W, Sabbe K, Danielidis DB (2002) Sexual reproduction,
462 mating system, and protoplast dynamics of *Seminavis* (Bacillariophyceae). *J Phycol*
463 38(5):1004-1019.
- 464 44. Basu S, et al. (2017) Finding a partner in the ocean: molecular and evolutionary bases of the
465 response to sexual cues in a planktonic diatom. *New Phytol* 215(1):140-156.
- 466 45. Thompson SEM, Taylor AR, Brownlee C, Callow ME, Callow JA (2008) The role of nitric
467 oxide in diatom adhesion in relation to substratum properties. *J Phycol* 44(4):967-976.

- 468 46. Gillard J, *et al.* (2008) Physiological and transcriptomic evidence for a close coupling between
469 chloroplast ontogeny and cell cycle progression in the pennate diatom *Seminavis robusta*. *Plant*
470 *Physiol* 148(3):1394-1411.
- 471 47. Tinevez J-Y, *et al.* (2017) TrackMate: An open and extensible platform for single-particle
472 tracking. *Methods* 115:80-90.
- 473 48. Team RC (2016) R: A language and environment for statistical computing (R Foundation for
474 Statistical Computing, Vienna, Austria).
- 475 49. Wickham H (2009) ggplot2: elegant graphics for data analysis (Springer-Verlag New York).
- 476 50. Pinheiro J, Bates D, DebRoy S, Sarkar D, Team RC (2015) nlme: Linear and Nonlinear Mixed
477 Effects Models. R package version 3.1-120.
- 478 51. Wood SN (2011) Fast stable restricted maximum likelihood and marginal likelihood estimation
479 of semiparametric generalized linear models. *J Roy Stat Soc Ser B (Stat Method)* 73:3-36.
- 480
- 481
- 482
- 483
- 484
- 485
- 486
- 487
- 488
- 489
- 490
- 491
- 492

493 **Figures**

494

495 **Figure 1. Attraction to nutrients.** Response of small-sized (24-27 μm) starved *S. robusta* to nutrient-
496 loaded beads. Cells in stationary phase were transferred to either dP, dSi, or dN (NH_4^+ or NO_3^-) -free
497 medium and were starved for 5, 3, or 12 days, respectively. For both dP and dN, the medium was
498 changed every second day to ensure that cells are under truly limiting condition for the respective
499 nutrient. Starved cells accumulated within ~10 min around dSi beads, ~30 min was needed for dP
500 accumulation, and no attraction was observed for dN beads even when varying loaded dN
501 concentration to the bead (data not shown). For further analysis as shown in Figure 2, the observation
502 area was divided into 3 bins, divided by circles with radii of 112 μm , 224 μm , and 336 μm (upper left).
503 Scale bar corresponds to 100 μm .



504

505 **Figure 2. Response of dP-starved *S. robusta* to bulk dP and dP-loaded beads.**

506 (A) Cells grown in dP-depleted medium for 5 days have higher mean speed than cells grown in dP-
 507 repleted medium ($p<0.001$). The cell speed dropped one hour after dP addition to starved cells
 508 ($p<0.001$), whereas blank addition of dP-depleted medium, did not affect motility ($p=0.160$).
 509 Data points are presented as mean \pm SEM of tracked cells from 30-s movies of each treatment
 510 ($n=3$, $n_{(\text{cells/movie})}=100-300$). Statistical analysis is linear mixed effects modeling (LME) with
 511 pair-wise Tukey's honest significance difference (HSD), detailed statistical analysis can be
 512 found in Table S3.

513 (B) Normalized cell counts (\pm SEM) showed a significant increase in cell density over time in dP-
 514 loaded beads for all bins compared to control. A value of 0 depicts the population mean. Cells
 515 exposed to dP-loaded beads showed significantly increasing trend over time while control
 516 showed a constant mean value of 0, indicating a stable population mean over time in all bins

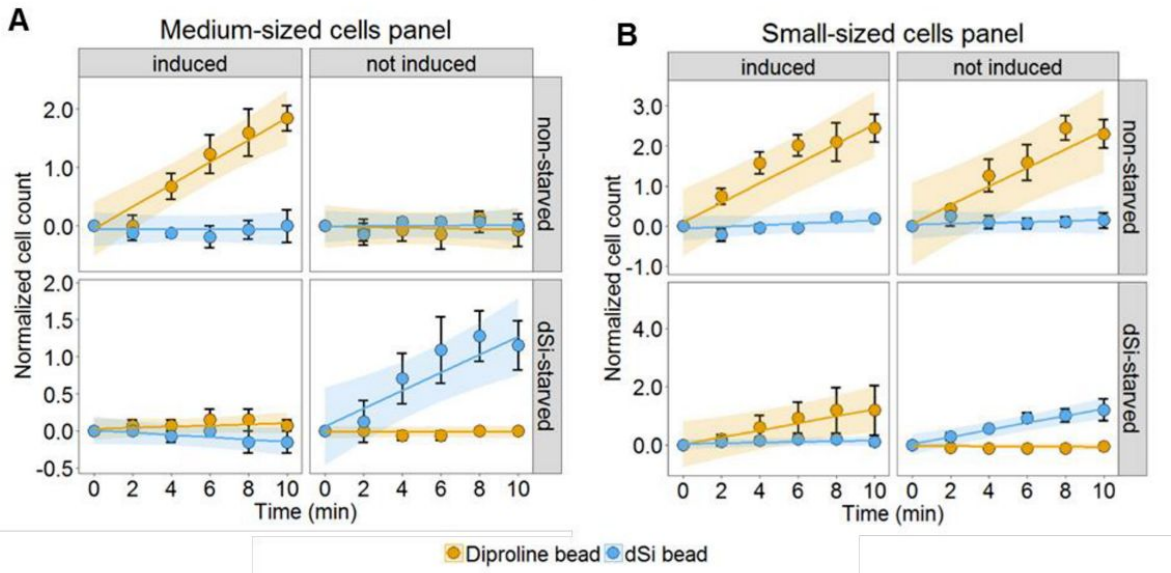
517 (Linear mixed effects modeling, n= 3 movies, for Bin A: p < 0.001, Bin B: p = 0.0097, Bin C: p
518 = 0.0189, Table S4). Both Bins A and B showed constant increase of cells over time with Bin
519 B reaching a steady influx of cells after 30 min. This demonstrates cell migration towards the
520 inner bins. The overlaid shaded area shows the LME model fit with 95% confidence intervals.
521 Detailed statistical analysis can be found in Table S4.

522 (C) The mean cell speeds (\pm SEM) over intervals of 2 min were taken for 1 h from track data of
523 each treatment (n=3, n_(cells/movie)=15). Bins A and B were combined to reach sufficient data
524 points. The log+1 transformed mean speeds were fitted using a generalized additive mixed
525 modeling (GAMM) approach for each bin. Cell speed increases over time in Bins A+B around
526 dP beads, reaching a peak at ~40 min, coinciding with higher cell densities accumulating
527 around the bead (p_{control bead}=0.598, p_{dP bead}<0.001). For Bin C, peak speeds were evident around
528 25-40 min, wherein cells presumably moved towards the dP gradient source (p_{control bead}=0.193,
529 p_{dP bead}<0.001). Detailed statistical analysis can be found in Table S6 and fitted cubic splines of
530 the model in Figure S3.

531 (D) The mean distance (\pm SEM) was determined from the last coordinate position of the cell
532 against the coordinate position of the bead (n =3, n_(cells/movie)=15). Both Bins B and C showed
533 lower mean distance of cells exposed to the dP-loaded bead compared to controls (pair-wise
534 Least square means, n= 3 movies, for Bin A: p=0.6791, Bin B: p<0.001, Bin C: p<0.001, Table
535 S5). This underscores the inward migration of cells. Detailed statistical analysis can be found in
536 Table S5.

537

538



539

540 **Figure 3. Behavioral switch of *S. robusta* depending on their cell size.**

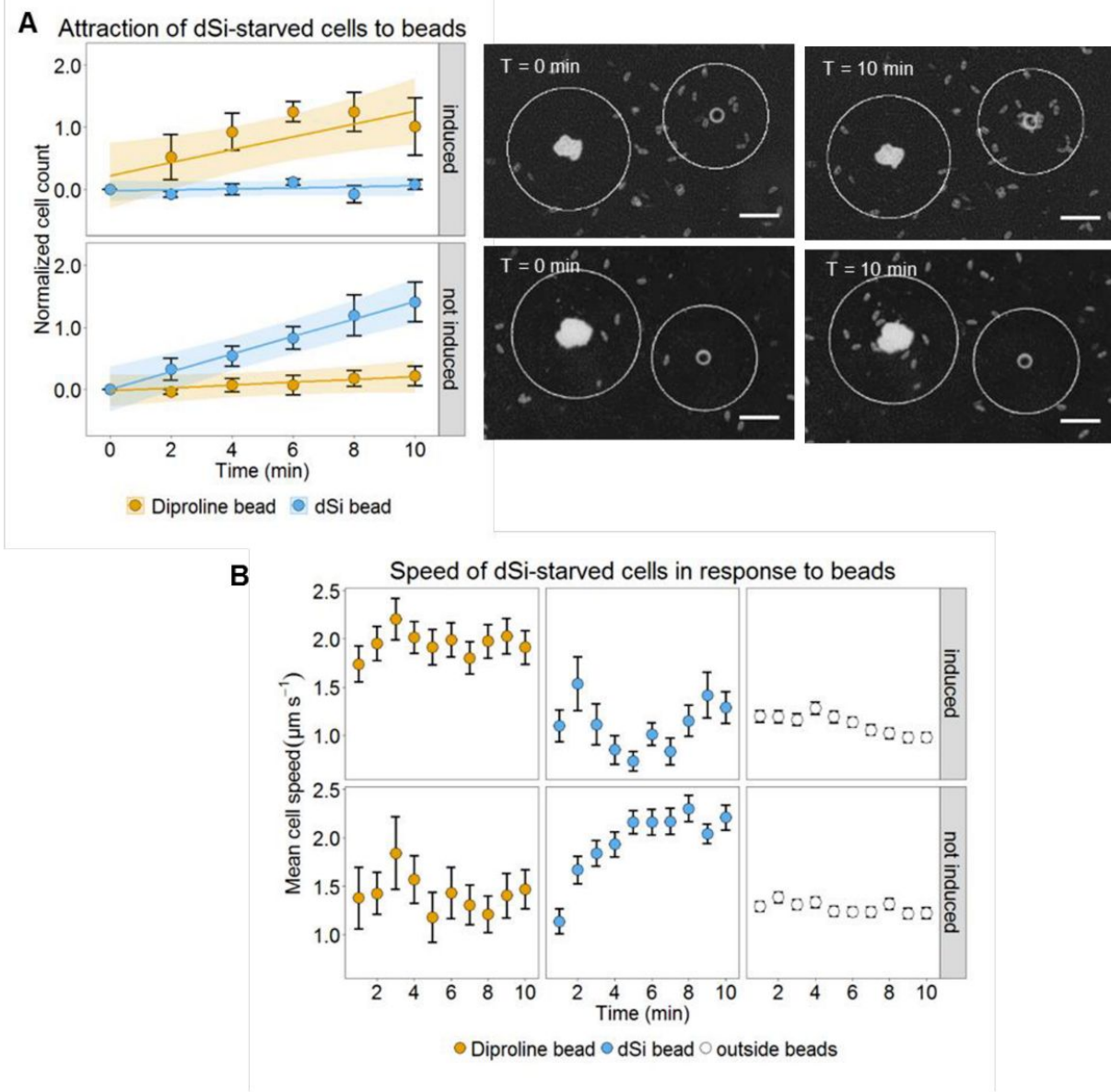
541 Experiments were done to determine the combination of effects of sex induction and dSi starvation on
 542 medium-sized ($\sim 40 \mu\text{m}$) and small-sized ($24\text{-}27 \mu\text{m}$) *S. robusta*. Pooled videos from different
 543 experimental sets were used and separate statistical analysis (Linear mixed effects modeling (LME)
 544 with pair-wise Tukey's honest significance difference (HSD) was done per bead and movie to
 545 determine specific conditions that affect chemoattraction. The detailed statistical analysis can be found
 546 in Table S7.

547 (A) Medium-sized cells were only attracted to diproline when grown with dSi and upon induction
 548 ($p < 0.001$ compared with all treatments). On the other hand, only dSi starvation and non-
 549 induction renders the cells to be attracted to dSi beads ($p < 0.01$ compared with all treatments).
 550 All data points are presented as mean \pm SEM of 3 movies per treatment. The overlaid shaded
 551 area shows the LME model fit with 95% confidence intervals.

552 (B) Non-starved, small-sized cells were always attracted to diproline, even without induction and at
 553 the same intensity as with induced cells ($p = 1$, $n_{(\text{movies})} = 3$) compared against the non-starved and
 554 induced treatment). However, these self-inducing cells were not attracted to the pheromone
 555 when they are starved, and it was only through induction that starved cells regained attraction to
 556 diproline ($p = 0.18$, $n_{(\text{movies})} = 6$). The induction medium used has traces of dSi ($\sim 50 \mu\text{M}$ per well)
 557 since it was collected from exponential phase cultures of the opposite mating type (MT^-). In
 558 contrast, only cells that are both not induced and starved were attracted to dSi bead ($p < 0.02$ for
 559 all comparisons). All data points are presented as mean \pm SEM of 3 movies with exception of

560 dSi-starved induced and not induced ($n_{\text{movies}}=6$) as cell responses showed variability between
561 sets. The overlaid shaded area shows the LME model fit with 95% confidence intervals.

562



563

564 **Figure 4. Choice experiments (dSi vs. diproline) on small-sized, self-inducing, dSi-starved cells of**
565 *S. robusta*. Choice experiments were performed using self-inducing and dSi-starved cells to determine
566 if they are capable of recognizing two different chemical signals under two different conditions (with
567 or without sex induction). Videos from different experimental sets were used ($n = 3$ from each
568 treatment) and separate statistical analysis (Linear mixed effects (LME) model) was done for each
569 condition to determine the preferred bead.

570 (A) Cell accumulation on beads. The left panel shows normalized cell counts from bins (depicted
571 here as white circles on microscopic photos from the right panel) having a size of 115 μm from
572 the edge of the bead. Cell density was determined after every 2 min for 10 min. The results
573 were consistent with the experiments with individual beads. Induced cells accumulated only on
574 diproline beads over time ($p=0.0259$). Presumably due to the exposure to residual amount of
575 dSi during induction cells are not fully depleted in dSi. On the other hand, the not induced cells
576 showed preference only to dSi beads ($p=0.0003$). Data points are presented as mean \pm SEM of 3
577 videos. The overlaid shaded area shows the LME model fit with 95% confidence intervals.
578 Detailed statistical analysis can be found in Table S8. Microscopic photos have a scale bar of
579 100 μm .

580 (B) The cell speed averaged over intervals of 1 min for 10 min were taken from automatically
581 tracked cells in five independent movies ($n_{(\text{cells/movie})}=80-100$). The track data was divided into 3
582 groups: the areas around the two beads and the area outside the beads. Induced cells showed a
583 consistent higher mean speed when cells are under the influence of diproline gradients
584 compared to dSi and outside the beads (LME with Tukey's HSD, $p<0.001$ for both). In contrast,
585 under not induced conditions, cells accumulating on dSi beads show the distinctive increase of
586 speed over time, whereas, diproline did not induce any change in speed ($p<0.001$). Data points
587 are presented as mean speed \pm SEM of 5 videos. Detailed statistical analysis can be found in
588 Table S9.

589

590

591 **Supporting Information**

592 **SI Materials and Methods**

593 ***Strains, maintenance of stock cultures, and microscopy***

594 Stock cultures of strains MT⁺ (PONTON36) and large-sized cells of MT⁻ (84A) were grown in buffered
595 artificial sea water (ASW) modified after Maier and Calenberg [46] with concentrations of 621 µM
596 NaNO₃ (VWR Chemicals, Leuven Belgium), 155 µM K₂HPO₄ (Roth, Karlsruhe, Germany) and 246
597 µM Na₂SiO₃ · 9 H₂O (Sigma-Aldrich, Steinheim, Germany). Stock cultures of strains MT⁺ (85A) and
598 small-sized MT⁻ (84A) were grown in 33g/l Instant Ocean® Sea Salt (Aquarium Systems, Sarrebourg,
599 France) dissolved in deionized water with f/2 supplements according to Guillard [47]. Experimental
600 cultures were prepared by inoculating 10% stock culture to fresh ASW or nutrient-depleted ASW and
601 kept in standard tissue culture flasks or well plates (Sarstedt, Nümbrecht, Germany). All cultures were
602 grown at 18 °C in a 12:12 h light:dark regime with cool-white fluorescent lamps at approximately 35
603 µmol photons m⁻² s⁻¹.

604

605 ***Monitoring diatom growth and nutrient analysis***

606 Stock cultures of small-sized cells (MT⁺, strain PONTON 36) were grown for 7 days to reach early
607 stationary phase before 1/10th of the initial culture was diluted into 25 ml fresh ASW medium. Growth
608 of experimental cultures (n=12) was monitored under an inverted microscope by taking triplicate
609 photos of 3 randomly chosen culture flasks every day. The cell density was calculated by counting the
610 number of cells per picture semi-automatically in Fiji (<http://fiji.sc/Fiji>) (S2). Every second day, the
611 medium of three replicates was harvested for nutrient analysis by sterile filtration (Filtropur S 0.2,
612 Sarstedt, Nümbrecht) and stored at -20 °C until measurement. Silicate and phosphate concentrations
613 were determined by standard photospectrometric methods (S3). The concentrations of nitrate, nitrite,

614 and ammonia were measured by flow analysis and photospectrometric detection according to ISO
615 11732-2005 and ISO 13395-1996.

616

617 ***Diatom growth under nutrient starvation and recovery experiment***

618 For monitoring cell growth under nutrient limitation, experimental cultures were inoculated into 25 ml
619 ASW where no dSi, dN, or dP was added, but which was supplemented with all other nutrients. As a
620 control, full ASW medium was used. Cell growth was monitored as described above (n=3) and the dN
621 or dP-depleted medium was exchanged every two days to avoid that other nutrients become limited.
622 Due to slow growth, this exchange was not required for the dSi-limited cultures. After 3, 5 or 12 days,
623 10 % of the dSi, dP, or dN depleted cultures, respectively were inoculated in fresh ASW and cell
624 growth was monitored as described above (n=3). A linear mixed effects (LME) model coupled with the
625 post-hoc Tukey's HSD was used to analyse the data (Supplementary Fig. 1, Supplementary Table 2).

626

627 ***Video and Statistical Analyses***

628 Only dP movies and their corresponding controls ($n_{movies}=3$, $n_{cells/movie}=15$) were evaluated since
629 dSi movies were previously analysed (S1) and dN movies showed no attraction. For dP experiments
630 with beads, the observation area was divided into three concentric circles, referred to as bins (bins A-
631 C), each having a radius of 112 μm with the bead in the middle. For individual dSi and diproline assays
632 and choice experiments, a radius of 115 μm from the edge of the bead was used for analysis.
633 Additionally, tracking outside the bead area for choice assays were done.

634 Our main data are either count data with or without trajectory analysis. We calculated
635 parameters such as speed and sum distance of cells from track data. Cell counts were transformed
636 either using log-normal for nutrient starvation and recovery studies, or Z-standard score for cell
637 accumulation sets. Whereas, speed was log+1 transformed. Depending on the longitudinal and nesting
638 of the experimental design, either LME or GAMM was used to fit the data. To correct for correlated

639 data between independent variables and residual spreads, an auto-regressive order 1 (AR-1) correlated
640 structure and a constant variance function structure (varIdent), respectively were added to the model
641 when necessary. For optimum model fitting, the Akaike Information Index (AIC), as well as residual
642 and model plots were checked. A Wald test to determine the significance of the fitted estimates was
643 performed on the chosen optimum model. For pair-wise comparisons of treatments, either a Tukey's
644 Honest Significance Difference (HSD) test or Least square (LS) means test was employed as a posthoc
645 test. The detailed model fit for each figure (Table S1), as well as results of each model (Tables S2-S11)
646 can be found in the Supplemental Information.

647

648 ***Diffusion of dP from the bead***

649 We determined the diffusion gradient formed by the dP-loaded beads for 1 h through a combination of
650 experimental and computational approach, as we have previously done for dSi and diproline gradient
651 determination (S1, S4). The total flux of dP diffused out (i) was calculated by exposing 100 mg dP-
652 loaded beads or control beads prepared as described previously with 50 ml ASW. After incubation at
653 room temperature for 1 h the medium was filtered (Filtropur 0.2, Sarstedt, Nümbrecht, Germany) and
654 stored at -20 °C until measurement. The phosphate concentrations were determined as described before
655 through standard colorimetric methods. We calculated i using the formula from Barbara and Mitchell
656 (S5).

657
$$C_{(r,t)} = i/4\pi r D$$

658 where i is the total diffusive flux of dP, r is the radius of the bead (55 μm), t is the time until steady
659 state was reached, and D is the diffusivity constant for small molecules (10^{-5} cm 2 s $^{-1}$) (S6). We then
660 determined the steady state gradient C by using the computed i ($8.16^{-15} \pm 6.42^{-16}$ mol s $^{-1}$) and
661 modifying \sqrt{r} as the radius of the observation area (336 μm) to correct for the shape of the gradient in a
662 flat chamber (S7). The time to steady state was determined as the time $\geq d^2/D$ where d is the diameter of
663 the whole observation area (672 μm). Supplementary Figure 2 depicts the formed gradient.

664

665 ***Attraction of large-sized cells to dSi-loaded beads***

666 Batch cultures of large-sized cells (MT⁻, strain 84A), as well as dSi and control beads were
667 prepared as described previously. Cells were starved for 1 week before exposing them to beads for 10
668 min, as shorter starvation period did not elicit any reaction. Photos were recorded every minute, but cell
669 counts were only determined every 2 min on a 115 µm observation area from the bead. Three replicates
670 per treatment were used. A linear mixed effects (LME) model coupled with the post-hoc Tukey's HSD
671 was used to analyse the data (Supplementary Fig. 4, Supplementary Table 10).

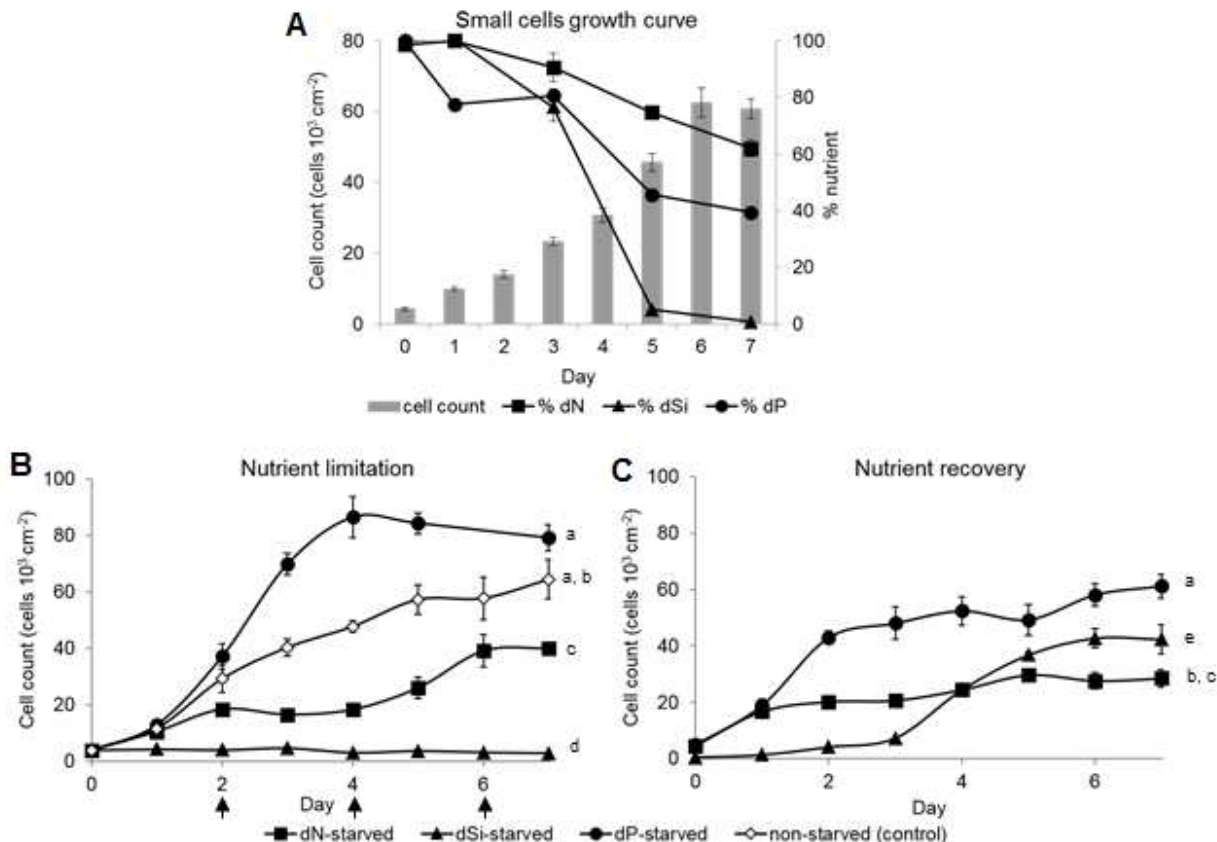
672

673 ***Motility of 85A small-sized cells under different conditions***

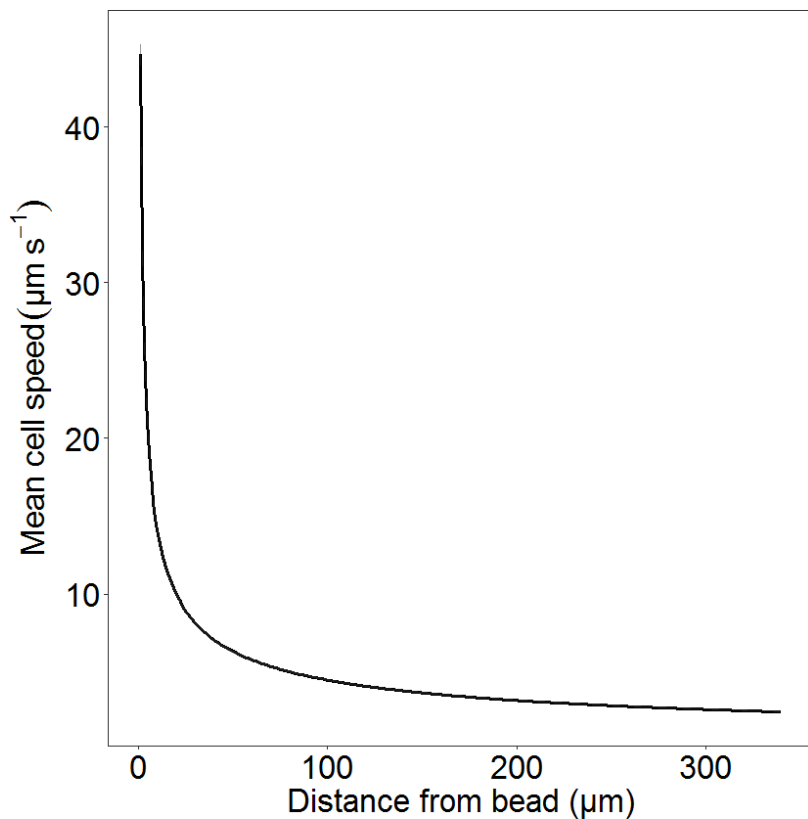
674 In conjunction with the panel experiments, we determined the cell motility of small cells under
675 different combinations of induction and starvation. Besides the induction medium, we also added the
676 equivalent amount of trace dSi we measured from the induced well plates (~50 µM) on dSi-starved
677 cells to compare the effect of dSi and induction on motility. After 6 h of light exposure and prior to
678 bead addition, we took 1 min movies of cells and processed them as described beforehand in our dP
679 medium exchange experiment. A linear mixed effects (LME) model coupled with the post-hoc Tukey's
680 HSD was used to analyze the speed data (Supplementary Fig. 5, Supplementary Table 11).

681

682

684
685686 **Figure S1.** Growth rate and nutrient dynamics of small-sized *Seminavis robusta* (strain PONTON 36,
687 24–27 μm).688 All data points are presented as mean \pm SEM.689 (A) As cells (n=3) reach late exponential phase, dSi was depleted in the medium (100% = 246 μM).
690 Meanwhile, concentrations of both dN (100% = 621 μM) and dP (100% = 15 μM) remained at
691 ~60% and ~40%, respectively.692 (B) Cells in stationary phase were transferred to medium depleted with dN, dSi, dP, or medium with
693 all nutrients (non-starved as control) and growth was observed for 1 week. The medium was
694 exchanged every two days (indicated by arrows) for dP and dN-starved cells. dSi-starved cells
695 showed no growth as compared with dN- and dP-starved cells and control (Linear mixed effects
696 (LME) modeling with pairwise Tukey's HSD for all p < 0.001, n=3). Cells limited of dN and dP
697 continued to grow, presumably due to stored nutrients. Treatments with same letters are not
698 statistically significant from each other. Statistical tests of this set were performed together with
699 data from Fig. 1c.700 (C) After starvation (3 days for dSi, 5 days for dP, and 12 days for dN), aliquots of starved cells
701 were transferred to nutrient replete medium. dSi- and dP-starved cells showed a remarkable
702 recovery in a matter of 3 days compared to dN-starved cells (LME with pairwise Tukey's HSD,
703 for dSi vs. dN: p < 0.001, for dP vs. dN: p = 0.001). Treatments with same letters are not
704 statistically significant from each other. Statistical tests of this set were performed together with
705 data from Fig. 1b.

706

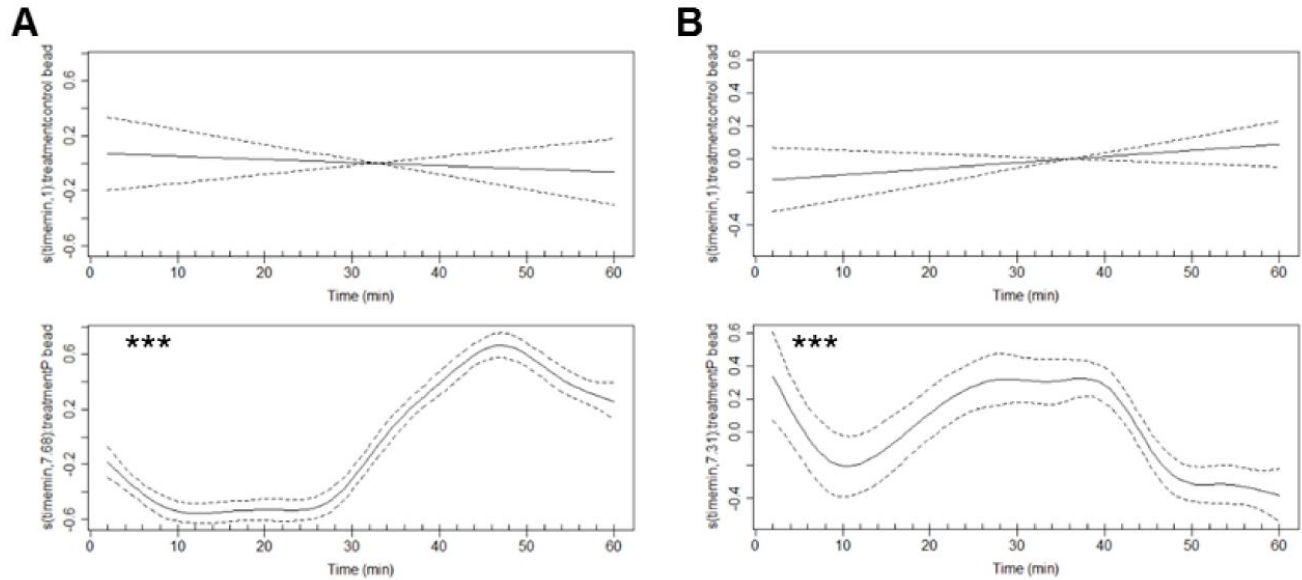


707

708 **Figure S2.** dP gradients were formed until the edge of the observation area in ~450 s. Bin A showed
709 steep concentrations of dP ranging from ~44 μM from the surface of the bead to ~4 μM , whereas, Bins
710 B and C have a constant 2-4 μM .

711

712



713

714 **Figure S3.** Fitted cubic splines of cell speed for the dP attraction experiment (upper panel: control,
 715 lower panel: dP-loaded bead) for Bins A+B (a) and Bin C (b) over 60 min. The y-axis shows the
 716 optimal smoothing knots (i.e. the number of connections for each data point over time). GAMM centers
 717 the mean of knots to 0. For the controls of both Bins A+B and Bin C, a straight line could be observed,
 718 suggesting that there were no observed changes on the mean speed over time. On the other hand, dP-
 719 loaded beads induced cells increased speed around ~30 min and ~15 min for both Bins A+B and Bin C,
 720 respectively, implying an orthokinetic response.

721

722

723

724

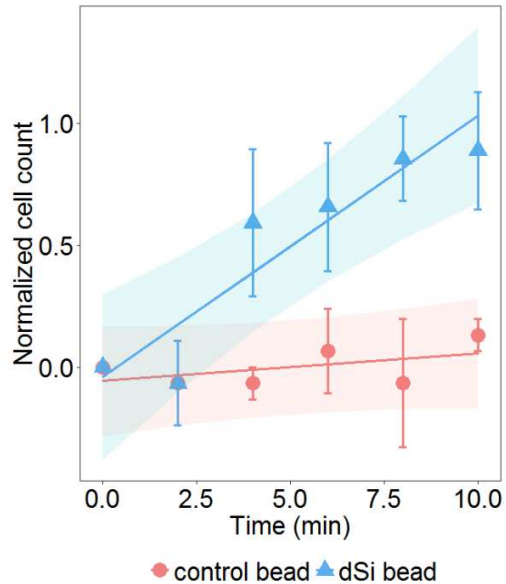
725

726

727

728

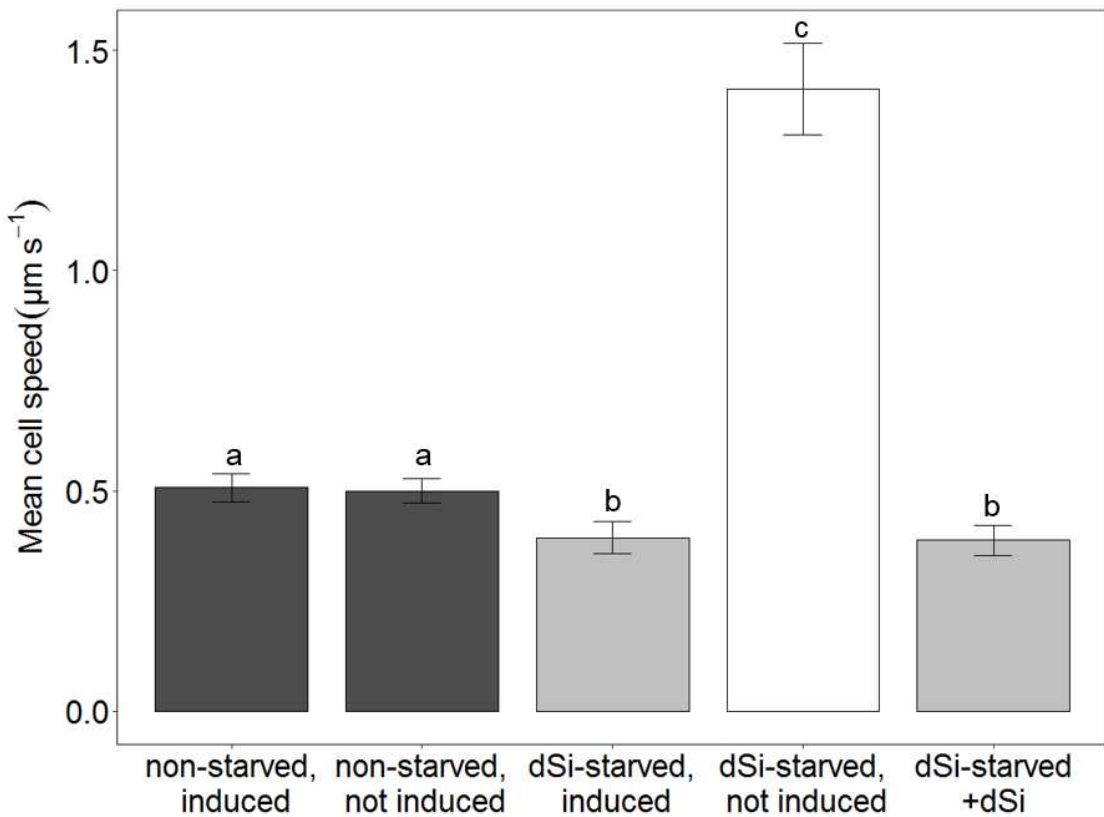
729



730

731 **Figure S4.** After 7 days of starvation, large-sized cells (MT⁻, strain 84A) responded to dSi-loaded
732 beads in the same manner as small- and medium-sized cells. A clear accumulation compared to the
733 control was observed (Linear mixed effects modeling, n=3 movies per treatment, p=0.0023). Error bars
734 indicate SEM of the mean and the gray shaded area shows the LME model fit with 95% confidence
735 intervals.

736



737

738 **Figure S5.** Cell speeds of small-sized 85A in different combination of starvation and induction. No
 739 difference in motility was observed for non-starved cells, whether induced or not (Linear mixed effects
 740 modeling (LME) with Tukey's HSD, $p= 0.9999$, $n=3$). On the other hand, dSi-starved and induced cells
 741 have significantly lower speed than its not induced counterpart (LME with Tukey's HSD, $p<0.0001$,
 742 $n=3$). To tease out whether the decreased motility is because of SIP⁻ or the residual dSi from the
 743 induction medium, we added the equivalent dSi measured (~50 μM per well) on dSi-starved cells.
 744 Indeed, the residual dSi was sufficient for the slowing down of the cells (LME with Tukey's HSD,
 745 $p=1.000$, $n=3$). Data points are presented as mean \pm SEM of all tracked cells ($n=50-175$ cells) from
 746 three 30-s movies for each treatment. Detailed statistical analysis can be found in Supplementary
 747 Table10.

748

749

750

Table S1. Detailed statistical parameters for each model fit of the corresponding figures mentioned.

Figure	Experimental Set	Supplementary Result Table	Sample Size (n)	Model	Random Factor	Correlation Structure	Variance Structure	Extra processing
2a	dP medium exchange experiment	Table 3	n _{movies} = 3, n _{cells/movie} = 100-300	LME with post-hoc test (Tukey's HSD); Vlog ^b ~ treatment	Track ID	-	Treatment	1 st 30s of video was removed, only complete 30s data were used for analysis
2b	dP-attraction: cell counts	Table 4	n _{movies} = 3	LME (per bin); cellsBase ^c ~ treatment	Replicate ID	Replicate ID and treatment	Replicate ID	-
2c	dP-attraction: speed	Table 5	n _{movies} = 3, n _{cells/movie} = 15	GAMM (per bin); Vlog ~ smoothed factor interaction of time*treatment penalized with cubic regression splines	Track ID	Track ID and treatment	Treatment	Bins A+B were combined, Outliers were removed
2d	dP-attraction: sum distance	Table 6		LME (all data) with post-hoc test (LS-means); distance ^d ~ treatment*bin	Track ID	Track ID and treatment	Bin	-
3	Medium-sized and small-sized panels	Table 7	n _{replicates} = 3; except for 85AS, dSi-starved, induced (diproline bead) which has 6	LME (per bead) with post-hoc test (Tukey's HSD); cellsBase ~ treatment*time	Replicate ID	Replicate ID and treatment	Treatment	-
4a	Choice: cell count	Table 8		LME (per treatment); cellsBase ~ bead*time	Replicate ID	Replicate ID and treatment	Bead	Cells in overlapping bins were excluded from analysis
4b	Choice: speed	Table 9	n _{movies} = 5, n _{cells/movie} = 80-100	LME (per treatment); Vlog ~ bead*time	Track ID	Track ID and bin	Bead	
Supp 1b and 1c	Nutrient starvation and recovery	Table 2	n _{replicates} = 3	LME with post-hoc test (Tukey's HSD); n _{cells} ^a ~ treatment*day	Replicate ID	Replicate ID and treatment	-	Outliers were removed
Supp 4	dSi attraction of large cells	Table 10	n _{movies} = 3	LME; cellsBase ~ bead*time	Replicate ID	-	Bead	-
Supp 5	Small-sized cells medium exchange experiment	Table 11	n _{movies} = 3, n _{cells/movie} = 50-175	LME with post-hoc test (Tukey's HSD); Vlog ~ treatment	Track ID	-	Treatment	1 st 30s of video was removed, only complete 30s data were used for analysis

^an_{cells}s = log normal transformation of cell counts^bVlog = log+1 transformation of speed^ccellsBase = Z standardized cell count calculated per treatment using the formula: $Z = (X-\mu)/\sigma$, where μ is mean, X is score and σ is standard deviation^ddistance = sum Euclidean distance from all track IDs calculated from the first and last coordinate position of the cell

757 **Table S2.** Pair-wise comparisons using Tukey's HSD of log normal cell counts of batch cultures
 758 during nutrient starvation and recovery. Cultures in full-nutrient ASW acted as control.

Pair-wise comparisons	Estimate	Std. error	z-value	Pr(> z)
control – dSi-starvation	1.94234	0.13590	14.293	< 0.001 ***
control – dN-starvation	0.41632	0.13590	3.063	0.03577 *
control – dP-starvation	-0.28641	0.14021	-2.043	0.38737
control – dSi-recovery	1.22408	0.13895	8.809	< 0.001 ***
control – dN-recovery	0.31864	0.13895	2.293	0.24711
control – dP-recovery	-0.22694	0.13895	-1.633	0.66049
dSi-starvation – dN-starvation	-1.52602	0.13590	-11.229	< 0.001 ***
dSi-starvation – dP-starvation	-2.22875	0.14021	-15.896	< 0.001 ***
dSi-starvation – dSi-recovery	0.71826	0.13895	5.169	< 0.001 ***
dSi-starvation – dN-recovery	-1.62370	0.13895	-11.685	< 0.001 ***
dSi-starvation – dP-recovery	-2.16928	0.13895	-15.611	< 0.001 ***
dSi-recovery – dN-recovery	-0.90544	0.14194	-6.379	< 0.001 ***
dSi-recovery – dP-recovery	-1.45102	0.14194	-10.222	< 0.001 ***
dSi-recovery – dN-starvation	-0.80776	0.13895	-5.813	< 0.001 ***
dSi-recovery – dP-starvation	-1.51049	0.14318	-10.550	< 0.001 ***
dN-starvation – dP-starvation	0.70274	0.14021	5.012	< 0.001 ***
dN-starvation – dN-recovery	0.09768	0.13895	0.703	0.99246
dN-starvation – dP-recovery	0.64326	0.13895	4.629	< 0.001 ***
dN-recovery – dP-starvation	0.60505	0.14318	4.226	< 0.001 ***
dN-recovery – dP-recovery	0.54558	0.14194	3.844	0.00243 **
dP-starvation – dP-recovery	-0.05948	0.14318	-0.415	0.99961

759 Signif. codes: 0 ‘***’ 0.001 ‘**’ 0.01 ‘*’ 0.05 ‘.’ 0.1 ‘ ’ 1 (Adjusted p values reported -- single-step method)

760

761 **Table S3.** Pair-wise comparisons using Tukey's HSD of speed (log+1 transformed) of dP-starved
 762 and non-starved cultures before and 1 h after addition of dP or blank.

Pair-wise comparisons	Estimate	Std. error	z-value	Pr(> z)
before medium exchange				
starved – non-starved	0.426028	0.025522	16.693	<1e-04 ***
after medium exchange				
starved – starved+dP	0.367292	0.026629	13.793	<1e-04 ***
starved – starved+blank	0.074003	0.033724	2.194	0.160
starved – non-starved+dP	0.435928	0.026118	16.691	<1e-04 ***
starved+dP – starved+blank	0.293289	0.024589	11.928	<1e-04 ***
starved+dP – non-starved+dP	0.068636	0.012225	5.614	<1e-04 ***
starved+dP – non-starved	0.058736	0.010893	5.392	<1e-04 ***
starved+blank - non-starved+dP	0.361925	0.024035	15.058	<1e-04 ***
non-starved – starved+blank	0.352025	0.023385	15.053	<1e-04 ***
non-starved – non-starved+blank	0.009900	0.009576	1.034	0.821

763 Signif. codes: 0 ‘***’ 0.001 ‘**’ 0.01 ‘*’ 0.05 ‘.’ 0.1 ‘ ’ 1 (Adjusted p values reported -- single-step method)

764

765 **Table S4.** Linear mixed effects (LME) model results on count data (Z-standard score
 766 transformed) on the dP attraction experiment (control bead vs. dP-loaded bead) for individual
 767 bins.

	numDF	denDF	F-value	p-value
Bin A				
(intercept)	1	34	22.06955	<.0001
treatment	1	4	42.56985	0.0028
time	1	34	17.67461	0.0002
treatment:time	1	34	36.13671	<.0001
Bin B				
(intercept)	1	34	0.767932	0.3870
treatment	1	4	3.81304	0.1226
time	1	34	0.0124	0.9120
treatment:time	1	34	7.511128	0.0097
Bin C				
(intercept)	1	34	3.323564	0.0771
treatment	1	4	0.001258	0.9734
time	1	34	7.093012	0.0117
treatment:time	1	34	6.072297	0.0189

768
 769 **Table S5.** Pair-wise comparisons using least square (LS) means of sum distance of cells on the
 770 dP attraction experiment (control bead vs. dP-loaded bead) for individual bins.

	Estimate	Std. error.	DF	t.ratio	p-value
Bin A	3.050294	7.346313	80	0.415	0.6791
Bin B	45.93821	9.744273	80	4.714	<.0001 ***
Bin C	43.24334	9.911365	80	4.363	<.0001 ***

771 Signif. codes: 0 ‘***’ 0.001 ‘**’ 0.01 ‘*’ 0.05 ‘.’ 0.1 ‘ ’ 1 (Adjusted p values reported -- single-step method)

772
 773 **Table S6.** General additive mixed model (GAMM) results on speed data (log+1 transformed) on
 774 the dP-attraction experiment (control bead vs. dP-loaded bead) for individual bins. Bins A and B
 775 were combined because of insufficient data points in Bin A.

	edf	Ref.df	F	p-value
Bins A+B				
s(time):controlbead	1.000	1.000	0.278	0.598
s(time):dPbead	7.684	7.684	60.811	<2e-16
Bin C				
s(time):controlbead	1.000	1.000	1.697	0.193
s(time):dPbead	7.311	7.311	14.502	<2e-16

776

777 **Table S7 (related to Fig. 3).** Pair-wise comparisons using Tukey's HSD of cell accumulation
 778 around a diproline or a dSi bead on different combinations of dSi and induction medium
 779 availability. Individual post-hoc tests were done per bead for both small and medium-sized cells.

Pair-wise comparisons	Estimate	Std. error	z-value	Pr(> z)
Medium-sized cells: diproline bead				
starved, induced – starved, not induced	-0.07962	0.06261	-1.272	0.55117
starved, induced – non-starved, induced	-0.83577	0.18414	-4.539	< 1e-04 ***
starved, not induced – non-starved, not induced	0.02181	0.13974	0.156	0.99847
starved, not induced – non-starved, induced	-0.91539	0.17930	-5.105	< 1e-04 ***
non-starved, induced – non-starved, not induced	-0.93720	0.22252	-4.212	0.00012 ***
Medium-sized cells: dSi bead				
starved, induced – starved, not induced	0.73348	0.20706	3.542	0.00207 **
starved, induced – non-starved, induced	-0.01826	0.13018	-0.140	0.99896
starved, induced – non-starved, not induced	-0.07387	0.12413	-0.595	0.93044
starved, not induced – non-starved, not induced	0.65961	0.22023	2.995	0.01404 *
starved, not induced – non-starved, induced	0.71522	0.22370	3.197	0.00694 **
non-starved, induced – non-starved, not induced	0.05561	0.15024	0.370	0.98181
Small-sized cells: diproline bead				
starved, induced – starved, not induced	-0.6705	0.3388	-1.979	0.18072
starved, induced – non-starved, induced	-0.6855	0.4914	-1.395	0.47845
starved, induced – non-starved, not induced	-0.5879	0.5587	-1.052	0.69845
starved, not induced – non-starved, not induced	-1.2585	0.4490	-2.803	0.02409 *
starved, not induced – non-starved, induced	-1.3560	0.3617	-3.749	0.00105 **
non-starved, induced – non-starved, not induced	-0.0975	0.5729	-0.170	0.99805
Small-sized cells: dSi bead				
starved, induced – starved, not induced	0.546984	0.149620	3.656	0.00133 **
starved, induced – non-starved, induced	0.051255	0.134189	0.382	0.98042
starved, induced – non-starved, not induced	0.000513	0.150551	0.003	1.00000
starved, not induced – non-starved, not induced	0.547497	0.189955	2.882	0.01972 *
starved, not induced – non-starved, induced	0.598240	0.177268	3.375	0.00379 **

non-starved, induced – non-starved, not induced	0.050742	0.178055	0.285	0.99167
--	----------	----------	-------	---------

780 Signif. codes: 0 ‘***’ 0.001 ‘**’ 0.01 ‘*’ 0.05 ‘.’ 0.1 ‘ ’ 1 (Adjusted p values reported -- single-step method)

781

782 **Table S8 (related to Fig. 4a).** Linear mixed effects (LME) model results on count data (Z-
 783 standard score transformed) on the choice experiment (diproline-loaded bead vs. dSi-loaded
 784 bead) for two different treatments (induced and not induced).

	numDF	denDF	F-value	p-value
Induced				
(intercept)	1	48	2.170292	0.1472
bead	1	8	14.231266	0.0054
time	1	48	1.902299	0.1742
bead:time	1	48	5.282655	0.0259
Not induced				
(intercept)	1	48	15.13610	0.0003
bead	1	8	14.01567	0.0057
time	1	48	19.14796	0.0001
bead:time	1	48	15.38768	0.0003

785

786

787 **Table S9 (related to Fig. 4b).** Pair-wise comparisons using Tukey's HSD of speed (log+1
 788 transformed) around a diproline, dSi, or outside the beads on the choice experiment for two
 789 different treatments (induced and not induced)

Pair-wise comparisons	Estimate	Std. error	z-value	Pr(> z)
Induced				
diproline – dSi	-0.21276	0.03375	-6.305	<0.001 ***
diproline – outside beads	-0.15616	0.02216	-7.048	<0.001 ***
dSi – outside beads	0.05660	0.02758	2.053	0.0953 .
Not induced				
diproline – dSi	0.14404	0.03555	4.052	0.000144 ***
diproline – outside beads	-0.02178	0.03192	-0.682	0.764509
dSi – outside beads	-0.16581	0.01845	-8.989	< 1e-05 ***

790 Signif. codes: 0 ‘***’ 0.001 ‘**’ 0.01 ‘*’ 0.05 ‘.’ 0.1 ‘ ’ 1 (Adjusted p values reported -- single-step method)

791

792

793 **Table S10 (related to Fig. S4).** Linear mixed effects (LME) model results on count data (Z-
 794 standard score transformed) on the dSi attraction experiment of large-sized cells (strain 84A)
 795 (dSi-loaded beads vs. control beads).

	numDF	denDF	F-value	p-value
(intercept)	1	27	5.515138	0.0264
bead	1	4	8.616357	0.0426
time	1	27	6.801745	0.0147
bead:time	1	27	11.34181	0.0023

796
 797 **Table S11 (related to Fig. S5).** Pair-wise comparisons using Tukey's HSD of cell speeds (log+1
 798 transformed) in different combinations of starvation and induction and with addition of trace
 799 amounts of dSi (~50 µM per well) 6 h after induction.

Pair-wise comparisons	Estimate	Std. error	z-value	Pr(> z)
not starved, not induced – starved, induced	0.0016413	0.0196737	0.083	0.99999
starved+dSi – not starved, induced	-0.0733831	0.0208220	-3.524	0.00342 **
starved, induced – not starved, induced	-0.0726083	0.0224860	-3.229	0.00976 **
starved, not induced – not starved, induced	0.3742123	0.0443702	8.434	< 0.001 ***
starved+dSi – not starved, not induced	-0.0750244	0.0206693	-3.630	0.00245 **
starved, induced – not starved, not induced	-0.0742497	0.0223446	-3.323	0.00718 **
starved, not induced – not starved, not induced	0.3725710	0.0442987	8.410	< 0.001 ***
starved, induced – starved+dSi	0.0007748	0.0233620	0.033	1.00000
starved, not induced – starved+dSi	0.4475954	0.0448205	9.986	< 0.001 ***

800 Signif. codes: 0 '***' 0.001 '**' 0.01 '*' 0.05 '.' 0.1 ' ' 1 (Adjusted p values reported -- single-step method)

801

802

803

804

805

806

807 **SI Movies**

808 **Movie S1.** This 1 h movie shows the chemoattraction of dSi-starved cells to a dSi-loaded bead.
809 Cells began to move towards the bead within ~3 min of bead exposure. After ~25 min, the cells
810 around the bead stopped moving as previously described by Bondoc et al.¹ The video speed was
811 accelerated 50 times and the scale bar indicates 100 μ m. Time stamp denotes min:s.

812 **Movie S2.** This 1 h movie shows the chemoattraction of dP-starved cells to a dP-loaded bead.
813 Cells began to move towards the bead within ~20 min of bead exposure. The video speed was
814 accelerated 50 times and the scale bar indicates 100 μ m. Time stamp denotes min:s.

815 **Movie S3.** This 1 h movie shows a dN-loaded bead (NH_4^+) eliciting no response from dN-starved
816 cells. The video speed was accelerated 50 times and the scale bar indicates 100 μ m. Time stamp
817 denotes min:s.

818 **Movie S4.** This 1 h movie shows a dN-loaded bead (NO_3^-) eliciting no response from dN-starved
819 cells. The video speed was accelerated 50 times and the scale bar indicates 100 μ m. Time stamp
820 denotes min:s.

821 **Movie S5.** This 1 h movie shows the control bead inducing no response from dP-starved cells.
822 The video speed was accelerated 50 times and the scale bar indicates 100 μ m. Time stamp
823 denotes min:s.

824 **Movie S6.** This 10 min movie shows dSi-starved, induced small-sized cells being attracted
825 towards a diproline bead. The video speed was accelerated 50 times and the scale bar indicates
826 100 μ m. Time stamp denotes min:s.

827 **Movie S7.** This 10 min movie shows dSi-starved, not induced small-sized cells being attracted
828 towards a dSi bead. We propose that dSi is needed for attraction towards diproline, as starvation
829 of auto-inducing cells did not induce diproline attraction. The video speed was accelerated 50
830 times and the scale bar indicates 100 μ m. Time stamp denotes min:s.

831

832

833

834 **SI References**

- 835 S1 Bondoc KGV, Heuschele J, Gillard J, Vyverman W, & Pohnert G (2016) Selective
836 silicate-directed motility in diatoms. *Nat. Com.* 7:10540.
- 837 S2 Schindelin J, *et al.* (2012) Fiji: an open-source platform for biological-image analysis.
838 *Nat. Methods* 9(7):676-682.
- 839 S3 Strickland J & Parsons T (1972) A practical handbook of seawater analysis 2nd. ed. *Bull.*
840 *Fish. Res. Board of Canada. Ottawa*:310.
- 841 S4 Bondoc KGV, Lembke C, Vyverman W, & Pohnert G (2016) Searching for a mate:
842 pheromone-directed movement of the benthic diatom *Seminavis robusta*. *Microb. Ecol.*
843 72(2):287-294.
- 844 S5 Barbara GM & Mitchell JG (2003) Marine bacterial organisation around point-like
845 sources of amino acids. *FEMS Microbiol. Ecol.* 43(1):99-109.
- 846 S6 Berg HC (1993) *Random walks in biology* (Princeton University Press).
- 847 S7 Blackburn N, Fenchel T, & Mitchell J (1998) Microscale nutrient patches in planktonic
848 habitats shown by chemotactic bacteria. *Science* 282(5397):2254-2256.
- 849
- 850
- 851
- 852
- 853
- 854

4 DISCUSSION AND FUTURE PERSPECTIVES

Patchiness of microscale communities is a product of microbe-microbe interaction and physiological and behavioural response to environmental gradients or chemical signals^{97,98,101}. Foraging for nutrients, finding mating partners, selecting suitable settlement sites, and avoiding predators for a microorganism occurs at a microscale. These processes collectively affect microbial trophodynamics and nutrient cycling on a larger scale^{97-100,124}. A benthic biofilm is an exemplary model of a patchy microscale community, possessing distinct hydrodynamic and physicochemical properties different from the overlying water⁶⁰. Typically, epipelagic pennate diatoms, primarily motile, biraphid species, dominate benthic biofilms^{38,63}. *Seminavis robusta* is a model organism among this group, and its behaviour can be stimulated individually and monitored readily. Understanding its behaviour could complement existing studies of nutrient dynamics on biofilm communities^{69,80,148} as well as offer new insights on mating dynamics within the biofilm. Foraging for nutrients and locating mating partners are two vital processes that can increase survival in a patchy environment. However, in such a complex habitat, diatoms also face diverse co-occurring stimuli, and behavioural prioritization would be advantageous.

I used chemoattraction assays through stimuli gradient-forming beads, in combination with video monitoring of cell behaviour. Cell tracking and statistical modelling uncovered specific cell motility patterns. In this study, insights were gained on (i) chemoattraction of *S. robusta* towards specific nutrient sources across its life cycle (Publications A and C); (ii) mate-finding mechanism of sexual cells through pheromones (Publications B and C); (iii) prioritization between nutrient acquisition and mating on sexual cells (Publication C); (iv) distinct motility patterns arising from sensing and signal perception (Publications A, B, and C); and (v) effect of directed motility on ecological and biogeochemical cascades. Fig. 9 depicts the summary of the results of this thesis.

4.1 Nutrient attraction across the life cycle

Two of the limiting inorganic macronutrients that most microalgae need are nitrogen, in the form of nitrate and ammonium, and phosphorus in the form of phosphate^{149,150}. Besides these, diatoms additionally require silicate to synthesize their intricately designed frustule or cell wall^{27,151}. Nutrient availability varies spatially as gradients exist with depth, and also temporally due to seasonal or even daily variability. Additionally, steep nutrient gradients can be formed on the benthos and in the

overlying water^{46,53,54,56}. Fluctuations in nutrient availability can inhibit growth and impair the physiology of diatoms. Hence, we determined the response of *S. robusta* to three dissolved inorganic nutrients: silicate (dSi), phosphate (dP), nitrate and ammonium (dN) in **Publications A and C**.

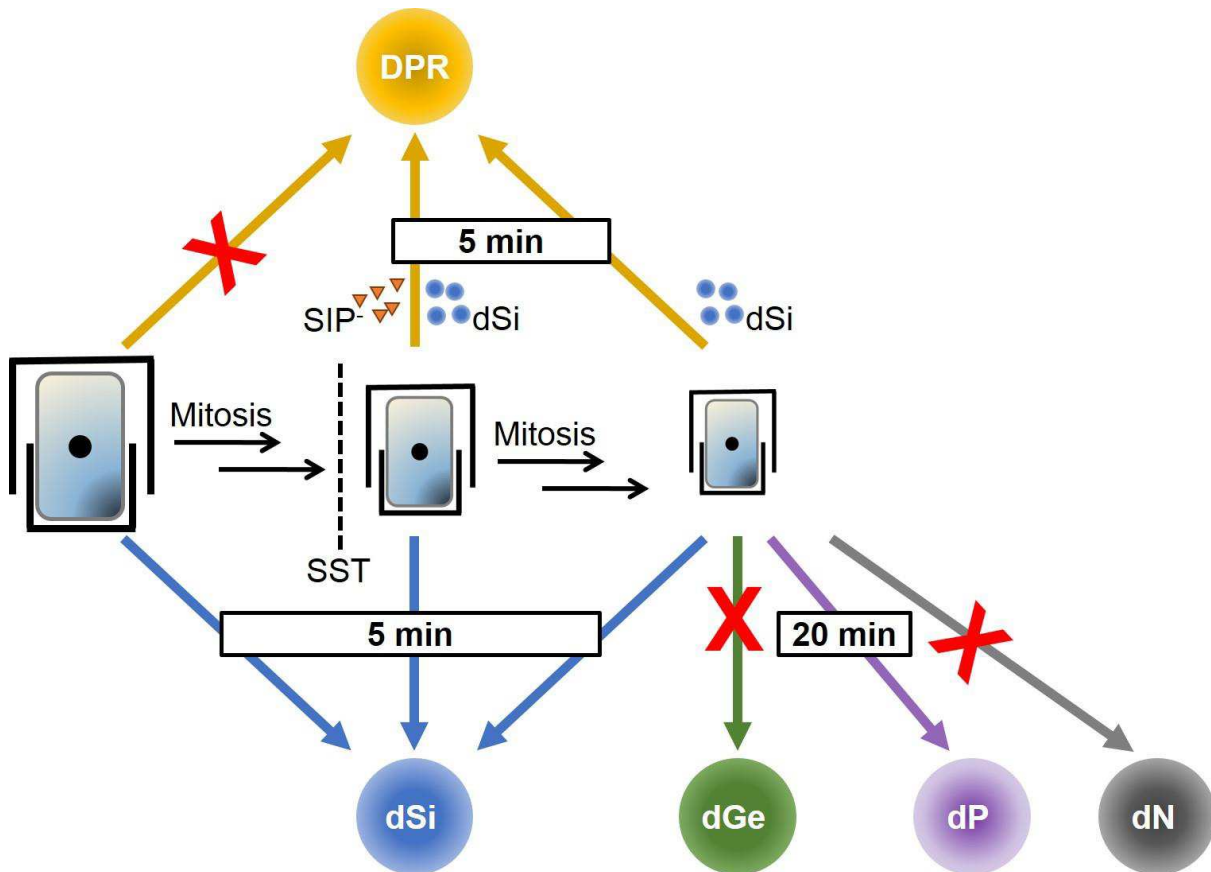


Figure 9. The adaptive motility of *Seminavis robusta* towards nutrient and pheromone sources across its life cycle.

During vegetative growth, cells experience a cell-size reduction of their biomineralized cell wall every mitotic division. Eventually, the cells reach a sexual size threshold (SST, $51.6 \pm 0.5 \mu\text{m}^{33}$) where they can either continue dividing mitotically or undergo pheromone-mediated sexual reproduction to escape programmed cell death and reconstitute their cell size. Throughout the life cycle, nutrients are needed for each cell division. Different sources of inorganic nutrients were tested to determine if there is a preferential migration towards specific gradients. Dissolved silicate (dSi) elicited attraction of starved cells within a 5 min time frame in all life stages, indicating that nutrient foraging is a typical strategy for benthic diatoms throughout their life cycle. The chemically-similar dissolved germanium (dGe) did not elicit any response pointing to a substrate-specific attraction. On the other hand, dissolved phosphate (dP)-loaded beads were also attractive to starved cells but only after 20 min of exposure while dissolved nitrate or ammonium (dN)-loaded beads were not attractive. Once cells reach SST, cells become attracted to the pheromone, diproline (DPR). Cells that recently crossed SST requires the addition of sex-inducing pheromone (SIP) and trace amounts of dSi to be attracted to DPR. On the other hand, critically small-sized cells can bypass the induction mechanism to locate the DPR-loaded bead. This self-priming mechanism could be a life-saving emergency mechanism for the cells on the verge of extinction.

4.1.1 Nutrient starvation and recovery

As with other diatoms, *S. robusta* completely ceased cell division when dSi-starved, but rapidly recover when re-supplemented with it^{131,132} (**Publication C**). This rapid recovery could be attributed

to upregulated genes for dSi assimilation during limiting conditions which allows rapid uptake upon replenishment¹³⁶. On *Thalassiosira weissflogii*, cell division was resumed upon replenishment after only ~3 hours^{131,132}. Although no hourly measurements were done for this experiment, the final cell yield of *S. robusta* after seven days of dSi replenishment was 100-fold higher compared to its initial cell density (**Publication C**), underlining the ability of diatoms to recover rapidly from dSi limitation.

On the other hand, dP-starved cells exhibited a remarkable increase in growth (**Publication C**) similar to those reported for the planktonic *Thalassiosira pseudonana* and *Skeletonema costatum* and the benthic *Nitzschia closterium* when resupplemented with phosphate^{134,137,152}. Luxury uptake, or the storage of excess dP as polyphosphates when dP concentration is high might be the prevailing mechanism for increased cell density even when the medium is dP-limited¹⁵³. However, this response may be species-specific as some diatoms, such as the tychoplanktonic *Cylindrotheca fusiformis*, *Cylindrotheca closterium*, and the benthic *Halimphora luciae* exhibited reduced growth rate^{137,154,155}. Additionally, diatoms can circumvent death from dP starvation through a sophisticated mechanism that enables them to recycle their phospholipid membranes and replace them with sulphur- and nitrogen-containing lipids, and increase their dP transport^{133,134,156}. This overall mechanism could have helped dP-starved cells to recover upon dP replenishment. However, the recovered cell density is 10-fold lower than dSi for replenished cells (**Publication C**), as dP-starved cells could experience a moderate reduction in photosystem efficiency and reduction in chloroplast size which can possibly affect cell division^{138,139,154,155}. Additionally, dP-starved cells could have reduced areola size¹⁵⁵ which can decrease nutrient uptake of cells via diffusion¹⁵⁵.

As for dN-starved cells, they continued to grow as well, although at a lower rate than dP-starved cells or the control (**Publication C**). They survived even after 12 days of starvation by putatively consuming alternative nitrogen resources such as free amino acids as a by-product of bacterial degradation or excreted by the diatom itself⁷⁶, intracellular reserves, and by recycling dN from plastid proteins and polar lipids¹³⁹. However, as a consequence of utilizing key proteins on the photosynthetic apparatus as dN sources in prolonged starvation, their chloroplasts could be reduced in size, drastically decreasing their photosystem efficiency^{138,139,155}, hence, affecting the recovery dynamics. Recovered final cell density was only 6-fold higher than their starting value after seven days of growth (**Publication C**). Moreover, dN starvation can cause the size of the areola to become smaller and have altered patterns¹⁵⁵ which can affect nutrient uptake greater than in dP-starved cells.

Previous model simulations complemented with experimental data of planktonic diatoms showed the rapid recovery of dSi-starved cells compared to dN-starved cells^{131,132,157}. While both dN and dP are necessary for basic life processes as building blocks of biomolecules and in the photosynthetic system, dSi is only crucial for cell wall development. Carbon metabolism is coupled to dN and dP assimilation, while dSi is uncoupled to it¹⁵⁸. In fact, even if dSi is depleted and cells halted their cell division, carbon sequestration and dP uptake can still happen¹⁵⁹, indicating a differential

regulation mechanism for dSi assimilation. Recovery in dSi might be higher because dN and dP are still available for cell use; conversely, the absence of dN and dP required the diatoms to compromise by using recycled alternative intracellular resources, which might have cascading effects on cellular processes. Consequently, regardless of the re-supply of nutrient after starvation, some cellular processes might have been impaired already resulting to lower recovery. Hence, diatoms are better poised to survive under dSi starvation than with the other two nutrients.

4.1.2 Behavioural response to nutrient starvation

In addition to a physiological control for circumventing death when faced with starvation, diatoms also have a complementary behavioural mechanism akin to the foraging behaviour of higher organisms^{94,95,160}. This thesis offers the first overview of such mechanism across the life cycle of a diatom using the model organism *S. robusta* (Fig. 9, lower panel). Together with large vegetative cells (>50 µm), we used two sizes of sexual cells: a medium one that just crossed SST (~40 µm), and a critically small one (24–27 µm). We utilized hotspot sources of nutrients delivered by beads producing steep gradients of specific nutrients, within the same range as reported in the sediment-water interface^{53,54}.

Starved cells exposed to nutrient gradients accumulated around the point-source within ~5 min for dSi (**Publication A**) and ~20 min for dP (**Publication C**). However, no obvious attraction was observed for cells exposed to dN sources even if they were starved for a longer period (~12 days) and exposed to varying concentrations and forms of dN (*i.e.*, NH₄⁺, NO₃⁻) (**Publication C**). Remarkably, dSi attraction was substrate-specific. When we exposed dSi-starved cells to dissolved germanium dioxide (dGe), a chemically-similar mineral, it did not elicit attraction (**Publication A**). Germanium (Ge) is a trace element located below Silicon (Si) in Group IV of the periodic table and is known to be an analogue of Si as it can be used as a replacement in siliceous minerals^{161–163}. Diatoms can uptake dGe and copolymerize it with dSi for the formation of their cell wall at Ge:Si ratios of <0.01. However, dGe can inhibit growth, cause toxicity and morphological aberrations, and decrease the mechanical integrity of the frustule at ratios of >0.05^{161,164,165}. We observed that *S. robusta* could discriminate between these two chemically similar compounds behaviourally by repulsion when dGe-loaded beads are introduced. The observed response to dSi was also reported for *Navicula sp.* indicating that dSi attraction is not species-specific but a universal response in benthic raphid diatoms (**Publication A**). In *S. robusta*, intraspecific variation was also not apparent; that is, chemoattraction to a dSi source was consistent in different strains of *S. robusta* (**Publication A**) and across its life stages in both vegetative (large-sized cells) and sexual cells (medium-sized and small-sized cells) (**Publication C**). The consistency indicates that diatoms rely on active foraging to gain limiting nutrients independent of size. However, compared to sexual cells, vegetative cells required longer starvation time before

responding to dSi-loaded beads (3 days vs. 7 days, respectively) (**Publication C**). Among the factors that may have affected uptake dynamics is the difference in their cell sizes. The decreased surface area to cell volume ratio of larger cells can dictate a higher nutrient uptake demand. However, they are biophysically constrained because nutrient uptake via diffusion is scaled inversely with the cell's radius squared^{166,167}. Additionally, large-sized cells have a thicker diffusion boundary layer, which is a nutrient-depleted area around the cell that inhibits transport of nutrients¹⁶⁸. Conversely, small-sized cells can assimilate dSi faster from the medium due to their thinner boundary layers. Hence, we only tested the chemoattraction of small-sized cells for dP and dN (**Publication C**).

To date, pennate diatoms investigated in this thesis are the only reported organism to have chemoattraction towards dSi even if some other microorganisms can also use dSi for the formation of their cell walls (silicoflagellates and thaumatomastigids) or their plates (testate amoebas) and spicules (flagellates)¹⁶⁹. In contrast, various organisms are known to respond to dP and dN. The dinoflagellate *Chatonella antiqua* and bacterioplankton *Thalassospira* sp. exhibited chemotaxis to dP sources^{170,171}. Most prokaryotes can chemotactically move towards dN sources. These include the cyanobacterium *Synechococcus*, non-sulphur photosynthetic purple bacterium *Rhodobacter sphaeroides*, and several species of the lake bacteria *Variovorax*, *Actinobacteria ACK-M1*, and *Methylophilaceae* family^{172,173}. Additionally, several lake bacteria in the *Sphingobacteriales* order showed attraction to both dN and dP sources¹⁷³. On the other hand, the chlorophyte phytoplankton *Dunaliella tertiolecta* was attracted to NH₄⁺¹⁷⁴, while the vegetative cells and non-competent pre-gametes of *Chlamydomonas reinhardtii* exhibited chemotaxis towards NH₄⁺^{175,176}, NO₃⁻¹⁷⁷, and NO₂⁻¹⁷⁸. However, green algae respond differently to dN starvation by increasing their C-stores to produce lipids, while, diatoms remobilize C sources as observed in cyanobacteria¹⁷⁹. Due to this remobilization, dN-starved pennate diatoms have low production and extrusion of extracellular polymeric substances (EPS) that are essential for motility,^{154,155,180} which could potentially lower foraging efficiency.

The response of motile organisms towards chemical signals could involve either taxis or kinesis. Both of these reactions can affect the accumulation or repulsion of cells¹⁴⁴. In chemotaxis, there is directed movement towards the stimuli, whereas chemokinesis is characterized by changes in motility parameters such as speed (orthokinesis) or turning frequency (klinokinesis) as cells perceive stimuli gradients^{144,146}.

We showed that foraging dSi- (**Publication A**) and dP-starved (**Publication C**) small-sized cells moved faster than non-starved cells, and can finely regulate their speed in response to bulk or gradients of such nutrients. Bulk replenishment of nutrients reversed this behaviour, pointing to an orthokinetic control of movement. Cells sped up in the immediate periphery of an attractive nutrient source, indicating their ability to sense gradients and, ultimately, direct their movement towards a high concentration area. The highest speeds were initially observed in the proximity of the bead, where nutrient concentrations are highest. Increased motility might aid cells to minimize diffusion-limitation

uptake by lowering diffusion boundary layer formation¹⁶⁸. One hour observation showed a continuous influx of cells towards the dSi source until ~25 min of exposure; after that, cells entered a satiation phase, which is characterized by decreased speed and cessation of movement in the proximity of the bead (**Publication A**). As uptake is diffusion mediated in high dSi concentrations¹⁸¹, the observed termination of motility could be a mechanism to control dSi uptake. In contrast, dP-starved cells did not reach satiation phase, as accumulation around the bead is evident until the end of the observation time. Chemoattracted cells also exhibited a tactic mechanism by increasing their forward steps towards the nutrient-loaded bead. Consequently, foraging cells mediated their movement by searching larger areas and persistently towards the source to maximize their encounter rate. The aforementioned kinetic mechanism of speed regulation and tactic response with directed persistence points out to a unique utilization of simultaneous tactic and kinetic mechanism in *S. robusta*. The concurrent use of both taxis and kinesis was also previously observed in another benthic biraphid diatom, *Navicula perminuta* in response to light wavelength⁷⁰. Marine bacteria also utilize a similar mechanism in moving toward sources of nutrients such as amino acids¹⁰⁵ and coral hosts¹¹⁶. Both marine bacteria and biraphid pennates share the same characteristic back-and-forth or run-and-reverse gliding strategy^{22,116}, which could enable them to simultaneously employ taxis and kinesis as a response to chemical signals.

4.1.3 Nutrient uptake enhanced by motility

Diatoms have a very low Reynold's number (~10⁻⁵–10⁻⁴) due to their small size and slow movement¹⁶. At this scale, the viscosity of the surrounding water can limit the transport of nutrients to the diffusive boundary layer, and nutrient transport is only via molecular diffusion in a one-dimensional gradient^{60,96,99}. When this layer is disturbed via motility of the organism or active flow of water, the nutrient influx is enhanced¹⁶⁸. The effect of motion on nutrient influx can be described using the relationship between the dimensionless parameters, Sherwood (*Sh*) and Peclet (*Pe*) numbers. *Sh* describes the enhancement of nutrient influx due to flow and is dependent on *Pe*, which is the ratio of advection to diffusion through a medium over a length scale. At *Pe* < 1, diffusive forces dominate, whereas advective forces are significant when *Pe* > 1^{96,182}. The *Pe* of *S. robusta* can be calculated using the formula:

$$Pe = \frac{ua}{D}$$

Where *u* is the speed of the cells (3–25 µm s⁻¹), *a* is the major radius (radius of the cell length) across the life cycle (10–35 µm), and *D* is the diffusivity of small molecules (10⁻⁵ cm² s⁻¹)¹⁸³. The resulting *Pe* is equivalent to 0.03–0.88. We can then calculate *Sh*¹⁸² as:

$$Sh = \frac{1 + (1 + 2Pe)^{1/3}}{2}$$

The resulting increase in uptake is computed as $Sh-1$. It is equivalent to 0.98–20% increase depending on the cell's size and speed. A small-sized cell will increase its uptake 7-fold if it increases its speed ten times, whereas a large-sized cell is 3-fold more efficient in nutrient uptake than a small-sized cell with the same speed. Hence, increasing speed seems to be a good strategy for a small cell. The observed increasing speed as cells approaches a nutrient-loaded bead could help increase nutrient uptake through lowering the diffusion limitation of cells.

Initial comparisons of enhancement of nutrient uptake through active foraging in pelagic and benthic diatoms show that the latter have a disadvantage. Large-sized pelagic centric diatoms (>100 µm in diameter) can increase their nutrient uptake rate up to 170% by altering their buoyancy in response to nutrient stress. Their start-stop sinking behaviour increases nutrient uptake via flow when they sink fast¹⁴. Unlike pelagic diatoms, benthic microalgae have the advantage of having exclusive access to nutrients from the substrata, while also being able to tap on the available nutrients in the water column^{45,46,50,86}. Field data also shows that motile biraphid diatoms actively seek out higher nutrient concentrations and can withstand water velocities of up to 0.43 m s⁻¹⁸⁰. Assuming that the active searching behaviour combined with water velocity can decrease the diffusive boundary layer significantly, the slower movement of benthic diatoms would not hamper their nutrient uptake efficiency. If Pe and Sh are re-computed using the water velocity mentioned and with the assumption that cells are not motile, the resulting value for $Pe = 43–150.5$ and for $Sh-1$ is 172–285%. It is possible that advection forces prevail in the benthos when the water velocity is high which could enhance nutrient uptake. Uptake can increase up to 174-fold for a small-sized cell, and 87-fold for a large-sized one compared to the values when cells have low speed, making the nutrient uptake rate of benthic diatoms is on par with pelagic ones.

Overall, the observed recovery and foraging mechanism of diatoms can increase their advantage in out-competing other algal groups. Fine tuning of motility parameters while foraging increases nutrient uptake to circumvent severe limitation scenarios in the benthic environment.

4.2 Pheromone-mediated chemoattraction of sexual cells

Sexual reproduction is a common proliferation strategy in eukaryotes, which enhances the genetic diversity in a species through gene recombination¹⁸⁴. In diatoms, sexual reproduction is essential for size restitution since failure to do so will result in programmed cell death^{27,28,184}. However, mating efficiency is dependent on secondary cues like environmental factors (light intensity, temperature, and nutrient availability)^{28,141}, and pheromone production by mating partners^{27,33–35,185}.

Pheromones synchronize behaviour of opposite mating types by signalling the presence and location of a mate, thereby, enhancing reproduction success¹⁸⁶. On **Publications B and C**, *S. robusta* served as our model for exploring the behavioural patterns induced by pheromone-mediated mate-finding in pennate diatoms (Fig. 9, upper panel).

The pheromone system of *S. robusta* harbours a complex cascade of signals. The sex-inducing pheromones (SIP⁺ and SIP⁻) produced by the respective mating types (MT⁺ and MT⁻) signal partners their sexual state and mediate perception and production of the attracting pheromone diproline, generated by MT⁻. Since sexual cells of *S. robusta* are morphologically identical, the behavioural observation was limited only to the migrating mating type (MT⁺). The diatom pheromone diproline from the attracting mating type (MT⁻) was chemically synthesized and used for bead experiments as previously described by Gillard *et al.*³³.

MT⁺ cells responded to pheromone gradients rapidly by moving towards the source and undergo repeated pairing attempts with the bead within ~5 min. Interestingly, cells respond to diproline with the combined tactic and kinetic manner similar to foraging cells. They also exhibit fine tuning of speed, by moving faster in the immediate periphery of the bead, indicative of a kinetic response. Attracted cells showed lack of angular orientation towards the bead, but with increasing forward steps, indicating a tactic response. As with nutrient chemoattraction, the combined tactic and kinetic response led to an increased encounter rate of the signal (**Publication B**).

Although sexual MT⁺ cells responded to diproline independent of cell size, the factors affecting their attraction varied. SIP induction was a necessary step for cells that recently crossed SST (medium-sized cells) to be attracted to diproline gradients. Sexual cells can continue to divide mitotically but with the risk of higher occurrence of abnormal morphology as they become smaller^{27,28}. When we exposed critically small-sized cells to diproline with and without SIP induction, they exhibited a similar degree of attraction. The small-sized cells then exhibit auto-induction, which could be a life-saving emergency mechanism, prompting the cells to prioritize sexual reproduction (**Publication C**). During auto-induction, pheromone-mediated priming is bypassed, enabling the cells to rapidly find a mating partner once the diproline cue is encountered. In previous experiments, a reduced cell size in *S. robusta* also led to a higher reproduction success¹⁴¹; the pressure to mate and subsequent auto-induction might be a reason behind this. The phenomenon of sex induction as a function of cell size clearly has to be further verified on other diatoms exhibiting pheromone-mediated mating as well, such as those reported on *Pseudostaurosira trainorii*³⁴ and *Pseudo-nitzschia multistriata*³⁵.

The use of pheromones is genetically and energetically costly¹⁸⁴, but their pervasiveness in a wide range of organisms is indicative of a central role in ensuring the initiation and success of sexual reproduction¹⁸⁶. Mate attraction using pheromones is only common among organisms that are over a millimetre in size, with a critical size between 0.2 and 5 mm. Below this threshold, pheromone use is inefficient, as the chemical diffuse faster than the organism can produce it. In fact, for microorganisms,

only ciliates are known to track their mate using pheromones¹⁸⁷. However, the case is different for organisms utilizing specialized haploid cells called gametes (*i.e.*, egg and sperm) that carry genetic information to recombine with a potential mate. Pheromone use in gametes is a special circumstance as the energy that they get from the parental cells are utilized solely for mate location¹⁴⁴. A wide range of aquatic photosynthetic organisms such as brown algae produce gametes that employ pheromones in mating^{144,145,147}. For diatoms, there are only two reported studies on mate-finding, and both of them utilize gametes. In the araphid pennates *Pseudostaurosira trainorii* and *Tabularia fasciculata*, induction from opposite mating types triggers gametogenesis or the production of haploid motile male and stationary female gametes^{32,34}. While mate-locating in *P. trainorii* is guided by unidentified pheromones³⁴, *T. fasciculata* requires physical contact to recognize its mate³². In contrast, the pheromone-mediated attraction of *S. robusta* is different as it is the gametangia or the diploid ‘adult cells’ that are involved in tracking the pheromone and mating.

MT- cells can leave a pheromone trail which the MT+ cells can follow, analogous to the trail tracking mechanism of copepods¹⁸⁸. A mate can detect a pheromone plume that has a defined length, and this length is independent of the speed of the opposite mating type. The trail length (L) reveals the sensitivity of tracking partners to the cue from the opposite mating type. This parameter can be estimated for MT- assuming that a patch of cells is releasing the same concentration of diproline as with the bead used in the attraction assays. The formula from Bagøien and Kiorboe¹⁸⁸ could be used:

$$L = \frac{Q}{4\pi DC}$$

Where Q is the release rate of diproline (synonymous with i from **Publication B**: $6.06^{-18} \pm 6.66^{-19}$ mol s⁻¹), D is the diffusivity of small molecules (10^{-5} cm² s⁻¹), and C is the concentration of diproline from the diffusion experiments (calculated to be $3.22^{-11} \pm 3.52^{-12}$ mol cm⁻³ in **Publication B**). The resulting trail length is 15.12 ± 1.58 μm, which is also equivalent to <1 body length. Even if the production of diproline is density-dependent³³, the estimated trail length here would still be similar assuming that the concentration and release rate of diproline are proportional to each other. That is, for an attractive bead or an MT- patch producing any concentration of diproline, the resulting trail length would still be ~15 μm. At this length, the attracted cells can directly follow a track of a motile MT- and do repeated contact for pairing, as we also observed in the bead experiments. For a bead loaded with 0.2 nM diproline, which is the lowest attractive concentration³³, the pheromone concentration at the 15 μm trail length would be 0.08 nM, highlighting the sensitivity of cells in tracking a pheromone trail. However, it was apparent that cells can change their direction 250 μm away from the bead, where a concentration of 0.019 nM or 19 pM diproline will occur. We could use this calculated value as the threshold concentration for diproline, that is the lowest concentration eliciting significant cell

attraction¹⁴⁵. The concentration is within the range of the measured threshold concentration of pheromone reception for planktonic flagellated brown algae¹⁴⁷, highlighting that pheromone sensitivity is widespread in marine algae regardless of their life history strategy (i.e. gametangiogamy or gametogamy).

4.3 Sensing mechanisms: How do diatoms find chemical signals?

Crucial to signal perception is the guiding mechanism for orientating towards or away from signals, depending on the information they convey. The simultaneous tactic and kinetic mechanism employed by diatoms to migrate towards a chemoattractant point out to a potentially combined sensing and guiding mechanism.

The majority of studies on diatom behaviour is about the light-regulated migratory reactions of benthic pennates, showing that they can respond both tactically and kinetically to specific light gradients^{24,25,70,71}. Motile benthic pennate diatoms can sense light on the tips of their cells, enabling a photophobic response at high irradiance, indicative of the presence of a cellular apparatus that can detect stimuli on both the trailing and leading ends of the cell^{24,25}. Through these receptors, diatoms can make simultaneous comparisons of signals spatially on both ends and directly guide cells to move either directly up or down along a gradient producing a tactic response⁹⁶. It might be possible that receptors for chemical stimuli are also localized on the tips of the cells since the directionality up or down a gradient is dictated by either moving forward or backwards through the leading and trailing end of the cell, respectively. On the other hand, the kinetic response of diatoms could also be described as a biased random walk, wherein steps forward or backwards have the same probability but tend to be of different lengths, analogous to the run-and-tumble mechanism of flagellated prokaryotes. Chemokinesis is a product of temporal sensing or the successive comparison of stimuli during movement resulting in the modulation of motility parameters which can lead to the indirect guiding of cells⁹⁶. Temporal sensing is highly dependent on the speed of the organism, that is, higher cell speed is more efficient for this mechanism than cells that move slower. Unlike bacteria that can travel ten times their body length in 1 s⁹⁸, *S. robusta* can only maximally travel ca. 1 body length s⁻¹, hence the use of temporal sensing alone would be unprofitable for a diatom. It is highly possible that to make up for its slow speed, a combined spatial and temporal sensing mechanism is employed by *S. robusta* since it increases nutrient foraging and mate-locating efficiency in a patchy environment.

4.4 Prioritization mechanisms: Food vs. sex on sexually-available diatoms

The interplay between acquiring nutrient and mating is complicated as it involves a cascade of signalling events and behaviour regulation. Also, chemical signal distribution is often spatially patchy

and temporally constrained. Dissolved nutrients would be more common for a diatom cell to encounter than patches of its mating partners as diproline is rapidly degraded after its release³³. Hence, cells increase their motility parameters drastically in search of the pheromone as compared to when they are foraging for nutrients, as was shown in **Publication B**. Both dSi and diproline elicited chemoattraction within a 10 min observation time. However, computational comparisons are oversimplified and tend to overlook the differences in the physiological conditions of the cell. Moreover, cells attracted to dSi can benefit in moving up towards the gradient to prevent diffusion limitation uptake, whereas cells attracted to the pheromone need to encounter the diproline-loaded bead directly. Hence, I designed an experimental set-up where sexual cells in different physiological conditions are faced with multiple stimuli to determine the decision-making mechanism of cells, mimicking the patchy and mixed condition they experience in their natural environment (**Publication C**).

While large-sized cells exhibited a definite attraction to dSi and non-attraction to diproline³³, information on prioritization of different sizes of sexual cells is lacking. Therefore, sexual cells that recently crossed SST (medium-sized cells) and critically small-sized cells were exposed to various combinations of dSi-starvation and priming. Individual beads loaded with dSi or diproline were applied to each treatment. Medium-sized cells exhibited attraction to diproline only when induced, while dSi attraction occurred when starved. Therefore, there is a clear physiological control of prioritization of cells on this size. On the other hand, only dSi-starvation can render dSi attraction in small-sized cells, as what was observed for all the other cell sizes. Besides the auto-induction observed in small-sized cells, a combination of dSi-starvation and SIP-induction still elicited pheromone attraction, albeit at a lower rate than SIP-induced cells alone and auto-induced cells. Induction introduced trace amounts of dSi (~50 µM) as the SIP was from the filtered spent medium of exponentially growing MT- cells. It is probable that residual dSi concentrations might be needed for diproline attraction since dSi is required in the formation of a new cell wall after pairing. Moreover, excess dSi could hamper mating even after the first round of cell division¹⁸⁹. In contrast, dSi-starved and non-induced cells were not attracted to diproline. Small-sized cells offered with both dSi and diproline-loaded beads on choice experiments showed similar response with those in the one-bead experiment. That is, dSi-starved and non-induced cells did not switch towards diproline within the observation time, highlighting the role of trace dSi before mating can progress. To further clarify the interplay of nutrient foraging and mating and the subsequent prioritization mechanism, additional experiments with purified SIP- in a combination of different concentrations of dSi can be conducted.

Our choice assay results suggest a signalling pathway integration and crosstalk between dSi-sensing and mating for *S. robusta*. Microeukaryotes like the yeast, *Saccharomyces cerevisiae* and the chlorophyte *C. reinhardtii* can integrate multiple stimuli enabling them to choose between nutrient uptake and mating^{175,190}. In *S. cerevisiae*, the pheromone-mediated mating is halted when glucose

becomes limiting. Briefly, when the carbon source is low, a cascade of G protein-coupled receptors (GPCRs) phosphorylation events reduce mating efficiency and increase survival through metabolic adaptation^{190,191}. In the case of *C. reinhardtii*, mating and chemotaxis to dN sources are coupled since both processes require flagellar motility which is mediated by the secondary messenger cAMP¹⁹²⁻¹⁹⁴. In a recent study, the planktonic diatom *P. multistriata* downregulated gene expression of nutrient transporters and cyclins when sexually induced. Furthermore, synthesis of the secondary messenger cyclic nucleotide cGMP which is responsible for downstream signalling for pheromone perception was upregulated, indicating that nutrient uptake is halted once the cells are induced¹⁴². Additionally, GPCRs, cell surface receptors that link nutrient and pheromone reception in *S. cerevisiae* were also detected in *Pseudonitzschia sp.*, indicating a potential role for such mechanisms in diatoms^{142,190,191,195}. First experiments on *S. robusta* showed that SIP⁺ induction also triggers the expression of a guanylyl cyclase/phosphodiesterase (GC/PDE) in MT⁻ cells; GC/PDE is responsible for the synthesis and breakdown of the cyclic nucleotides, cyclic adenosine monophosphate (cAMP) or cyclic guanosine monophosphate (cGMP)³⁶. Also, secondary messengers appear crucial for motility in *S. robusta*. A NO/cGMP signalling mediates motility and biofilm formation in *S. robusta* by reducing adhesiveness of EPS and allowing the cell to choose suitable habitats²¹. As motility is mediated by both foraging and mate searching, the possible role of secondary messengers as a mediating molecule might be possible. However, this highly sophisticated mechanism requiring fine control of genetic and behavioural aspects should be further examined.

Indeed, the interplay between nutrient foraging and mating is a complicated mechanism involving signalling events and regulation of behaviour. This thesis offers the first insight into the behavioural response of a diatom to multiple stimuli and lends explanation on the patchy distribution of diatoms within a biofilm. The active searching behaviour to specific stimuli depending on physiological conditions, as well as the on/off switch for mate recognition, can help in understanding how diatoms gained dominance in benthic communities.

4.5 Implications of directed motility – evolutionary aspects and ecological cascades

An integral part for both nutrient-searching and mate-locating in *S. robusta* is the raphe system, a product of evolution synonymous with the evolution of flight in birds. The evolution of raphe greatly helped in niche expansion, and consequently in diatom diversification in submerged habitats¹⁹⁶. On an evolutionary time scale, araphid pennates were the first diatoms to colonize benthic surfaces. Araphids are mostly immotile except for a few that can glide via excretion of mucilage as raphid diatoms do, albeit at a lower speed¹². Interestingly, both araphids and raphids exhibit gametangiogamy as a life history strategy with araphid having no strict requirement for it. Additionally, pheromone mediation is optional for araphid pennates^{32,34,197}. As gametangiogamy evolved first before the raphe system,

some araphids would need to rely on slow gliding and passive transport in the water for mating. It would be a driving mechanism to support faster motility as a way to increase chances of successful pairing in a crowded habitat. Hence the evolution of a raphe system emerged in raphid pennate diatoms^{28,196}. Additionally, active motility could have also aided in exploiting hotspot sources of nutrients effectively, highlighting the adaptation of raphid pennates to a patchy environment.

Directed motility towards nutrient sources can alleviate nutrient limitation as diatoms exhibiting this behaviour can position themselves in beneficial environments. Besides being highly motile, biraphids are also nutrient-sensitive and can perform better in highly eutrophic habitats^{57,148}. If the observed dSi and dP-foraging behaviour from my study applies to all motile biraphids, we can infer that it is the reason behind their abundance in a patchy environment, as they can avoid nutrient limitation effectively through modulation of their behaviour. Their proliferation in this habitats can also control the availability of DOM in the environment, in turn mediating the abundance of heterotrophic bacteria. Additionally, diatoms as the base of most benthic food webs can affect the abundance of consumers, such as macro- and meiofauna^{42,43}.

Most community studies focused on dN or dP enrichment in sediment, artificial substrates, or even in overlying water^{50,57,77-81}. From these studies, the addition of dN into dN-limited environments resulted in higher diatom biomass⁷⁹⁻⁸¹, so it seems logical to assume that there is an underlying foraging behaviour for dN as well. However, based on our results, diatoms were not attracted to either NH₄⁺ or NO₃⁻, regardless of concentrations used. However, the possible utilization of organic nitrogen sources cannot be excluded, as an explanation for the lack of observed diatom attraction to dN. Besides their mechanisms to overcome dN limitation by NH₄⁺ and NO₃⁻ uptake, benthic diatoms have been shown to uptake dissolved free amino acids (DFAAs) even in the presence of high inorganic dN sources. DFAAs are released to the sediment by excretion of both algae and bacteria, as well as through the process of lysing and breakdown of algal cells^{82,198,199}. The uptake preference for DFAAs might be the reason behind the non-attraction of *S. robusta* to dN-loaded bead. However, it might still be possible that other benthic pennates would have a different response to a dN-loaded bead. On the other hand, dP foraging was observed on *S. robusta*, which could be explained by the patchy distribution of dP, as well as dSi, as both nutrients come from mineral sources in the benthos. However, bacteria can out-compete diatoms in taking up dP and dissolved organic phosphorus (DOP)^{152,153,200}. Hence, the observed dP-foraging mechanism in diatoms could be an adaptive effort to explore dP hotspots in the benthos²⁰¹.

Si is mostly released from settled amorphous biogenic silica from the water column or mineral quartz in the sediment^{202,203}, with only the latter releasing dSi, which is the form preferred by diatoms for uptake^{84,202}. Brehm *et al.*²⁰⁴ previously showed that diatoms, with the help of associated bacteria, could leach dSi from quartz sand in a particle-size/surface area-dependent manner. Quartz sand and the beads I used in my experiments can be within the same size range, thus mimicking the particles

sizes that foraging cells may encounter in nature. The unprecedented attraction of *S. robusta* towards dSi-diffusing beads might be a dominant mechanism for motile diatoms in the benthos in their attempt to seek out particles diffusing dSi.

Motility can confer an advantage for mate-searching in a dense microhabitat. Sexualized mating types continuously secrete low concentrations of priming pheromones to signal each other of their presence³⁶. In a biofilm where chemical signals are diverse, this would be an advantageous mechanism that enables the cells to gain information on the presence and abundance of the opposite mating type. Spatial information on the exact location of MT⁻ will be given by diproline, which is produced in relatively higher concentrations than the priming pheromones^{33,36}. The production of the attraction pheromone is not just density-dependent but also light-activated,³³ suggesting that cells maximize their encounter rate to a mating partner to potentially coincide with the diel vertical migration. Emission of species-specific attracting pheromone coupled with temporal interspecific differences in vertical migratory patterns⁶⁹ could aid in higher mating success in a patchy environment.

The life cycle of diatoms can have an impact on biogeochemical cycles^{2,184}. Mitotically-dividing cells reduce CO₂ by efficiently fixing dissolved inorganic carbon to particulate organic matter through photosynthesis². When cells switch to sexual reproduction, empty frustules from auxosporeulation are discarded²⁷ which can be a source for re-mobilized sources of dSi. During a mass sexual phase, as in the case of blooms, empty silica cell walls can contribute significantly to Si flux on the benthos²⁰⁵. Furthermore, organic carbon could be recycled into the benthic microbial loop or released back into the euphotic zone when cells undergo lysis after failing to find its mate or when gametes do not fuse^{2,184}.

The overall processes discussed here gave insights on how microscale-processes such as the directed movement towards nutrients and chemical signals can have an impact on a larger scale. Additionally, the evolutionary significance of such mechanism also lends an incredible illustration on how behaviour is selected. The active behaviour in both nutrient foraging and mate-locating of benthic diatoms as an adaptation to a patchy environment could have been one of the factors driving the diversification of pennates on benthic habitats¹⁴⁰.

4.6 Future perspectives

Behavioural response of an organism is a product of both its inherited genome and external stimuli such as environmental cues and chemical signals⁹⁶. This thesis dealt largely with behaviour analyses, and it would be intuitive to complement the studies undertaken herein with molecular techniques, physiological experiments, and additional behavioural observations that mimic the environment of benthic diatoms.

Methods in the -omics field could help in elucidating the cross-talk between nutrient foraging, and mate-locating, and their regulatory effect in motility, to provide a coherent analysis/overview and a potential model pathway for diatom sensing and behaviour, similar to the yeast and *C. reinhardtii* model discussed above^{190,192}. In fact, metabolomics was already used to isolate, elucidate, and characterize the attraction pheromone diproline in *S. robusta* with a complementary behavioural assay also utilized in this thesis³³. Moreover, the proposed structure of SIP⁺, as well as its effect on the transcriptome of MT⁻ including the production of diproline, has recently been elucidated³⁶. The effect of SIP⁻ on MT⁺ could complement the previous study with a focus on elucidating potential diproline and dSi receptors, as well as motility factors. Experiments could initially focus on the possible roles of secondary messengers and GPCRs to determine how diatoms integrate signals and mediate behaviour as discussed beforehand^{21,36,142,195}. The existence of auto-induction in other diatoms with pheromone-mediated sexual phase^{34,35} and elucidate the genetic control of this mechanism could also be an aspect that could be investigated. Elucidation of silicic acid transporters (SITs) in *S. robusta* could also give insights in determining genetic controls for dSi sensing and assimilation. Specific SIT clades are hypothesized to have differential functions and are lineage-specific. Particularly interesting is SIT clade D which is present in major diatom lineages and hypothesized to function on sensing and signalling²⁰⁶. Furthermore, the possibility of co-limitation of nutrients, as well as the utilization of organic substrates should be explored. Co-limitation of one or two nutrients is highly possible in multi-species habitat since different species would have different uptake preferences for various forms of specific nutrients^{131,132,134,137,152,154,155}. Diatoms are also well-known to utilize a broad range of organic substrates²⁰⁷, and it would be interesting to see if cells would employ active movement to locate different chemical forms of specific substrates. Additionally, the foraging behaviour to dP and dN of other biraphids could be checked to determine universality of simultaneous tactic and kinetic responses. Quartz sand could also be used to determine if it would elicit similar responses to that of a dSi-loaded bead. A first step would be to determine the diffusion of dSi from this source and compare it directly with the diffusion of loaded beads. Additionally, the microscale foraging processes observed in this thesis can be scaled-up to determine effects in nutrient cycles, which could be useful for determining how marine ecosystems adapt to global change²⁰⁸. Similar to Tréguer and De La Rocha²⁰³, I also suggest that the effects of active nutrient foraging and uptake on the benthos should be included in silica cycle models since silification links the carbon and silica cycle²⁰⁶. To prove both the foraging and mating dynamics in a patchy environment, one can also design experimental set-ups wherein cells can migrate vertically (Fig. 10). The use of a medium containing agar with overlying seawater could mimic not just the benthic environment but also the sediment-water interface. Nutrients, whether inorganic or organic, could be introduced from the agar (mimicking sources from sediments) or from the water column. Co-limitation experiments or choice assays could be done through the introduction of diffusing signals from different locations on the plate (Fig. 10A). Additionally, both mating types

could be cultured in a set-up, divided by a removable mesh that would allow chemical signal exchange but not physical contact, synonymous to the co-culture chambers for planktonic diatoms²⁰⁹ (Fig. 10B). The mesh barrier would permit the exchange of priming pheromones, which consequently trigger the production of diproline. Once diproline is produced, the mesh could be removed to allow cell contact. The mechanism of auto-induction could also be tested here by utilizing both medium-sized and small-sized MT⁺ in one co-culture plate and checking the effect of cell size, density, and even other factors such as light. Additionally, the link between vertical migration patterns and diproline production could be determined here by determining if both events are synchronized. However, technical preparations of this set-up would need optimization to allow microscopic observations.

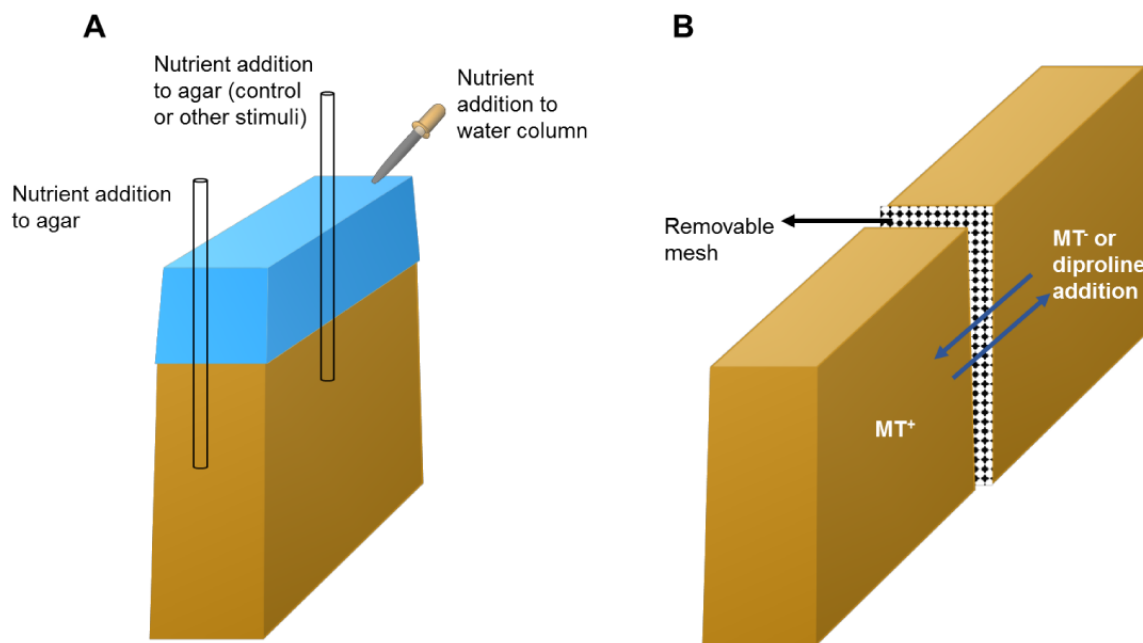


Figure 10. Suggested experimental set-up to determine nutrient foraging and mate-locating in a patchy environment.

(A) Nutrients can be introduced to either the water column or to the agar part by insertion of pipette tips filled with diffusing specific nutrients, or to the water column. (B) Co-culture set-up for MT⁺ and MT⁻ *S. robusta* cells. Two agar blocks could be separated by a mesh where cells cannot have cell contact but can exchange nutrient signals to each other.

Overall, consolidating techniques from different fields can give a more comprehensive overview of the connection between behavioural adaptation, genetic and physiological control of diatoms on stimuli sensing, and could offer a model system that could link individual behaviour to ecosystem dynamics.

5 REFERENCES

- 1 Field, C. B., Behrenfeld, M. J., Randerson, J. T. & Falkowski, P. Primary production of the biosphere: Integrating terrestrial and oceanic components. *Science* **281**, 237-240, (1998).
- 2 Smetacek, V. Diatoms and the ocean carbon cycle. *Protist* **150**, 25-32, (1999).
- 3 Mann, D. G. & Droop, S. J. M. 3. Biodiversity, biogeography and conservation of diatoms. *Hydrobiologia* **336**, 19-32, (1996).
- 4 Kooistra, W. H. C. F., De Stefano, M., Mann, D. G. & Medlin, K. in *Silicon Biomineralization: Biology — Biochemistry — Molecular Biology — Biotechnology* (ed Werner E. G. Müller) 59-97 (Springer-Verlag Berlin Heidelberg, 2003).
- 5 Adl, S. M. *et al.* The new higher level classification of eukaryotes with emphasis on the taxonomy of protists. *J. Eukaryot. Microbiol.* **52**, 399-451, (2005).
- 6 Hildebrand, M. & Lerch, S. J. in *Semin. Cell Dev. Biol.* 27-35 (Elsevier).
- 7 Brümmer, F. in *Silicon Biomineralization: Biology — Biochemistry — Molecular Biology — Biotechnology* (ed Werner E. G. Mueller) 3-10 (Springer-Verlag Berlin Heidelberg, 2003).
- 8 Hale, M. S. & Mitchell, J. G. Functional morphology of diatom frustule microstructures: hydrodynamic control of Brownian particle diffusion and advection. *Aquat. Microb. Ecol.* **24**, 287-295, (2001).
- 9 Hamm, C. E., Merkel, R., Springer, O. & Jurkojc, P. Architecture and material properties of diatom shells provide effective mechanical protection. *Nature* **421**, 841, (2003).
- 10 Round, F. E., Crawford, R. M. & Mann, D. G. *Diatoms: biology and morphology of the genera*. (Cambridge University Press, 1990).
- 11 Underwood, G. J. & Paterson, D. M. The importance of extracellular carbohydrate production by marine epipelagic diatoms. *Adv. Bot. Res.* **40**, 183-240, (2003).
- 12 Sato, S. & Medlin, L. K. Motility of non-raphid diatoms. *Diatom Res.* **21**, 473-477, (2006).
- 13 Gross, F. & Zeuthen, E. The buoyancy of plankton diatoms: a problem of cell physiology. *Proc. R. Soc. Lond., Ser. B: Biol. Sci.* **135**, 382-389, (1948).
- 14 Gemmell, B. J., Oh, G., Buskey, E. J. & Villareal, T. A. Dynamic sinking behaviour in marine phytoplankton: rapid changes in buoyancy may aid in nutrient uptake. *Proc. R. Soc. Lond., Ser. B: Biol. Sci.* **283**, (2016).
- 15 Edgar, L. A. & Pickett-Heaps, J. The mechanism of diatom locomotion. I. An ultrastructural study of the motility apparatus. *Proc. R. Soc. Lond., Ser. B: Biol. Sci.* **218**, 331-343, (1983).
- 16 Edgar, L. A. Diatom locomotion: A consideration of movement in a highly viscous situation. *Br. Phycol. J.* **17**, 243-251, (1982).
- 17 Poulsen, N. C., Spector, I., Spurck, T. P., Schultz, T. F. & Wetherbee, R. Diatom gliding is the result of an actin-myosin motility system. *Cell Motil. Cytoskeleton* **44**, 23-33, (1999).
- 18 Cooksey, K. & Wigglesworth-Cooksey, B. Adhesion of bacteria and diatoms to surfaces in the sea: a review. *Aquat. Microb. Ecol.* **9**, 87-96, (1995).
- 19 Cooksey, K. E. Requirement for calcium in adhesion of a fouling diatom to glass. *Appl. Environ. Microbiol.* **41**, 1378-1382, (1981).
- 20 Cohn, S. A. & Disparti, N. C. Environmental factors influencing diatom cell motility. *J. Phycol.* **30**, 818-828, (1994).
- 21 Thompson, S. E. M., Taylor, A. R., Brownlee, C., Callow, M. E. & Callow, J. A. The role of nitric oxide in diatom adhesion in relation to substratum properties. *J. Phycol.* **44**, 967-976, (2008).
- 22 Wang, J. D., Cao, S., Du, C. & Chen, D. R. Underwater locomotion strategy by a benthic pennate diatom *Navicula sp.* *Protoplasma* **250**, 1203-1212, (2013).

- 23 Consalvey, M., Paterson, D., M. & Underwood, G., J.C. The ups and downs of life in a benthic biofilm: Migration of benthic diatoms. *Diatom Res.* **19**, 181–202, (2004).
- 24 Cohn, S. A. *et al.* Comparative analysis of light-stimulated motility responses in three diatom species. *Diatom Res.* **30**, 213-225, (2015).
- 25 Cohn, S. A., Spurck, T. P. & Pickett-Heaps, J. D. High energy irradiation at the leading tip of moving diatoms causes a rapid change of cell direction. *Diatom Res.* **14**, 193-206, (1999).
- 26 Cooksey, B. & Cooksey, K. E. Chemical signal-response in diatoms of the genus *Amphora*. *J. Cell Sci.* **91**, 523-529, (1988).
- 27 Chepurnov, V. A., Mann, D. G., Sabbe, K. & Vyverman, W. Experimental studies on sexual reproduction in diatoms. *Int. Rev. Cytol.* **237**, 91-154, (2004).
- 28 Edlund, M. B. & Stoermer, E. F. Ecological, evolutionary, and systematic significance of diatom life histories. *J. Phycol.* **33**, 897–918, (1997).
- 29 Geitler, L. Der Formwechsel der pennaten Diatomeen. *Arch. Protistenkd.* **78**, 1-226, (1932).
- 30 Moore, E. R. *et al.* Morphological and transcriptomic evidence for ammonium induction of sexual reproduction in *Thalassiosira pseudonana* and other centric diatoms. *PLoS ONE* **12**, e0181098, (2017).
- 31 Chepurnov, V. A. *et al.* In search of new tractable diatoms for experimental biology. *Bioessays* **30**, 692–702, (2008).
- 32 Edgar, R., Drolet, D., Ehrman, J. M. & Kaczmarcza, I. Motile male gametes of the araphid diatom *Tabularia fasciculata* search randomly for mates. *PLoS ONE* **9**, e101767, (2014).
- 33 Gillard, J. *et al.* Metabolomics enables the structure elucidation of a diatom sex pheromone. *Angew. Chem. Int. Ed. Engl.* **52**, 854-857, (2013).
- 34 Sato, S., Beakes, G., Idei, M., Nagumo, T. & Mann, D. G. Novel sex cells and evidence for sex pheromones in diatoms. *PLoS ONE* **6**, e26923, (2011).
- 35 Scalco, E., Stec, K., Iudicone, D., Ferrante, M. I. & Montresor, M. The dynamics of sexual phase in the marine diatom *Pseudo-nitzschia multistriata* (Bacillariophyceae). *J. Phycol.* **50**, 817-828, (2014).
- 36 Moeys, S. *et al.* A sex-inducing pheromone triggers cell cycle arrest and mate attraction in the diatom *Seminavis robusta*. *Sci. Rep.* **6**, 19252, (2016).
- 37 MacIntyre, H. L., Geider, R. J. & Miller, D. C. Microphytobenthos: the ecological role of the “secret garden” of unvegetated, shallow-water marine habitats. I. Distribution, abundance and primary production. *Estuaries* **19**, 186-201, (1996).
- 38 Underwood, G. J. C. & Kromkamp, J. Primary production by phytoplankton and microphytobenthos in estuaries. *Adv. Ecol. Res.* **29**, 93-153, (1999).
- 39 Decho, A. W. Microbial biofilms in intertidal systems: an overview. *Cont. Shelf Res.* **20**, 1257-1273, (2000).
- 40 Saburova, M. A. & Polikarpov, I. G. Diatom activity within soft sediments: behavioural and physiological processes. *Mar. Ecol. Prog. Ser.* **251**, 115-126, (2003).
- 41 Van Cullen, C., Underwood, G. J., Serôdio, J. & Paterson, D. M. Ecology of intertidal microbial biofilms: Mechanisms, patterns and future research needs. *J. Sea Res.* **92**, 2-5, (2014).
- 42 Maria, T. F., De Troch, M., Vanaverbeke, J., Esteves, A. M. & Vanreusel, A. Use of benthic vs planktonic organic matter by sandy-beach organisms: a food tracing experiment with ^{13}C labelled diatoms. *J. Exp. Mar. Biol. Ecol.* **407**, 309-314, (2011).
- 43 Middelburg, J. J. *et al.* The fate of intertidal microphytobenthos carbon: An in situ ^{13}C -labeling study. *Limnol. Oceanogr.* **45**, 1224-1234, (2000).
- 44 Qian, P.-Y., Lau, S. C., Dahms, H.-U., Dobretsov, S. & Harder, T. Marine biofilms as mediators of colonization by marine macroorganisms: implications for antifouling and aquaculture. *Mar. Biotechnol.* **9**, 399-410, (2007).
- 45 Sigmon, D. E. & Cahoon, L. B. Comparative effects of benthic microalgae and phytoplankton on dissolved silica fluxes. *Aquat. Microb. Ecol.* **13**, 275-284, (1997).
- 46 Sundbäck, K., Enoksson, V., Graneli, W. & Pettersson, K. Influence of sublittoral microphytobenthos on the oxygen and nutrient flux between sediment and water: A laboratory continuous-flow study. *Mar. Ecol. Prog. Ser.* **74**, 263-279, (1991).

- 47 Sundbäck, K. & Granéli, W. Influence of microphytobenthos on the nutrient flux between sediment and water: a laboratory study. *Mar. Ecol. Prog. Ser.*, 63-69, (1988).
- 48 Stal, L. J. Microphytobenthos as a biogeomorphological force in intertidal sediment stabilization. *Ecol. Eng.* **36**, 236-245, (2010).
- 49 Battin, T. J., Besemer, K., Bengtsson, M. M., Romani, A. M. & Packmann, A. I. The ecology and biogeochemistry of stream biofilms. *Nat. Rev. Microbiol.* **14**, 251-263, (2016).
- 50 Pringle, C. M. Nutrient spatial heterogeneity: Effects on community structure, physiognomy, and diversity of stream algae. *Ecology* **71**, 905-920, (1990).
- 51 Saburova, M. A., Polikarpov, I. G. & Burkovsky, I. V. Spatial structure of an intertidal sandflat microphytobenthic community as related to different spatial scales. *Mar. Ecol. Prog. Ser.* **129**, 229-239, (1995).
- 52 Azovsky, A., Chertoprod, M., Kucheruk, N., Rybnikov, P. & Sapozhnikov, F. Fractal properties of spatial distribution of intertidal benthic communities. *Mar. Biol.* **136**, 581-590, (2000).
- 53 Magni, P. & Montani, S. Seasonal patterns of pore-water nutrients, benthic chlorophyll a and sedimentary AVS in a macrobenthos-rich tidal flat. *Hydrobiologia* **571**, 297-311, (2006).
- 54 Leynaert, A., Longphuirt, S. N., Claquin, P., Chauvaud, L. & Ragueneau, O. No limit? The multiphasic uptake of silicic acid by benthic diatoms. *Limnol. Oceanogr.* **54**, 571-576, (2009).
- 55 Parsons, T. & Harrison, P. in *Physiological Plant Ecology IV* (eds OL Lange, PS Nobel, CB Osmond, & H Ziegler) 85-115 (Springer, 1983).
- 56 Longphuirt, S. N. et al. Dissolved inorganic nitrogen uptake by intertidal microphytobenthos: nutrient concentrations, light availability and migration. *Mar. Ecol. Prog. Ser.* **379**, 33-44, (2009).
- 57 Passy, S. I. Diatom ecological guilds display distinct and predictable behavior along nutrient and disturbance gradients in running waters. *Aquat. Bot.* **86**, 171-178, (2007).
- 58 Barnett, A. et al. Growth form defines physiological photoprotective capacity in intertidal benthic diatoms. *ISME J.* **9**, 32-45, (2015).
- 59 Blommaert, L., Huysman, M. J. J., Vyverman, W., Lavaud, J. & Sabbe, K. Contrasting NPQ dynamics and xanthophyll cycling in a motile and a non-motile intertidal benthic diatom. *Limnol. Oceanogr.* **62**, 1466-1479, (2017).
- 60 Borchardt, M. *Algal Ecology: Freshwater Benthic Ecosystems*. 183-227 (Academic Press, 1996).
- 61 Amin, S. A., Parker, M. S. & Armbrust, E. V. Interactions between diatoms and bacteria. *Microbiol. Mol. Biol. Rev.* **76**, 667-684, (2012).
- 62 Vanelslander, B. et al. Daily bursts of biogenic cyanogen bromide (BrCN) control biofilm formation around a marine benthic diatom. *Proc. Natl. Acad. Sci. USA* **109**, 2412-2417, (2012).
- 63 Admiraal, W., Peletier, H. & Brouwer, T. The seasonal succession patterns of diatom species on an intertidal mudflat - an experimental analysis. *Oikos* **42**, 30-40, (1984).
- 64 Round, F. & Happey, C. Persistent, vertical-migration rhythms in benthic microflora: Part IV a diurnal rhythm of the epipelagic diatom association in non-tidal flowing water. *Br. Phycol. Bull.* **2**, 463-471, (1965).
- 65 Serôdio, J., Marques da Silva, J. & Catarino, F. Nondestructive tracing of migratory rhythms of intertidal benthic microalgae using in vivo chlorophyll a fluorescence. *J. Phycol.* **33**, 542-553, (1997).
- 66 Kromkamp, J., Barranguet, C. & Peene, J. Determination of microphytobenthos PSII quantum efficiency and photosynthetic activity by means of variable chlorophyll fluorescence. *Mar. Ecol. Prog. Ser.*, 45-55, (1998).
- 67 Harper, M. Movement and migration of diatoms on sand grains. *Br. Phycol. J.* **4**, 97-103, (1969).
- 68 Longphuirt, S. N. et al. Discovery of microphytobenthos migration in the subtidal zone. *Mar. Ecol. Prog. Ser.* **328**, 143-154, (2006).
- 69 Underwood, G. et al. Patterns in microphytobenthic primary productivity: Species-specific variation in migratory rhythms and photosynthetic efficiency in mixed-species biofilms. *Limnol. Oceanogr.* **50**, 755-767, (2005).
- 70 McLachlan, D. H., Brownlee, C., Taylor, A. R., Geider, R. J. & Underwood, G. J. C. Light-induced motile responses of the estuarine benthic diatoms *Navicula perminuta* and *Cylindrotheca closterium* (Bacillariophyceae). *J. Phycol.* **45**, 592-599, (2009).

- 71 Nultsch, W. Phototactic and photokinetic action spectra of the diatom *Nitzschia communis*. *Photochem. Photobiol.* **14**, 705-712, (1971).
- 72 Coelho, H., Vieira, S. & Serôdio, J. Endogenous versus environmental control of vertical migration by intertidal benthic microalgae. *Eur. J. Phycol.* **46**, 271-281, (2011).
- 73 Frankenbach, S. *et al.* Evidence for gravitactic behaviour in benthic diatoms. *Eur. J. Phycol.* **49**, 429-435, (2014).
- 74 Round, F. & Palmer, J. Persistent, vertical-migration rhythms in benthic microflora.: II. Field and laboratory studies on diatoms from the banks of the River Avon. *J. Mar. Biol. Assoc. U.K.* **46**, 191-214, (1966).
- 75 Fenchel, T. The ecology of marine microbenthos IV. Structure and function of the benthic ecosystem, its chemical and physical factors and the microfauna communities with special reference to the ciliated protozoa. *Ophelia* **6**, 1-182, (1969).
- 76 Jauffrais, T. *et al.* Physiological and photophysiological responses of the benthic diatom *Entomoneis paludosa* (Bacillariophyceae) to dissolved inorganic and organic nitrogen in culture. *Mar. Biol.* **163**, (2016).
- 77 Sommer, U. Nutrient competition experiments with periphyton from the Baltic Sea. *Mar. Ecol. Prog. Ser.* **140**, 161-167, (1996).
- 78 Sundbäck, K., Lindehoff, E. & Granéli, E. Dissolved organic nitrogen: an important source of nitrogen for the microphytobenthos in sandy sediment. *Aquat. Microb. Ecol.* **63**, 89-100, (2011).
- 79 Underwood, G. J., Phillips, J. & Saunders, K. Distribution of estuarine benthic diatom species along salinity and nutrient gradients. *Eur. J. Phycol.* **33**, 173-183, (1998).
- 80 Cochero, J., Licursi, M. & Gomez, N. Changes in the epipelagic diatom assemblage in nutrient rich streams due to the variations of simultaneous stressors. *Limnologica* **51**, 15-23, (2015).
- 81 Porubsky, W. P., Velasquez, L. E. & Joye, S. B. Nutrient-replete benthic microalgae as a source of dissolved organic carbon to coastal waters. *Estuar Coasts* **31**, 860-876, (2008).
- 82 Admiraal, W., Riaux-Gobin, C. & Laane, R. W. Interactions of ammonium, nitrate, and D-and L-amino acids in the nitrogen assimilation of two species of estuarine benthic diatoms. *Mar. Ecol. Prog. Ser.*, 267-273, (1987).
- 83 Admiraal, W. Tolerance of estuarine benthic diatoms to high concentrations of ammonia, nitrite ion, nitrate ion and orthophosphate. *Mar. Biol.* **43**, 307-315, (1977).
- 84 Amo, Y. D. & Brzezinski, M. A. The chemical form of dissolved Si taken up by marine diatoms. *J. Phycol.* **35**, 1162-1170, (1999).
- 85 Treguer, P. *et al.* The silica balance in the world ocean: a reestimate. *Science* **268**, 375-375, (1995).
- 86 Carlton, R. G. & Wetzel, R. G. Phosphorus flux from lake sediments: Effect of epipelagic algal oxygen production. *Limnol. Oceanogr.* **33**, 562-570, (1988).
- 87 Leynaert, A. *et al.* Tidal variability in benthic silicic acid fluxes and microphytobenthos uptake in intertidal sediment. *Estuar. Coast. Shelf Sci.* **95**, 59-66, (2011).
- 88 Sakamaki, T., Nishimura, O. & Sudo, R. Tidal time-scale variation in nutrient flux across the sediment-water interface of an estuarine tidal flat. *Estuar. Coast. Shelf Sci.* **67**, 653-663, (2006).
- 89 Kuwae, T., Kibe, E. & Nakamura, Y. Effect of emersion and immersion on the porewater nutrient dynamics of an intertidal sandflat in Tokyo Bay. *Estuar. Coast. Shelf Sci.* **57**, 929-940, (2003).
- 90 Laruelle, G. G. *et al.* Benthic-pelagic coupling and the seasonal silica cycle in the Bay of Brest (France): new insights from a coupled physical-biological model. *Mar. Ecol. Prog. Ser.* **385**, 15-32, (2009).
- 91 Van Luijn, F., Van der Molen, D., Luttmer, W. & Boers, P. Influence of benthic diatoms on the nutrient release from sediments of shallow lakes recovering from eutrophication. *Water Sci. Technol.* **32**, 89-97, (1995).
- 92 Gillard, J. *et al.* Physiological and transcriptomic evidence for a close coupling between chloroplast ontogeny and cell cycle progression in the pennate diatom *Seminavis robusta*. *Plant Physiol.* **148**, 1394-1411, (2008).
- 93 Pouličková, A., Hašler, P., Lysáková, M. & Spears, B. The ecology of freshwater epipelagic algae: an update. *Phycologia* **47**, 437-450, (2008).

- 94 Levitis, D. A., Lidicker, W. Z. & Freund, G. Behavioural biologists do not agree on what constitutes behaviour. *Anim. Behav.* **78**, 103-110, (2009).
- 95 Bell, W. J. *Searching behaviour: the behavioural ecology of finding resources*. (Chapman and Hall, London, England, 1991).
- 96 Dusenbery, D. *Living at microscale: The unexpected physics of being small*. (Harvard University Press, 2011).
- 97 Son, K., Brumley, D. R. & Stocker, R. Live from under the lens: exploring microbial motility with dynamic imaging and microfluidics. *Nat. Rev. Microbiol.* **13**, 761, (2015).
- 98 Stocker, R. The 100 μm length scale in the microbial ocean. *Aquat. Microb. Ecol.* **76**, 189-194, (2015).
- 99 Stocker, R. & Seymour, J. R. Ecology and physics of bacterial chemotaxis in the ocean. *Microbiol. Mol. Biol. Rev.* **76**, 792-812, (2012).
- 100 Seymour, J., Marcos & Stocker, R. Resource patch formation and exploitation throughout the marine microbial food web. *Am. Nat.* **173**, E15-E29, (2009).
- 101 Stocker, R. Marine microbes see a sea of gradients. *Science* **338**, 628-633, (2012).
- 102 Seymour, J. R., Simo, R., Ahmed, T. & Stocker, R. Chemoattraction to Dimethylsulfoniopropionate throughout the marine microbial food web. *Science* **329**, 342-345, (2010).
- 103 Smriga, S., Fernandez, V. I., Mitchell, J. G. & Stocker, R. Chemotaxis toward phytoplankton drives organic matter partitioning among marine bacteria. *Proc. Natl. Acad. Sci. USA* **113**, 1576-1581, (2016).
- 104 Stocker, R., Seymour, J. R., Samadani, A., Hunt, D. E. & Polz, M. F. Rapid chemotactic response enables marine bacteria to exploit ephemeral microscale nutrient patches. *Proc. Natl. Acad. Sci. USA* **105**, 4209-4214, (2008).
- 105 Barbara, G. M. & Mitchell, J. G. Marine bacterial organisation around point-like sources of amino acids. *FEMS Microbiol. Ecol.* **43**, 99-109, (2003).
- 106 Barbara, G. M. & Mitchell, J. G. Bacterial tracking of motile algae. *FEMS Microbiol. Ecol.* **44**, 79-87, (2003).
- 107 Blackburn, N., Fenchel, T. & Mitchell, J. Microscale nutrient patches in planktonic habitats shown by chemotactic bacteria. *Science* **282**, 2254-2256, (1998).
- 108 Fossing, H., Gallardo, V. A., Jorgensen, B. & Huttel, M. Concentration and transport of nitrate by the mat-forming sulphur bacterium *Thioploca*. *Nature* **374**, 713, (1995).
- 109 Huttel, M., Forster, S., Kloster, S. & Fossing, H. Vertical migration in the sediment-dwelling sulfur bacteria *Thioploca spp.* in overcoming diffusion limitations. *Appl. Environ. Microbiol.* **62**, 1863-1872, (1996).
- 110 Schulz, H. N. & Jørgensen, B. B. Big bacteria. *Annu. Rev. Microbiol.* **55**, 105-137, (2001).
- 111 Adler, J. Chemoreceptors in bacteria. *Science* **166**, 1588-1597, (1969).
- 112 Adler, J. A method for measuring chemotaxis and use of the method to determine optimum conditions for chemotaxis by *Escherichia coli*. *J. Gen. Microbiol.* **74**, 77-91, (1973).
- 113 Nossal, R. Growth and movement of rings of chemotactic bacteria. *Exp. Cell Res.* **75**, 138-142, (1972).
- 114 Berg, H. C. How to track bacteria. *Rev. Sci. Instrum.* **42**, 868-871, (1971).
- 115 Berg, H. C. & Brown, D. A. Chemotaxis in *Escherichia coli* analysed by three-dimensional tracking. *Nature* **239**, 500-504, (1972).
- 116 Garren, M. et al. A bacterial pathogen uses dimethylsulfoniopropionate as a cue to target heat-stressed corals. *ISME J.* **8**, 999-1007, (2014).
- 117 Tinevez, J.-Y. et al. TrackMate: An open and extensible platform for single-particle tracking. *Methods* **115**, 80-90, (2017).
- 118 Chenouard, N. et al. Objective comparison of particle tracking methods. *Nat. Methods* **11**, 281-289, (2014).
- 119 Meijering, E., Dzyubachyk, O. & Smal, I. 9 Methods for cell and particle tracking. *Methods Enzymol.* **504**, 183-200, (2012).
- 120 Drescher, K., Dunkel, J., Cisneros, L. H., Ganguly, S. & Goldstein, R. E. Fluid dynamics and noise in bacterial cell-cell and cell-surface scattering. *Proceedings of the National Academy of Sciences* **108**, 10940-10945, (2011).

- 121 Seymour, J., Ahmed, T. & Stocker, R. A microfluidic chemotaxis assay to study microbial behavior in diffusing nutrient patches. *Limnol. Oceanogr. Methods* **6**, 477-488, (2008).
- 122 Bell, W. & Mitchell, R. Chemotactic and growth responses of marine bacteria to algal extracellular products. *Biol. Bull.* **143**, 265-277, (1972).
- 123 Miller, L. D., Russell, M. H. & Alexandre, G. Diversity in bacterial chemotactic responses and niche adaptation. *Adv. Appl. Microbiol.* **66**, 53-75, (2009).
- 124 Azam, F. Microbial control of oceanic carbon flux: The plot thickens. *Science* **280**, 694-696, (1998).
- 125 Kiene, R. P., Linn, L. J. & Bruton, J. A. New and important roles for DMSP in marine microbial communities. *J. Sea Res.* **43**, 209-224, (2000).
- 126 Kirst, G. *et al.* Dimethylsulfoniopropionate (DMSP) in ice algae and its possible biological role. *Mar. Chem.* **35**, 381-388, (1991).
- 127 Sunda, W., Kieber, D., Kiene, R. & Huntsman, S. An antioxidant function for DMSP and DMS in marine algae. *Nature* **418**, 317, (2002).
- 128 Bates, T. S., Charlson, R. J. & Gammon, R. H. Evidence for the climatic role of marine biogenic sulphur. *Nature* **329**, 319-321, (1987).
- 129 Charlson, R. J., Lovelock, J. E., Andreaei, M. O. & Warren, S. G. Oceanic phytoplankton, atmospheric sulphur, cloud. *Nature* **326**, 655-661, (1987).
- 130 Falciatore, A., d'Alcalà, M. R., Croot, P. & Bowler, C. Perception of environmental signals by a marine diatom. *Science* **288**, 2363-2366, (2000).
- 131 De La Rocha, C. L. & Passow, U. Recovery of *Thalassiosira weissflogii* from nitrogen and silicon starvation. *Limnol. Oceanogr.* **49**, 245-255, (2004).
- 132 De La Rocha, C. L., Terbruggen, A., Volker, C. & Hohn, S. Response to and recovery from nitrogen and silicon starvation in *Thalassiosira weissflogii*: growth rates, nutrient uptake and C, Si and N content per cell. *Mar. Ecol. Prog. Ser.* **412**, 57-68, (2010).
- 133 Dyhrman, S. T. *et al.* The transcriptome and proteome of the diatom *Thalassiosira pseudonana* reveal a diverse phosphorus stress response. *PLoS ONE* **7**, e33768, (2012).
- 134 Martin, P., Van Mooy, B. A. S., Heithoff, A. & Dyhrman, S. T. Phosphorus supply drives rapid turnover of membrane phospholipids in the diatom *Thalassiosira pseudonana*. *ISME J.* **5**, 1057-1060, (2011).
- 135 Mock, T. *et al.* Whole-genome expression profiling of the marine diatom *Thalassiosira pseudonana* identifies genes involved in silicon bioprocesses. *Proc. Natl. Acad. Sci. USA* **105**, 1579-1584, (2008).
- 136 Shrestha, R. P. *et al.* Whole transcriptome analysis of the silicon response of the diatom *Thalassiosira pseudonana*. *BMC Genomics* **13**, (2012).
- 137 Urbani, R., Magaletti, E., Sist, P. & Cicero, A. M. Extracellular carbohydrates released by the marine diatoms *Cylindrotheca closterium*, *Thalassiosira pseudonana* and *Skeletonema costatum*: Effect of P-depletion and growth status. *Sci. Total Environ.* **353**, 300-306, (2005).
- 138 Geider, R. J., Laroche, J., Greene, R. M. & Olaizola, M. Response of the photosynthetic apparatus of *Phaeodactylum tricornutum* (Bacillariophyceae) to nitrate, phosphate, or iron starvation. *J. Phycol.* **29**, 755-766, (1993).
- 139 Levitan, O. *et al.* Remodeling of intermediate metabolism in the diatom *Phaeodactylum tricornutum* under nitrogen stress. *Proc. Natl. Acad. Sci. USA* **112**, 412-417, (2015).
- 140 Bowler, C. *et al.* The *Phaeodactylum* genome reveals the evolutionary history of diatom genomes. *Nature* **456**, 239-244, (2008).
- 141 Chepurnov, V. A., Mann, D. G., Vyverman, W., Sabbe, K. & Danielidis, D. B. Sexual reproduction, mating system, and protoplast dynamics of *Seminavis* (Bacillariophyceae). *J. Phycol.* **38**, 1004-1019, (2002).
- 142 Basu, S. *et al.* Finding a partner in the ocean: molecular and evolutionary bases of the response to sexual cues in a planktonic diatom. *New Phytol.* **215**, 140-156, (2017).
- 143 Davidovich, N. A., Kaczmarska, I. & Ehrman, J. M. Heterothallic and homothallic sexual reproduction in *Tabularia fasciculata* (Bacillariophyta). *Fottea* **10**, 251-266, (2010).
- 144 Maier, I. Gamete orientation and induction of gametogenesis by pheromones in algae and plants. *Plant, Cell Environ.* **16**, 891-907, (1993).

- 145 Maier, I. & Muller, D. G. Sexual pheromones in algae. *Biol. Bull.* **170**, 145, (1986).
- 146 Amsler, C. D. & Iken, K. B. in *Marine Chemical Ecology* (eds J. B. McClintock & B. J. Baker) 413-430 (CRC Press, 2001).
- 147 Pohnert, G. & Boland, W. The oxylipin chemistry of attraction and defense in brown algae and diatoms. *Nat. Prod. Rep.* **19**, 108-122, (2002).
- 148 Passy, S. I. & Larson, C. A. Succession in stream biofilms is an environmentally driven gradient of stress tolerance. *Microb. Ecol.* **62**, 414-424, (2011).
- 149 Lin, S. J., Litaker, R. W. & Sunda, W. G. Phosphorus physiological ecology and molecular mechanisms in marine phytoplankton. *J. Phycol.* **52**, 10-36, (2016).
- 150 Moore, C. M. et al. Relative influence of nitrogen and phosphorous availability on phytoplankton physiology and productivity in the oligotrophic sub-tropical North Atlantic Ocean. *Limnol. Oceanogr.* **53**, 291-305, (2008).
- 151 Martin-Jezequel, V., Hildebrand, M. & Brzezinski, M. A. Silicon metabolism in diatoms: Implications for growth. *J. Phycol.* **36**, 821-840, (2000).
- 152 Admiraal, W. & Werner, D. Utilization of limiting concentrations of orthophosphate and production of extracellular organic phosphates in cultures of marine diatoms. *J. Plankton Res.* **5**, 495-513, (1983).
- 153 Thingstad, T. F., Skjoldal, E. F. & Bohne, R. A. Phosphorous cycling and algal-bacterial competition in Sandsfjord, Western Norway. *Mar. Ecol. Prog. Ser.* **99**, 239-259, (1993).
- 154 Alcoverro, T., Conte, E. & Mazzella, L. Production of mucilage by the Adriatic epipelagic diatom *Cylindrotheca closterium* (Bacillariophyceae) under nutrient limitation. *J. Phycol.* **36**, 1087-1095, (2000).
- 155 Daglio, Y., Maidana, N. I., Matulewicz, M. C. & Rodriguez, M. C. Changes in motility and induction of enzymatic activity by nitrogen and phosphate deficiency in benthic *Halamphora luciae* (Bacillariophyceae) from Argentina. *Phycologia* **55**, 493-505, (2016).
- 156 Van Mooy, B. A. S. et al. Phytoplankton in the ocean use non-phosphorus lipids in response to phosphorus scarcity. *Nature* **458**, 69-72, (2009).
- 157 Flynn, K. J. & Martin-Jezequel, V. Modelling Si-N-limited growth of diatoms. *J. Plankton Res.* **22**, 447-472, (2000).
- 158 Claquin, P., Martin-Jezequel, V., Kromkamp, J. C., Veldhuis, M. J. W. & Kraay, G. W. Uncoupling of silicon compared with carbon and nitrogen metabolisms and the role of the cell cycle in continuous cultures of *Thalassiosira pseudonana* (Bacillariophyceae) under light, nitrogen, and phosphorus control. *J. Phycol.* **38**, 922-930, (2002).
- 159 Dell'Aquila, G. et al. Nutrient consumption and chain tuning in diatoms exposed to storm-like turbulence. *Sci. Rep.* **7**, 1828, (2017).
- 160 Pyke, G. H. Optimal foraging theory: A critical review. *Annu. Rev. Ecol. Syst.* **15**, 523-575, (1984).
- 161 Azam, F., Hemmingsen, B. B. & Voleani, B. E. Germanium incorporation into the silica of diatom cell walls. *Arch. Microbiol.* **92**, 11-20, (1973).
- 162 Lewin, J. Silicon metabolism in diatoms. V. Germanium dioxide, a specific inhibitor of diatom growth. *Phycologia* **6**, 1-12, (1966).
- 163 Rorrer, G. L. et al. Biosynthesis of silicon-germanium oxide nanocomposites by the marine diatom *Nitzschia frustulum*. *Journal of nanoscience and nanotechnology* **5**, 41-49, (2005).
- 164 Froelich, P. N. & Andrae, M. O. The marine geochemistry of germanium : Ekasilicon. *Science* **213**, 205-207, (1981).
- 165 Basharina, T. N. et al. The effect of titanium, zirconium and tin on the growth of diatom *Synedra acus* and morphology of its silica valves. *Silicon*, 1-11, (2012).
- 166 Geider, R. J., Platt, T. & Raven, J. A. Size dependence of growth and photosynthesis in diatoms: a synthesis. *Mar. Ecol. Prog. Ser.* **30**, 93-104, (1986).
- 167 Kiørboe, T. *A mechanistic approach to plankton ecology*. (Princeton University Press, 2008).
- 168 Paschak, W. J. & Gavis, J. Transport limitation of nutrient uptake in phytoplankton. *Limnol. Oceanogr.* **19**, 881-898, (1974).
- 169 Ehrlich, H., Demadis, K. D., Pokrovsky, O. S. & Koutsoukos, P. G. Modern views on desilicification: Biosilica and abiotic silica dissolution in natural and artificial environments. *Chem. Rev.* **110**, 4656-4689, (2010).

- 170 Hütz, A., Schubert, K. & Overmann, J. *Thalassospira sp.* isolated from the oligotrophic Eastern Mediterranean Sea exhibits chemotaxis toward inorganic phosphate during starvation. *Appl. Environ. Microbiol.* **77**, 4412-4421, (2011).
- 171 Ikegami, S., Imai, I., Kato, J. & Ohtake, H. Chemotaxis toward inorganic phosphate in the red tide alga *Chatonella antiqua*. *J. Plankton Res.* **17**, 1587-1591, (1995).
- 172 Willey, J. M. & Waterbury, J. B. Chemotaxis toward nitrogenous compounds by swimming strains of marine *Synechococcus* sp. *Appl. Environ. Microbiol.* **55**, 1888-1894, (1989).
- 173 Dennis, P. G., Seymour, J., Kumbun, K. & Tyson, G. W. Diverse populations of lake water bacteria exhibit chemotaxis towards inorganic nutrients. *ISME J.* **7**, 1661-1664, (2013).
- 174 Sjöblad, R. D., Chet, I. & Mitchell, R. Chemoreception in the green alga *Dunaliella tertiolecta* *Curr. Microbiol.* **1**, 305-307, (1978).
- 175 Ermilova, E. V., Zalutskaya, Z. M., Lapina, T. V. & Nikitin, M. M. Chemotactic behavior of *Chlamydomonas reinhardtii* is altered during gametogenesis. *Curr. Microbiol.* **46**, 261-264, (2003).
- 176 Sjöblad, R. D. & Frederikse, P. H. Chemotactic responses of *Chlamydomonas reinhardtii*. *Mol. Cell. Biol.* **1**, 1057-1060, (1981).
- 177 Ermilova, E. V., Zalutskaya, Z. M. & Lapina, T. V. Chemotaxis of *Chlamydomonas reinhardtii* to nitrate is changed during gametogenesis. *Protistology* **6**, (2009).
- 178 Ermilova, E. & Zalutskaya, Z. Regulation by Light of Chemotaxis to Nitrite during the Sexual Life Cycle in *Chlamydomonas reinhardtii*. *Plants* **3**, 113-127, (2014).
- 179 Hockin, N. L., Mock, T., Mulholland, F., Kopriva, S. & Malin, G. The response of diatom central carbon metabolism to nitrogen starvation is different from that of green algae and higher plants. *Plant Physiol.* **158**, 299-312, (2012).
- 180 Guerrini, F., Cangini, M., Boni, L., Trost, P. & Pistocchi, R. Metabolic responses of the diatom *Achnanthes brevipes* (Bacillariophyceae) to nutrient limitation. *J. Phycol.* **36**, 882-890, (2000).
- 181 Thamatrakoln, K. & Hildebrand, M. Silicon uptake in diatoms revisited: a model for saturable and nonsaturable uptake kinetics and the role of silicon transporters. *Plant Physiol.* **146**, 1397-1407, (2008).
- 182 Karp-Boss, L., Boss, E. & Jumars, P. Nutrient fluxes to planktonic osmotrophs in the presence of fluid motion. *Oceanogr. Mar. Biol. Annu. Rev.* **34**, 71-108, (1996).
- 183 Berg, H. C. *Random walks in biology*. (Princeton University Press, 1993).
- 184 von Dassow, P. & Montresor, M. Unveiling the mysteries of phytoplankton life cycles: patterns and opportunities behind complexity. *J. Plankton Res.* **33**, 3-12, (2010).
- 185 Frenkel, J., Vyverman, W. & Pohnert, G. Pheromone signaling during sexual reproduction in algae. *Plant J.* **79**, 632-644, (2014).
- 186 Johansson, B. G. & Jones, T. M. The role of chemical communication in mate choice. *Biol. Rev.* **82**, 265-289, (2007).
- 187 Dusenbery, D. B. & Snell, T. W. A critical body size for use of pheromones in mate location. *J. Chem. Ecol.* **21**, 427-438, (1995).
- 188 Bagøien, E. & Kiørboe, T. Blind dating—mate finding in planktonic copepods. I. Tracking the pheromone trail of *Centropages typicus*. *Mar. Ecol. Prog. Ser.* **300**, 105-115, (2005).
- 189 Gillard, J. *The pennate diatom life cycle: a genetic, physiological and biochemical study using Seminavis robusta as a new experimental model*, Ghent University, (2009).
- 190 Schmidt, M. C. Signaling crosstalk: Integrating nutrient availability and sex. *Sci. Signal.* **6**, (2013).
- 191 Clement, S. T., Dixit, G. & Dohlman, H. G. Regulation of yeast G protein signaling by the kinases that activate the AMPK homolog Snf1. *Sci. Signal.* **6**, (2013).
- 192 Goodenough, U., Lin, H. & Lee, J. H. Sex determination in *Chlamydomonas*. *Semin. Cell Dev. Biol.* **18**, 350-361, (2007).
- 193 Goodenough, U. W. Cyclic AMP enhances the sexual agglutinability of *Chlamydomonas* flagella. *J. Cell Biol.* **109**, 247-252, (1989).
- 194 Pan, J. M. & Snell, W. J. Regulated targeting of a protein kinase into an intact flagellum - An aurora/Ipl1p-like protein kinase translocates from the cell body into the flagella during gamete activation in *Chlamydomonas*. *J. Biol. Chem.* **275**, 24106-24114, (2000).

- 195 Port, J. A. *et al.* Identification of G protein-coupled receptor signaling pathway proteins in marine diatoms using comparative genomics. *BMC Genomics* **14**, 503, (2013).
- 196 Sims, P. A., Mann, D. G. & Medlin, L. K. Evolution of the diatoms: insights from fossil, biological and molecular data. *Phycologia* **45**, 361-402, (2006).
- 197 Chepurnov, V. A. & Mann, D. G. Auxosporulation of *Licmophora communis* (Bacillariophyta) and a review of mating systems and sexual reproduction in araphid pennate diatoms. *Phycol. Res.* **52**, 1-12, (2004).
- 198 Flynn, K. & Wright, C. The simultaneous assimilation of ammonium and L-arginine by the marine diatom *Phaeodactylum tricornutum* Bohlin. *J. Exp. Mar. Biol. Ecol.* **95**, 257-269, (1986).
- 199 Nilsson, C. & Sundbäck, K. Amino acid uptake in natural microphytobenthic assemblages studied by microautoradiography. *Hydrobiologia* **332**, 119-129, (1996).
- 200 Johannes, R. Uptake and release of dissolved organic phosphorus by representatives of a coastal marine ecosystem. *Limnol. Oceanogr.* **9**, 224-234, (1964).
- 201 Karl, D. M. Microbially mediated transformations of phosphorus in the sea: New views of an old cycle. *Annu. Rev. Mar. Sci.* **6**, 279-337, (2014).
- 202 Capellacci, S. *et al.* Bioavailability of different chemical forms of dissolved silica can affect marine diatom growth. *Mar. Ecol.* **34**, 103-111, (2013).
- 203 Treguer, P. J. & De La Rocha, C. L. The world ocean silica cycle. *Annu. Rev. Mar. Sci.* **5**, 477-501, (2013).
- 204 Brehm, U., Gorbushina, A. & Mottershead, D. The role of microorganisms and biofilms in the breakdown and dissolution of quartz and glass. *Palaeogeogr., Palaeoclimatol., Palaeoecol.* **219**, 117-129, (2005).
- 205 Crawford, R. M. The role of sex in the sedimentation of a marine diatom bloom. *Limnol. Oceanogr.* **40**, 200-204, (1995).
- 206 Durkin, C. A., Koester, J. A., Bender, S. J. & Armbrust, E. The evolution of silicon transporters in diatoms. *J. Phycol.* **52**, 716-731, (2016).
- 207 Tuchman, N. C., Schollett, M. A., Rier, S. T. & Geddes, P. Differential heterotrophic utilization of organic compounds by diatoms and bacteria under light and dark conditions. *Hydrobiologia* **561**, 167-177, (2006).
- 208 Azam, F. & Malfatti, F. Microbial structuring of marine ecosystems. *Nat. Rev. Microbiol.* **5**, 782-791, (2007).
- 209 Paul, C., Mausz, M. A. & Pohnert, G. A co-culturing/metabolomics approach to investigate chemically mediated interactions of planktonic organisms reveals influence of bacteria on diatom metabolism. *Metabolomics*, 1-11, (2012).

6 DECLARATIONS

Selbstständigkeitserklärung

Ich erkläre, dass ich die vorliegende Arbeit selbstständig und unter Verwendung der angegebenen Hilfsmittel, persönlichen Mitteilungen und Quellen angefertigt habe.

Jena, den

Karen Grace V. Bondoc

Weitere Erklärungen

Erklärung zu den Eigenanteilen des Promovenden/der Promovendin sowie der weiteren Doktoranden/Doktorandinnen als Koautoren an den Publikationen Zweitpublikationsrechten bei einer kumulativen Dissertation. Die Koautoren der in dieser kumulativen Dissertation verwendeten Manuskripte sind sowohl über die Nutzung, als auch über die oben angegebenen Eigenanteile der weiteren Doktoranden/Doktorandinnen als Koautoren an den Publikationen und Zweitpublikationsrechten bei einer kumulativen Dissertation informiert und stimmen dem zu. Die Anteile des Promovenden/der Promovendin sowie der weiteren Doktoranden/Doktorandinnen als Koautoren an den Publikationen und zweitpublikationsrechten bei einer kumulativen Dissertation sind vor der jeweiligen Publikation aufgeführt. Für alle in dieser kumulativen Dissertation verwendeten Manuskripte liegen die notwendigen Genehmigungen der Verlage („Reprint permissions“) für die Zweitpublikation vor.

Jena, den

Karen Grace V. Bondoc

Einverständniserklärung des Betreuers

Ich bin mit der Abfassung der Dissertation als publikationsbasiert, d.h. kumulativ, einverstanden und bestätige die vorstehenden Angaben. Eine entsprechend begründete Befürwortung mit Angabe des wissenschaftlichen Anteils des Doktoranden/der Doktorandin an den verwendeten Publikationen werde ich parallel an den Rat der Fakultät der Chemisch-Geowissenschaftlichen Fakultät richten.

Jena, den

Prof. Dr. Georg Pohnert

AFTERWORD

A doctoral thesis tells the story of the research topic—how you did it and what new knowledge you contributed to science, but it barely tells the personal journey that every doctoral student went through. A mark is given based on your output, but the effort behind this bounded piece of work is not often discussed. This is the only page where dedications and acknowledgements are made, often written in a sentence or two, while not fully understanding the impact of each person and how much they helped the author.

I decided early that I will finish this thesis, no matter what happens, and in the course of it, my chronic illnesses worsened. To do a PhD is already a task itself, one that you need to devote all you have and to have it together with health problems is a disaster-in-progress. I risked a lot, but I was one of the blessed ones, who had the means and support to finish this task, and for that, I am deeply indebted to these people:

To my supervisor, Prof. Dr. Georg Pohnert, thank you for the opportunity to work in your group and for supporting my research. The direction of my thesis went in a different way than expected, but you continued to trust my work. Thank you for the independence that you gave me, the insightful inputs especially in manuscript writing, for extending my stay in Jena for the last part of my experiments, and for correcting my thesis in such a short time,

To my funding agency, International Max Planck Research School. I am also indebted to two wonderful graduate school coordinators - Dr. Karin Groten and Dr. Claudia Voelkel. I also want to extend my gratitude to Richard-Winter-Stiftung for the support during my writing months.

To Christine Lembke, my co-author for the two papers in this thesis and a friend. Thank you for being patient in experiments and writing, for telling me when it is enough, for correcting my thesis in such a short time, translating my summary, and for the open communication every single time.

To Dr. Jan Heuschele, for introducing me to R and the ropes of mixed modelling, for answering all my questions and troubleshooting scripts that do not work. To Dr. Jens Schumacher for giving me advices on how to design mix models.

To Dr. Wim Vyverman for all the corrections and advice that greatly improved all the three manuscripts in this thesis. I want to thank you and Olga Chepurnova for the endless supply of *Seminavis robusta*. To Dr. Jeroen Gillard, thank you for designing the bead bioassays that formed the basis of my work.

To the entire Pohnert group for their help throughout the PhD. I owe special thanks to the awesome (former) Rm. 228 people who welcomed an English-speaking girl on the office with warmth, tea, and sweets. To Dr. Raphael Seidel thank you for all the prayers, encouragement, jokes, and chocolates. To Katharina Eick, for all the sushi lunches, cakes and tea breaks, for an epic Spain adventure, and for being as sweet as always. To Marcel Ritter, for all the logical advice, encouragement, and translating my summary. Thank you also to Dominique Jacquemond for helping me troubleshoot my initial R scripts. To Dr. Stefanie Wolfram for giving me her thesis template. To Dr. Johannes Frenkel for teaching me how to deal with *Seminavis* the first time I worked with it. To Emilio Cirri for all the *Seminavis* that I borrowed. To Kathleen Thume, Constanze Kuhlish, Dr. Marine Vallet, Lydia Papanikolopoulou for all the chats about work and life. To Madlen Kühn and Sarah Tippner for all the help in the administrative stuff.

I also gained some friends in Jena who became family to me. To Purva Kulkarni-Singh, my roommate during recruitment, my first flatmate in Jena, and with whom I have parallel events. Thank you for being there with throughout all the difficult times in Jena. Thank you to my porter guys Luke Donald Halder and Vincensius Oetama for always helping me in carrying my luggage around Jena, for all the food, laughter, and friendship. To Christina Glock, for being my first close German friend, for all our epic Asian holidays, and for being as warm and sweet as you are despite distance. To the MiCom 2015 organizing team for all the experience in arranging a fun conference, all the dinners, discussions, and laughter. I owe gratitude especially to Shraddha Shitut, for being my partner in MiCom and a friend whom I can count on always. To Dr. Ayu Okvitawanli and Dr. Martin Fischer, for all our dinners, game nights, and a lovely time in Austria. To Wiwin Winjaya, for all the Sunday lunches, encouragements, and for listening a lot.

I found my home in Jena because I have been blessed with the best flatmates ever. Thank you to Sarah Hummel, Meike Haag, Sarah Schmidt, Liesa-Marie Fischer, and Sophia Sczesny for taking care of me whenever I am sick, for calling doctors, for translating, for the prayers, for the homey atmosphere and encouragements, and for the friendship and warmth from all of you.

To the Filipinos in Jena, thank you for bringing a part of home in Germany. Thank you for all the karaoke parties filled with Filipino food, laughter, and singing. Special thanks to the only other Filipina PhD student, Marivic Martin. I am thankful that you came in Jena and that I have someone whom I can talk to in Tagalog about anything under the sun, for the endless support and sleepovers. To Dr. Leilani Torres-Mapa and Louise Mapa, for adopting me literally during their stay in Jena and for welcoming me to Hannover whenever I needed a break.

To my spiritual family – Der Eckstein and Internationaler Kreis. Thank you for all the prayers, support, and encouragement. I owe special thank you to Karoline Panepinto for all the dinners and stories that we had. To the recent and former IK staff – Deborah Schäl, Antonia Dainat, Yu-Chun Pynn, Hannah Africiska Duruk, and Dr. Markus Müller for the friendship and warm welcome that greatly

helped me to adjust here in Germany. I greatly appreciate the warmth of Dorothea Reeps, for all the visits, stories, hugs, and encouragements.

To the friends who supported my nomadic lifestyle in Jena during my writing stage by welcoming me to their homes – thanks to Shraddha Shitut, Lydia Papanikolopoulou, the Stärker family, and my flatmates.

To my long-distance and long-time friends who have stood with me constantly, supported me, and prayed for me since I met them years ago. Thank you for giving me a soft landing every single time. To Jennie Talao, my "to-go-to" person and my branded best friend, for always being there for me and for all the snail mails, postcards, surprise food deliveries, and for welcoming me home every time I am in the Philippines. To the other third of dinner club, Meljay Santos, thank you for your humor, free food, and sometimes sensible advice. To Gerlie Bautista, for being an awesome nurse and friend who takes good care of me whenever I got sick in the Philippines. To Wilfred John Santiañez, thank you for being my koyang (big brother), for all the (un)solicited advice and, honest criticisms, and tons of corrections to my manuscripts and thesis, for your everyday humour (and good looks), and for not getting tired of me (yet). To Joyce Nieva, thank you for being my ating (in this case little sister), for being one of my constant rant pages where I can sort my anxious thoughts, for all the video and voice calls, and for standing with me through everything. To Charisma Maga and Veronica Escaño, for making the load of chronic illness lighter, and for all the prayers and encouragements.

To all my doctors in Jena and the Philippines. I know it is weird to thank doctors in a dissertation, but I owe a lot to you. Thank you for your help in keeping my health stable, and giving me advice on how to live despite my illnesses.

To my family. I would not have done it without your unwavering love, support and prayers. For my parents, thank you for letting me choose my own path. All I am is because of all what you have instilled to me. Thank you for showing me how to be hardworking and persistent, and for constantly reminding me about the value of education. I also owe a lot to my sister, who selflessly supported my academic career, followed me all the way from Philippines to Germany, and finally understood my passion for science.

And I owe my utmost praise and thank you to my God who sustained me throughout this journey and who will continue to keep me in His grace. This is just the start.

He named it Ebenezer, explaining, "The LORD has helped us to this point." - 1 Sam 7:12b

Maraming salamat.